Leif Rune Hellevik

Wave propagation and pressure drop in precordial veins

A study of the fetal ductus venosus-umbilical vein bifurcation and the adult pulmonary veins

NTNU Trondheim
Norges teknisk-naturvitenskapelige universitet

Doktor ingeniøravhandling 1999:61
Institutt for mekanikk, termo- og fluiddynamikk

MTF-rapport 1999:181

Wave propagation and pressure drop in precordial veins

A study of the fetal ductus venosus-umbilical vein bifurcation and the adult pulmonary veins

Leif Rune Hellevik

Department of Applied Mechanics
Thermodynamics and Fluid Dynamics

National Center for Fetal Medicine
University Hospital Trondheim

Norwegian University of Science and Technology

Trondheim, August, 1999

Summary

In this thesis, consisting of an introduction and five separate papers, wave propagation and pressure drop in blood vessels are studied by means of mathematical and numerical models. The first four papers are related to the hemodynamics of the fetal ductus venosus-umbilical vein bifurcation, while the fifth paper relates to pressure and flow waves in the pulmonary veins of man.

In paper I we deduce a generalized Bernoulli equation for pressure drop estimates in bifurcations. Further, physiological measurements were used as the basis for a rigid-walled, three-dimensional computational model of the umbilical vein-ductus venosus bifurcation. Based on results of this computer model, energy dissipation is estimated to constitute from 24 to 31 percent of the pressure drop between the umbilical vein and the ductus venosus inlet, depending on the Reynolds number and the curvature ratio. Thus, energy dissipation should be taken into account in pressure drop estimates.

Information about the mechanical properties of fetal ductus venosus and the umbilical vein is presented in paper II. The information is based on pressure-area measurements of the ductus venosus and the umbilical vein of five fetal sheep in vitro. Each data set is fitted to an exponential function to determine the stiffness parameter and the area of the ductus venosus and umbilical vein at a standard pressure. The mechanical properties of fetal veins are comparable to those described for veins later in life. The stiffness parameter represents the elastic properties at all pressure levels and conveniently permits inference of compliance and pulse wave velocity.

A mathematical model to identify the mechanical factors that influence pulsation in the umbilical vein is presented in paper III. The umbilical vein is modeled as a compliant reservoir and the umbilical vein pressure is assumed to be equal to the stagnation pressure at the ductus venosus inlet. The pulsatility of the umbilical vein pressure and the reflection and transmission factors at the ductus venosus inlet, are quantified numerically and with estimates. The results indicate that wave transmission and reflection in the umbilical vein-ductus venosus bifurcation depend on the impedance ratio between the umbilical vein and the ductus venosus, as well as on the ratio of the mean velocity and the pulse wave velocity in the ductus venosus. The impedances, in turn, depend on the mechanical properties of the veins, the pressure level, and their dimensions. These findings are in agreement with in vivo observations. Thus, we believe that the mathematical model is suitable for analyzing the factors involved in the occurrence of umbilical venous pulsations.

In paper IV the effect of ductus venosus tapering on the reflection coefficient is investigated with a mathematical model incorporating wave propagation. The results in this

ɔer indicate that the only effective reflection site in the ductus venosus is located at
: ductus venosus inlet. The tapered geometry of the ductus venosus is of minor impor-
ıce. The differences between the ductus venosus inlet and outlet flow are also minor for
dium to large umbilical vein-ductus venosus diameter ratios. The results of this model
·ee well with those of paper III.

The pulmonary venous systolic flow wave in man has been attributed both to left
ırt phenomena, such as left atrial relaxation and descent of the mitral annulus, and
propagation of the pulmonary artery pressure pulse through the pulmonary bed from
: right ventricle. In paper V we hypothesize that all waves in the pulmonary veins
ginate in the left heart, and that the gross wave features observed in measurements
ı be explained simply by wave propagation and reflection. A mathematical model of
: pulmonary vein and the pulmonary bed in man is developed; the pulmonary vein
modeled as a lossless transmission line and the pulmonary bed by a 3-element lumped
ɾameter model. We conclude that the gross features of the pressure and flow waves in the
lmonary vein can be explained in the following manner: the waves originate in the left
ırt and travel towards the pulmonary bed, where reflections give rise to waves traveling
ck towards the left atrium. Although the gross features of the measured pressure were
ɔtured well by the model predicted pressure, there was still some discrepancy between
: two. Thus, other factors initiating or influencing waves traveling towards the LA can
t be excluded.

Preface

This thesis could not have been realized without extensive help and support from others. First of all I want to express my sincere gratitude to my supervisor Professor Fridtjov Irgens, who so willingly accepted me as his student in the field of biomechanics, a field more or less unknown to both of us in the beginning. His interest and curiosity in the whole field of mechanics have been a continuous source of inspiration.

Grateful thanks go to my co-supervisor Professor Tor Ytrehus, for advice, discussions, and for granting me the confidence to teach his course "Viscous fluid flows" while he was on sabbatical leave.

Professor Torvid Kiserud is the one who introduced me to the fascinating world of fetal hemodynamics, while I served my "civil service" at the National Center for Fetal Medicine in Trondheim. Since then, his genuine interest in the field, his enormous capacity, and his never failing interest and guidance have been of indispensable help. He was always there with his swift responses when I needed him. Additionally, his wit and humor has made him a highly regarded friend.

Professor Sturla Hall Eik-Nes, head of the National Center for Fetal Medicine, with his ability to grasp the essentials in unfamiliar areas of science, his energetic manner and his enthusiasm, has been a cornerstone for me in my work. The financial support he has provided is also highly appreciated.

I would also like to thank my colleagues and advisors at the University of Gent for their hospitality, friendship and support. Professor Pascal Verdonck, for inviting me to Gent and letting me benefit from his extensive scientific network, his guidance, and his friendship extending far beyond scientific matters. Professor Erik Dick for including me in his group and for advice in numerical methods. Special thanks to Drs. Jan Vierendeels and Patrick Segers for invaluable advice, help, encouragement, and friendship.

Professor Otto Smiseth, Rikshospitalet, introduced me to the dynamics of pulmonary veins and to wave intensity analysis with vigor and enthusiasm. Further, my stay in Gent would not have been possible without his financial support through the Medinnova project.

Special thanks are rendered to Professor Nikos Stergiopulos, EPFL, who welcomed me so willingly in Lausanne and provided valuable ideas, which proved to be vital for the progress of my work. His gentle and friendly nature has been a true inspiration.

Thanks are also due to chief scientist, Professor II Stein Tore Johansen and research scientist Harald Laux at SINTEF Materials Technology for help with CFD-simulations.

PhD-student Stein Inge Rabben, at the Department of physiology and biomedical engineering, my only fellow in biomechanics at NTNU, is entitled my most sincere thanks

advice, help, discussions, and fruitful collaboration. His dedicated interest in the field, stayer-instinct, and his friendship have been a true inspiration and example for me. supervisor, Professor Bjørn Angelsen, is also entitled my gratitude; he has contributed many discussions with his astonishing mathematical and physical intuition and skills. The partial financial support provided by Vingmed Sound was vital in the initial stages ny work and is most appreciated.

Nancy Lea Eik-Nes has revised all but one of the papers in this thesis. Her skills in ntific writing and her interest in etymology has improved my manuscripts significantly. ther, her humor, warmth and care has meant "more than words" to me.

Thanks also to Associate Professor Reidar Kristoffersen, the rest of the dr.ing. students MTF/Divsion of Applied Mechanics, and to the "computer-guys": Sevald Berg, Anders rp, Bjarte Østvold, Andreas Heimdal, and Atle Kleven for help with LaTeX 2_ε, emacs l numerous computer-hacks.

My family has always been a constant source of help and support; they have with love l patience endured all my "ups" and "downs". My sister Turid has always been there, ding the way for her kid-brother three years down the road. Thank you for setting such ood example Turid.

Finally, I will express my gratitude to Ingrid for encouragement, help, and pleasant tractions during the last stages of my work.

ondheim, May 1999

if Rune Hellevik

Contents

Introduction

This thesis consists of an introduction and five separate papers. The papers are self-contained and complete with abstracts and references. In what follows the papers will be referred to by their respective Roman numerals.

The introduction is divided into four parts. In the first the clinical problems relevant for this thesis are presented. The 1D governing equations for wave propagation along with selected examples of applications in biofluid dynamics are introduced in the second part. In the third part, estimates are presented of the counteracting effects of viscous dissipation and pressure recovery in the human fetal ductus venosus. In the last part validation simulations are presented for the computational fluid dynamics (CFD) package employed in paper I.

1 Motivation

Examination of the precordial venous flow is an increasingly important part of the clinical hemodynamic evaluation. This is particularly true for the evaluation of the fetal circulation which is entirely dependent on ultrasound techniques. However, the lack of information about the mechanical properties and an insufficient understanding of the fluid dynamics of this section of the circulation hampers the use and interpretation of the venous Doppler recordings. The first four papers are related to fetal hemodynamics. For a general introduction to fetal circulation and physiology the reader is referred to textbooks on fetal physiology (e.g. Thorburn and Harding, 1994; Moore and Persaud, 1993). In the following, a short outline of the fetal cardiovascular system (FCS) will be presented.

The FCS is the single most important system responsible for nourishment and exchange of gas, water, and electrolytes between the maternal and the fetal tissue. The system is designed to serve the prenatal needs and to adapt rapidly to the totally different environment after birth. In the FCS, the umbilical circulation plays a dominating role during most of the pregnancy. The fact that 50% of the total fetal blood volume is contained within the placenta and that the placenta receives 40% of the fetal combined cardiac output reflects the importance of this circulatory section (Rudolph, 1985). The oxygenated placental blood that returns to the fetus through the umbilical vein (UV) enters the liver tissue or is shunted through the ductus venosus (DV), to reach the heart directly (Fig. 1). The DV is a narrow, trumpet-shaped vein that connects the UV to the hepatic veins and the inferior vena cava (IVC) below the atrial inlet (Chako and Reynolds, 1953; Blanc,

0). At eight weeks of gestation the DV is well defined, whereas during the early stages ntra-uterine life the vascular system has a different arrangement (Chako and Reynolds, 3; Lassau and Bastian, 1983).

In animals, 50% of the oxygenated blood is directed through the DV, but the proportion reases to 70% during reduced oxygen content or reduced blood volume (Behrman et al., '0; Edelstone and Rudolph, 1979; Edelstone et al., 1978). In the human fetus, a similar chanism of preferential streaming (Fig. 1) exists (Kiserud et al., 1991) but with a smaller ction of shunting (20-30%) through the ductus vensosus (Kiserud et al., 1998b). Both animal and human fetuses the oxygenated blood accelerates in the DV and is directed vards the foramen ovale to generate the preferential streaming to the left atrium (Fig. 1). is flow mixes only to a small extent with the less oxygenated blood in the inferior vena a which otherwise is directed to the right atrium. There is a small contribution of oxygenated blood from the pulmonary circulation to the left atrium. The net effect of se flow patterns is a 10-12% higher oxygen saturation of the blood in the left atrium mpared to the right atrium), which is sufficient to ensure an abundant oxygen supply the coronary arteries and the brain via the ascending aorta. On the other hand, the od in the right side of the heart has the lower oxygen saturation and predominantly ws through the ductus arteriosus to reach the lower parts of the body and the placenta.

Knowledge about the central venous pressure is generally accepted as a key to under- nding central blood circulation and the underlying hemodynamics changes in disease. e high velocity in the DV, both in normal (Huisman et al., 1992; Kiserud et al., 1992) d complicated pregnancies (Kiserud et al., 1992; Oepkes et al., 1993; Hecher et al., 95a), has been suggested to reflect a major proportion of the pressure drop from the V to the fetal heart. Attempts to calculate the UV-DV pressure drop by means of a nple Bernoulli equation have been reported (Kiserud et al., 1994b; van Splunder et al., 95). By employing such a method in conjunction with measurements of the UV pressure ned by needling, one may obtain an estimate of the pressure in the fetal heart. How- er, until the methodological limitations are controlled, the formulation cannot reliably used in clinical practice. In paper I a rigid-walled, 3D computational model of the V-DV bifurcation for stationary flow conditions is established. The energy dissipation this model constitute 24% to 31% of the pressure drop from the UV to the DV inlet, pending on the Reynolds number and the curvature ratio. Note, however, that only the essure drop from the UV to the DV inlet is discussed in this paper, while the long term al is to estimate the pressure drop from the UV to the IVC or the fetal heart. This is very complex problem and remains to be investigated. In section 3 a brief outline of an imation procedure for the counteracting effects of viscosity and pressure recovery along e DV is provided.

In contrast to the pulsatile flow in precordial veins, the blood flow in the umbilical n (UV) is usually stationary. In 1986, Lingman et al. described a pulsatile veloc- in the UV in fetuses with imminent asphyxia (Lingman et al., 1986); Gudmundsson al., who found the same pulsations in fetuses with congestive heart disease, suggested s sign as a marker of poor prognosis (Gudmundsson et al., 1991). Similarly, such lsations were found in cases with fetal cardiac malformations (Kiserud et al., 1993), rhythmias (Gembruch et al., 1995), serious growth restriction (Kiserud et al., 1994a) d twin-twin transfusion syndrome (Hecher et al., 1995b). However, UV pulsation is a

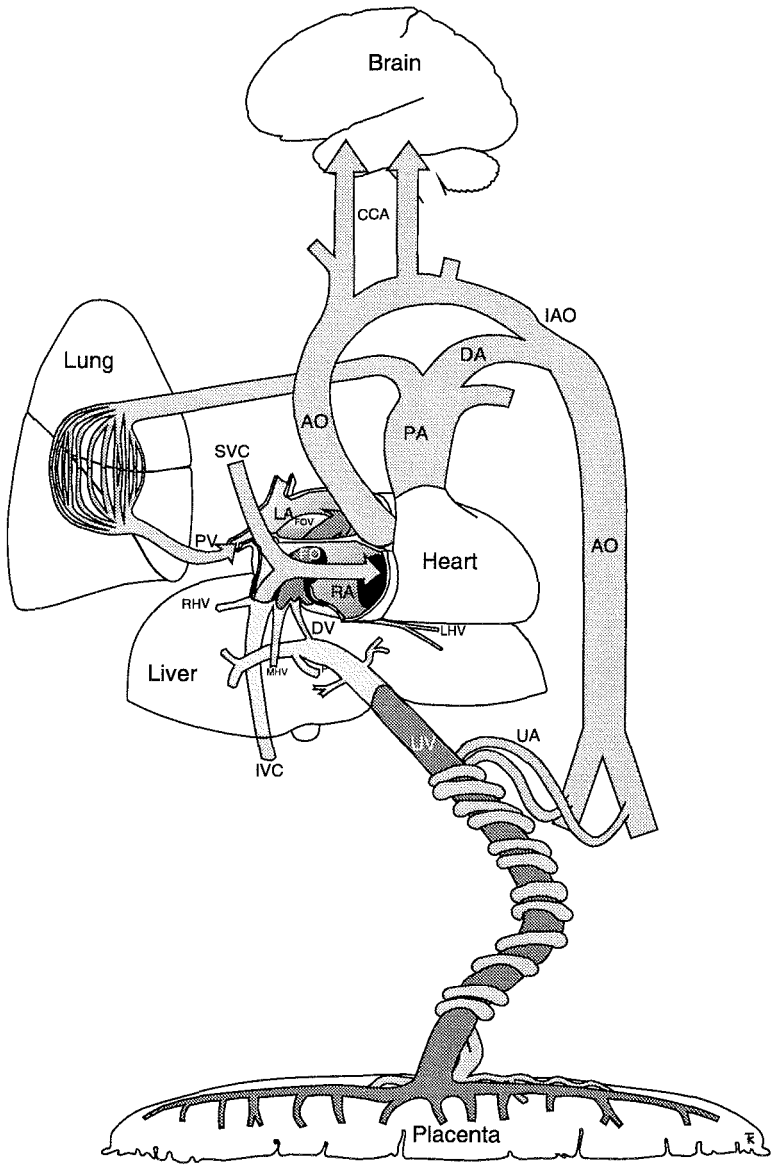

Figure 1: Fetal vascular anatomy showing the three shunts: the ductus arteriosus (DA), ductus venosus (DV) and foramen ovale (FO). Observe that three shunts permit most of the blood to bypass the liver and the lungs. The left portion of the fetal liver is relatively large compared to its size in adult life. The umbilical vein (UV) is connected to the left branch of the portal system which is usually called the intra-abdominal UV. The main stem of the portal vein (P) is a modest vessel during fetal life. In contrast to adult life, the left hepatic vein (LHV) and the medial branch (MHV) are well defined in the fetus. Note the close anatomical relationship between the DV and the FO, a detail that is commonly neglected, but important for understanding the function of the FO. AO, aorta; CCA, common carotid artery; FOV, foramen ovale valve; IAO, isthmus of the aorta; LA, left atrium; PA, pulmonary artery; PV, pulmonary vein; RA, right atrium; RHV, right hepatic vein; SVC, superior vena cava; UA, umbilical artery. (Adapted from Hanson and Kiserud, 1999)

:mal phenomenon in fetuses of a gestational age of 13 weeks and younger (Rizzo et al.,)2; Nakai et al., 1995), and its occurrence is described even in normal fetuses during e pregnancy, particularly in the deep intra-abdominal portion of the vein (van Splunder al., 1994). Fetal sheep experiments have shown that such waves are transmitted to the ' during adrenergic stimulation and hypoxic challenge (Reuss et al., 1983; Hasaart and Haan, 1986), and that the transmission of such waves is blocked by the agenesis of the ctus venosus (Kiserud et al., 1998a). The mechanisms that govern the transmission and :urrence of pulsations in the UV are not well understood. In papers II-IV, information the mechanical properties of the UV and DV is presented, and mathematical models the UV-DV bifurcation are established in order to identify the factors that influence lsation in the UV.

In the adult human being the pulmonary venous flow pattern is believed to provide ormation about left atrial pressure and to improve noninvasive assessment of left ven- cular diastolic function (Kücherer and Schiller, 1993). The concept of what causes the lmonary venous systolic flow wave is controversial and has been attributed both to left art phenomena, such as left atrial relaxation and descent of the mitral annulus, and to opagation of the pulmonary artery pressure pulse through the pulmonary bed from the ;ht ventricle. In paper V all waves in pulmonary veins are assumed to originate in the t heart and a lumped mathematical model including wave transmission and reflection established to address this issue.

1D governing equations

ıe one-dimensional equations for flow in an impermeable, uniform elastic tube can be ·itten as (Anliker et al., 1971; Raines et al., 1974; Pedley, 1980):

$$\frac{\partial A}{\partial t} + \frac{\partial Q}{\partial x} = 0 \tag{1}$$

$$\frac{\partial Q}{\partial t} + \frac{\partial}{\partial x}\left(\frac{Q^2}{A}\right) = -\frac{A}{\rho}\frac{\partial p}{\partial x} + \frac{\pi D \tau_0}{\rho} \tag{2}$$

ıere p and A denote pressure and cross-sectional tube area, D the tube diameter, ρ the id density, Q the volume flow ($Q = u\,A$), u the spatially averaged velocity, and τ_0 the ear stress at the wall. This model is based on the following assumptions:

- The fluid is incompressible and Newtonian.
- Gravitational effects are negligible.
- The primary variables change only along the longitudinal axis x, i.e. the radial dependency of pressure and velocity is neglected. Consequently, the momentum coefficient defined by:

$$\gamma = \frac{1}{u^2\,A}\int_A u_x^2\,dA \tag{3}$$

is assumed to be $\gamma = 1$. The velocity component in the axial direction is denoted by u_x. Local Poiseuille flow could be accounted for by the following correction of the convective term in Eq. (2):

$$\frac{\partial}{\partial x}\left(\gamma \frac{Q^2}{A}\right)$$

Young and Tsai (1973) approximated the shear stress by comparing with the analytical solution for harmonically, oscillating, laminar, Newtonian, and incompressible flow in a long tube of constant cross-sectional area and obtained:

$$\tau_0 = -\frac{\rho}{\pi D}\left[\frac{8\pi\nu c_v}{A}\, Q + (c_u - 1)\frac{\partial Q}{\partial t}\right] \tag{4}$$

where c_u and c_v, the inertia and viscous coefficients, respectively, are functions of the Womersley number $\alpha = (D/2)\sqrt{\omega/\nu}$ (Womersley, 1957). The kinematic viscosity and the angular frequency of the primary variables are denoted by ν and ω, respectively.

To close the system of equations (Eqs. (1) and (2)) the constitutive equation for the tube is normally taken to be represented by a single-valued function p of A:

$$p = p(A) \tag{5}$$

Thus, the viscoelasticity (Holenstein et al., 1980) of the vessel wall is neglected. The significance of viscoelastic correction in human arteries has been estimated to be comparable to nonlinear and dissipation corrections (Pythoud, 1996), i.e. 10-20%, while information on both the dynamic and the static mechanical properties of veins is scarce.

Various approaches to represent the pressure-area relations for blood vessels have been suggested. Hayashi reviewed recent studies on the elastic properties of arterial walls (Hayashi, 1993) and argued that a simple constitutive relation, such as an exponential or logarithmic one, is more advantageous than the more elaborated relations based on strain energy functions (Vaishnav et al., 1973; Fung et al., 1979). In these simple formulations the number of coefficients are reduced, while their physical meaning is retained. Constitutive equations based on linear elasticity theory for a thin-walled cylinder have also been proposed (Bergel, 1972), but these require the knowledge or assumption of the vessel wall thickness. A three-parameter arc tangent model was suggested to capture the S-shape of the arterial pressure-area relation, i.e. the presence of an inflection point, better than an exponential function (Langewouters et al., 1985a,b). Our pressure-area measurements, in paper II, of the UV and the DV showed no inflection point (i.e. S-shape), most probably because the pressure variation is much smaller in fetal veins than in adult arteries. Thus, we preferred the simplest regression model that gave a statistically satisfying representation of the data, i.e. the exponential model.

Such a pressure-area relationship may be introduced into Eqs. (1) and (2) to eliminate either the cross-sectional area or the pressure. Normally the area is eliminated and by introducing the area compliance C:

$$C = \frac{\partial A}{\partial p}$$

ich is derived from the constitutive equation and in general is pressure dependent. This s also been found to be the case for the UV and DV in paper II.

From the linearized and inviscid forms of Eqs. (1) and (2) the widely used pulse wave ocity c and the characteristic impedance Z_c may be derived (Fung, 1984):

$$c^2 = \frac{\partial p}{\partial A}\frac{A}{\rho} = \frac{A}{\rho C}, \quad Z_c = \frac{\rho c}{A} \tag{6}$$

Founded on the inviscid and linearized forms of Eqs. (1) and (2), the concept of wave paration for analysis of wave propagation in arteries was first introduced by Westerhof al. in 1972. This concept has been developed further to incorporate both nonlinearities d viscous dissipation (Pythoud et al., 1996). However, due to limitations in measure-nts in vivo, the classical method of Westerhof et al. is the method of choice to estimate e forward and backward running wave components.

Wave intensity (WI), is another useful concept related to wave propagation in blood ssels. Based on theory for acoustic intensity (Lighthill, 1978), WI was first introduced in terial dynamics by Parker et al. (Parker et al., 1988; Parker and Jones, 1990; Jones et al., 94). Any finite wave can be analyzed as the sum of "wavelets", defined as infinitesimal anges in pressure and velocity. Along the characteristic directions the flow is steady and e relationships between wavelets of pressure (dp) and velocity (du) are:

$$dp_f = \rho c\, du_f, \quad dp_b = -\rho c\, du_b \tag{7}$$

here the subscripts f and b denote forward and backward propagating wavelets, respec-vely. Wavelets with positive pressure changes $dp > 0$, are generally called compression avelets and those with negative changes $dp < 0$ expansion wavelets. The instantaneous anges in p and u are the result of intersecting forward and backward wavelets at the ne and location of measurements:

$$dp = dp_f + dp_b, \quad du = du_f + du_b \tag{8}$$

ne wave intensity $WI = dp\, du$, is the rate of energy flux per unit area associated with e wavelet, and from Eqs. (7) and (8) the following expression for WI may be derived:

$$WI = \frac{dp_f^2 - dp_b^2}{\rho c} \tag{9}$$

nus, the WI has the useful property that forward propagating wavelets make a positive ntribution to the WI, whereas backward propagating waves make a negative contribu-on. This is the case regardless of whether or not they are compression or expansion avelets. In paper V the WI is derived with volume flow and *not* velocity as the primary riable for convenience. Thus, the WI dimension in paper V is W and not $W\,s^{-2}$ (Parker al., 1988; Parker and Jones, 1990; Jones et al., 1994); i.e. strictly speaking it does not present wavelet *intensity* but rather wavelet *power*. However, the interpretation of the I remains unchanged with respect to identifying the direction of net energy transport.

Further, the Eqs. (1) and (2) have, with varying degrees of simplification, also been plied to develop a wide range of distributed models of the human arterial system (West-hof et al., 1969; Schaaf and Abbrecht, 1972; Raines et al., 1974; Avolio, 1980; Zagzoule

and Marc-Vergnes, 1986; Stergiopulos et al., 1992). Arterial network models allow for calculation of the pressure and flow waves along the arterial tree and exhibit the observed wave phenomena such as: the systolic pressure rise, diastolic pressure decay, wave attenuation and wave reflection. In a study by Segers et al. (1997) the relative importance of elastic nonlinearities in a nonlinear time-domain approach by Stergiopulos et al. was compared to that of viscoelastic effects in a linearized frequency domain approach by Avolio. In paper IV, Eqs. (1) and (2) are used to study wave propagation phenomena in the human fetal ductus venosus.

3 1D estimate of DV tapering impact on pressure drop

In paper I results are presented on energy dissipation and UV/DV inlet pressure drop in a 3D computational model of the UV/DV bifurcation. The energy dissipation in these models was estimated to constitute 24% to 31% of the pressure drop, depending on the Reynolds number and the curvature ratio. Thus, energy dissipation should be taken into account in pressure drop estimates at the DV inlet. For a physician, however, the primary concern is the pressure drop between the UV and the outlet of the trumpet-shaped DV. The DV shape resembles a relatively low-Re diffusor (White, 1988). The diffusor effect was not accounted for in the paper as we wanted to study the inlet effects first and leave the diffusor effect for future studies. However, in the discussion section of paper I we do stress the need to study the effect of DV tapering and refer to 1D estimates of its effects for certain physiological parameters. The rationale for these 1D estimates is outlined below.

For stationary flow and with the spatially averaged velocity u as the primary variable, the momentum equation (Eq. (2)) reduces to:

$$-\frac{\partial p}{\partial x} = -4\,\frac{\tau_0}{D} + \rho u \frac{\partial \gamma u}{\partial x} \tag{10}$$

Further, let the pressure drop be defined by: $\Delta p = p_i - p_o$, assume that γ is constant, and let the subscripts i and o refer to inlet and outlet, respectively. Then, integration along the flow yields:

$$\Delta p = -\int_0^L 4\,\frac{\tau_0}{D}\,dx + \rho\gamma \int_{u_i}^{u_o} u\,du$$

Further, the pressure drop may be split into viscous (Δp_v) and inviscid (Δp_r) parts:

$$\Delta p_v = -\int_0^L 4\,\frac{\tau_0}{D}\,dx, \quad \Delta p_r = \rho\gamma \int_{u_i}^{u_o} u\,du \tag{11}$$

i.e. $\Delta p = \Delta p_v + \Delta p_r$, which normalized by the dynamic pressure $\frac{1}{2}\,\rho\,u_i^2$ gives the corresponding diffusor (k_d), viscous (k_v), and inviscid (k_r), pressure loss coefficients:

$$k_d = k_v + k_r, \quad k_v = \frac{\Delta p_v}{\frac{1}{2}\rho u_i^2}, \quad k_r = \frac{\Delta p_r}{\frac{1}{2}\rho u_i^2} \tag{12}$$

To obtain quantitative approximations of the pressure loss coefficients, a wall friction law and a momentum coefficient have to be prescribed.

1 Estimate of the viscous pressure loss coefficient

ɔject to the assumption of local Poiseuille flow ($\gamma = 4/3$) the wall shear stress takes the m:

$$-\tau_0 = \tau_\omega = \frac{64}{Re}\,\frac{\rho u^2}{8} \quad \text{and} \quad Re = \frac{uD}{\nu} \tag{13}$$

ere Re denotes the Reynolds number. From the principle of mass conservation it follows ıt:

$$u = \frac{D_i^2 u_i}{D^2} \tag{14}$$

ɹen, from Eqs. (12), (13) and (14) an integral expression for the viscous pressure loss ɜfficient k_v may be obtained:

$$k_v = \frac{64}{Re_i}\,D_i^3 \int_0^L \frac{1}{D^4}\,dx \tag{15}$$

suming the diameter of the tube to vary linearly along the axis yields:

$$D = D_i + \frac{D_o - D_i}{L}\,x, \quad \frac{dD}{dx} = \frac{D_o - D_i}{L} \tag{16}$$

d an analytical approximation of k_v may be found:

$$k_v = \frac{64}{Re_i}\,D_i^3\,\frac{L}{D_o - D_i} \int_{D_i}^{D_o} D^{-4}\,dD$$

ıich by the introduction of the expansion factor $f = D_o/D_i$ and the monotonously creasing function:

$$h_1(f) = \frac{1}{3}\,\frac{1 + f + f^2}{f^3} \tag{17}$$

lduces to:

$$k_v = \frac{64}{Re_i}\,\frac{L}{D_i}\,h_1(f) = \frac{16\,\pi\,\mu\,L}{Q}\,h_1(f) \tag{18}$$

ıus, the larger the expansion factor f the smaller the viscous pressure loss coefficient . Observe that, $h_1(1) = 1$; thus for $f = 1$ the viscous pressure loss coefficient equals the dinary Poiseuille form for a straight tube. Note further that h_1 will always be positive the expansion factor per definition is positive. Consequently, k_v will always contribute a streamwise pressure reduction.

2 Estimate of inviscid pressure loss coefficient

om the inviscid pressure drop expression Eq. (11) and with:

$$du = -\frac{u_i\,D_i^2}{D^3}\,dD$$

an expression for the inviscid pressure drop coefficient k_r in Eq. (12) may be found:

$$k_r = \gamma\, h_2(f), \quad \text{with} \quad h_2(f) = (f^{-4} - 1)$$

For expansion factors f larger than one, h_2 will be negative and consequently k_r will yield a pressure recovery. Observe that $h_2(1) = 0$, which corresponds to no inviscid effects for a straight tube. Further, as f^{-4} drops very fast to zero, k_r will be close to its maximum value γ for relatively modest expansion factors.

3.3 The diffusor pressure loss coefficient

Subject to the assumptions above an approximate expression for the diffusor pressure loss coefficient was obtained:

$$k_d = \frac{64}{Re_i}\,\frac{L}{D_i}\, h_1(f) + \gamma\, h_2(f)$$

For $k_d \approx 0$ the inviscid pressure recovery will approximately cancel the viscous pressure drop, and thus an approximate criterion for pressure drop cancellation may be expressed:

$$h(f) = -\frac{h_2(f)}{h_1(f)} \approx \frac{64L}{\gamma Re\, D_i} = \frac{16\, L\nu\pi}{\gamma\, Q} \tag{19}$$

The estimate in paper I is based on an expansion factor $f = 2$, a DV inlet diameter of $D_i = 1.65\,10{-}3$ m, a DV length of $8.4\,D_i$ (the length downstream of the branch junction at $1.6\,D_i$ to the outlet at $10\,D_i$), $\gamma = 4/3$, and a UV Reynolds number of 163. For a flow split of 0.45 this corresponds to $u_i = 0.46$ m/s and $Re_i = 191$. These parameters yield a $k_d = -0.43$, whereas simulated pressure drop from the UV to the DV inlet was approximately 1.5 mmHg, corresponding to a bifurcation loss coefficient k_b of 1.8, i.e. the diffusor pressure loss coefficient k_d is about 24% of the k_b and makes a significant contribution to the over all pressure loss. By changing the expansion factor to $f \approx 1.75$ and the DV length to $10D_i$, k_d is close to zero. Thus, the estimates outlined above suggest that the DV geometry is also of importance for estimates of the pressure drop from the UV to the DV outlet.

However, it should be stressed that the estimates presented in this section are one-dimensional only. The fluid dynamics of a diffusor may be very complex; for instance the flow may separate along the wall in the case of an adverse pressure gradient. Thus, we suggest that a parametric study of these effects should be performed in the future, where the factors suggested by White (1988) are taken into account:

- Expansion factor f
- Divergence angle $2\theta = 2\arctan\left(\frac{D_o - D_i}{2\,L}\right)$ or slenderness L/D
- Inlet Reynolds number Re_i.
- Inlet boundary layer *blockage factor* $B_t = D_{bl}^2/D_i^2$, where $\pi\, D_{bl}^2$ is the wall area blocked, or displaced, by the retarded boundary-layer flow in the inlet.

Validation

paper I we employed a commercially available CFD package (Fluent, 1991) to investigate ssure drop and energy dissipation in a simplified computer model of the bifurcation of human fetal umbilical vein and the ductus venosus. In this code, the governing mass d momentum equations are discretized with the finite volume method (FVM) (Rizzi and ouye, 1973). To investigate the applicability of the FVM-code to flow regimes similar to one presented in the first paper, some preliminary validation simulations were carried t. The results of these investigations are outlined in this section.

1 2D validation

merical simulations were carried out for steady, laminar and incompressible flow through 2D T-bifurcation and compared with numerical and experimental results (Collins and i, 1990; Liepsch et al., 1982).

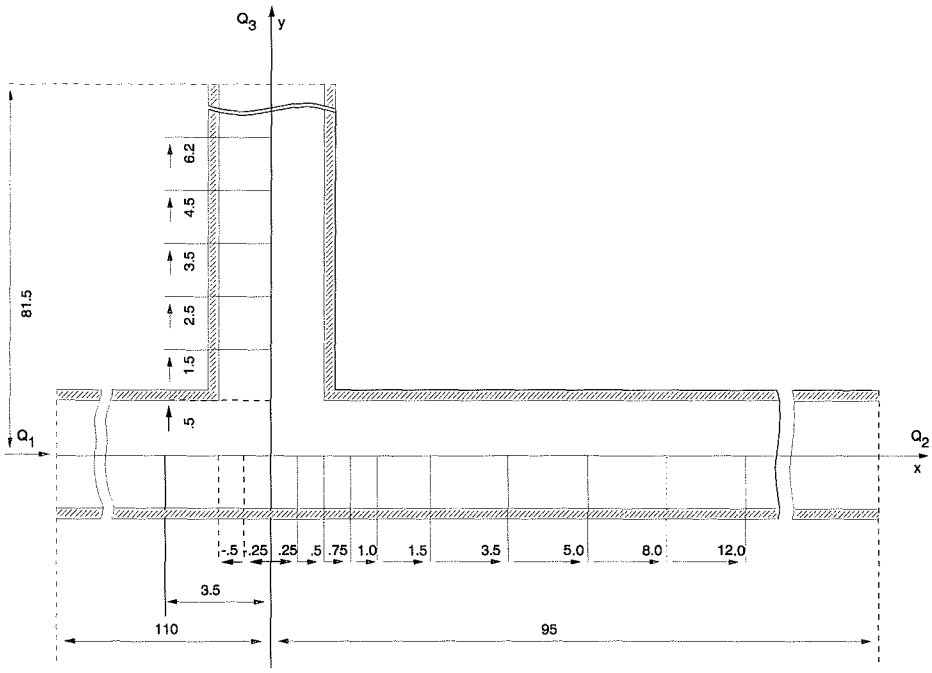

gure 2: 2D T-bifurcation geometry and measurements locations scaled by the channel width: cations of Liepsch et al. (solid line), additional locations for comparison in the present study d by Collins and Xu (dashed lines). The location excluded in the present study and by Collins d Xu, but included in the measurements by Liepsch et al. (dotted line). All lengths are n-dimensionalized with the channel width D.

Liepsch et al. used a one-component direction-sensitive laser Doppler anemometer DA) to measure the velocity profiles in their experimental setup. The test section

consisted of a 90° glass bifurcation of 10mm × 80mm cross-section. They found this aspect ratio to provide two-dimensional flow in the individual channels and the measurements were carried out along the center lines of the corresponding channels. The geometry and the measurement locations are shown in Fig. 2. All lengths are scaled by the channel width D. Measurements were performed for various Reynolds numbers, ranging from $Re = 496$ to $Re = 1130$ (Reynolds number based on the hydraulic diameter $D_h = 2D$), and various flow ratios, ranging from $Q_3/Q_1 = 0.23$ to $Q_3/Q_1 = 0.64$. In this study however, only the results of the $Re = 496$ and $Q_3/Q_1 = 0.44$ configuration will be used for validation.

The simulations of Collins and Xu were performed using ASTEC, a fluid flow code in which finite volume methods are applied to a finite element mesh (Lonsdale, 1988). For pressure velocity coupling the SIMPLE algorithm was employed (Patankar, 1980), and a vector upwind scheme was used for the advection terms. To reduce computational costs they reduced the upstream main tube (MT) length to $3.5\,D$, the downstream MT length to $11.8\,D$ and the branch length to $6.2\,D$. Their mesh consisted of 840 elements and 1870 nodes, with a refined distribution in the bifurcation junction.

We discretized the governing mass and momentum equations by employing a finite volume formulation (Fluent, 1991). The SIMPLEC algorithm (van Doormaal and Raithby, 1984) was utilized for the pressure velocity coupling in order to improve convergence. For the advection terms we used power law, second order, and Quick upwind schemes to evaluate their impact on the solution. The fluid was assumed to be Newtonian and all simulations were performed at $Re = 496$. At the inlet plane a fully developed profile with zero normal velocities was specified. Further, at the MT outlet a fully developed profile was also imposed, whereas a zero velocity gradient condition was used at the branch outlet. The assumption at the branch outlet implies a fully developed profile. Collins and Xu imposed a constant pressure at the branch outlet; this implies a fully developed profile.

Due to the relatively short branch length ($6.2\,D$) (Collins and Xu, 1990), we found it necessary to investigate the upstream impact on the imposed boundary conditions at the branch outlet. The *inlet length* x_L, is normally defined as the point where the developing center line velocity equals 99% of the fully developed maximum velocity. In the book by Schlichting (Schlichting, 1968, pp. 176-178) an outline of an analytical estimation method of the inlet length in a straight channel is presented, based on a previous and more comprehensive paper (Schlichting, 1934). Schlichting found that the inlet length may be taken as:

$$\frac{x_L}{D} \approx 0.02Re \tag{20}$$

The numerical values quoted are modified for use of Re based on the hydraulic diameter $D_h = 2\,D$, rather than the channel width D.) Several others have reported similar results for steady flow in circular cylindrical tubes (e.g. (Schiller, 1922; Targ, 1951) cited in Fung 1984, p. 141) and Chang and Atabek (1961) cited in McDonald (1973, p. 111)). Note, however, that these approximations do not apply when the Reynolds number tends to zero. In their study, Shah and London (1978) report that the inlet length tends to a constant as the Reynolds number tends to zero and suggest the following correlation for the inlet

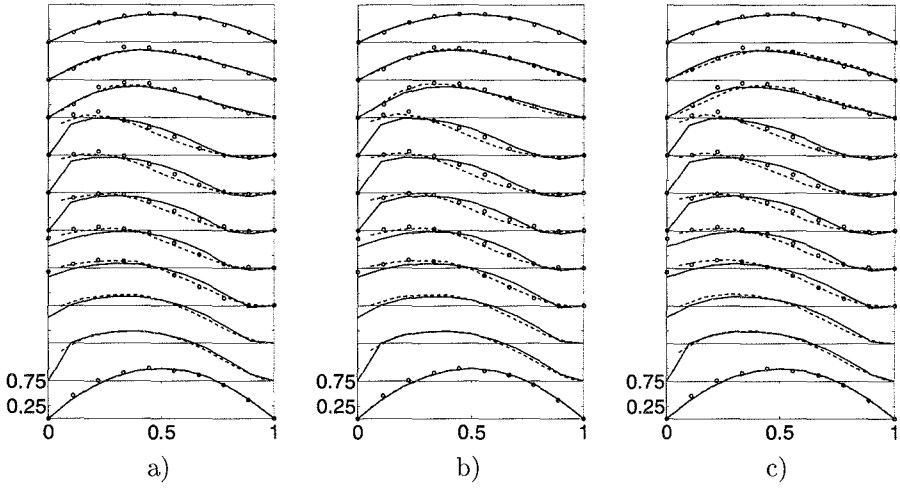

gure 3: Comparisons for the different upwind schemes in the extended model of the present ıdy with the axial MT velocity profiles of Collins and Xu (solid lines) and Liepsch et al. (circles), the various MT locations. The upwind schemes of the present study (dashed lines) are in panel second order, b) power law, and c) Quick. The velocities are scaled by the maximum velocity the MT inlet. The profiles are plotted in increasing consecutive order, starting at the bottom the figure.

ıgth (Shah and London, 1978):

$$\frac{x_L}{D} \approx \frac{0.6}{1 + 0.0175Re} + 0.028Re \tag{21}$$

For the Reynolds number in our validation case ($Re = 496$) both inlet length approx-ıations in Eqs. (20) and (21) by far exceed the branch length of 6.2 D ($x_L \approx 10\,D$ and $\approx 14\,D$, respectively). Thus, in order to study the appropriateness of the imposed ɔundary conditions at the branch outlet, simulations were conducted, both on the trun-ted geometry proposed by Collins and Xu with branch length $6.2\,D$, and on an extended ometry with branch length of $14\,D$. This geometry is the same as that employed by epsch et al. in their numerical simulations (not included here for brevity).

In Figs. 3 and 4, the axial velocity profiles in the MT and the branch of the extended odel are plotted against the non-dimensionalized diameter at different locations. The sults of the three upwind schemes in the present study are compared with the numerical sults of Collins and Xu and the experimental results of Liepsch et al.. The velocity ofiles at the different locations are plotted in increasing consecutive order, starting at e bottom of the figures. Note that we, like Collins and Xu, have excluded the velocity ofile at $8.0\,D$ and included velocity profiles at $-0.5\,D$ and $-0.25\,D$ in the MT and $0.5\,D$ the branch (i.e. at the branch inlet) in addition to the measurement locations of Liepsch al. (Fig. 2). Further, as the numerical grid points did not always coincide with the easurement locations, some of the profiles were linearly interpolated. In Fig. 3 the MT

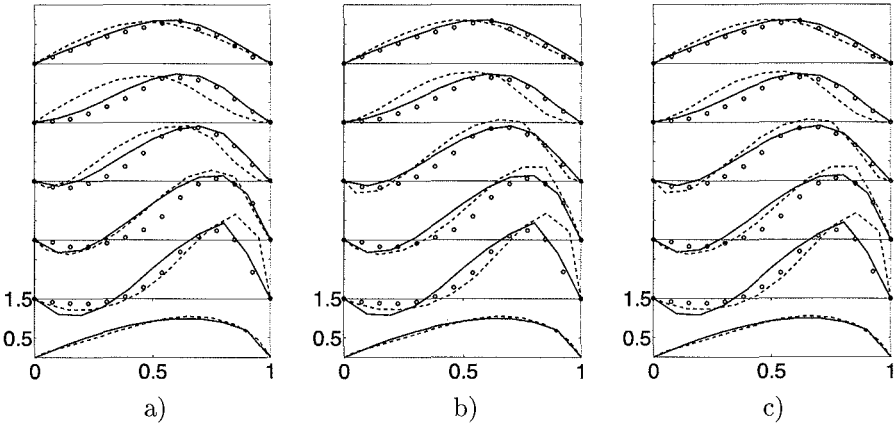

Figure 4: Comparisons for the different upwind schemes in the extended model of the present study with the axial branch velocity profiles of Collins and Xu (solid lines) and Liepsch et al. (circles), at the various branch locations. The upwind schemes of the present study (dashed lines) are in panel a) second order, b) power law, and c) Quick. The velocities are scaled by $3/2\ v_m$. The profiles are plotted in increasing consecutive order, starting at the bottom of the figure.

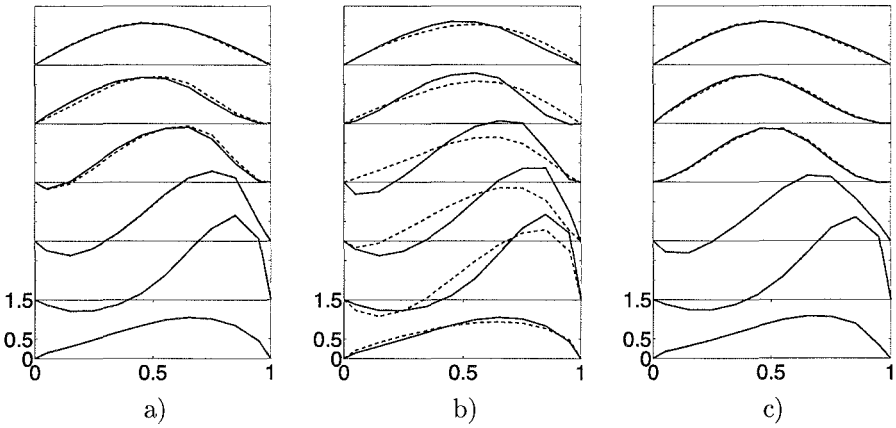

Figure 5: Comparison of the extended (solid lines) versus truncated (dashed lines) branch model of the present study. Panel a) second order, b) power law and c) Quick. The velocities are scaled by $3/2\ v_m$.

ocities are scaled by the maximum inlet velocity, whereas in Figs. 4 and 5 the velocities
scaled by $3/2\,v_m$, where v_m is the axial mean velocity in the branch, i.e. the maximum
al velocity for fully developed flow. The lines used in the figures are obtained by linear
erpolation between discrete values. Unless otherwise stated, this convention is adopted
the following.

The velocity profiles in the MT show quantitative agreement for all upwind schemes
ig. 3). The velocity profile upstream of the bifurcation is parabolic, whereas at the
urcation the velocities increase in the upper part due to the upstream influence of flow
o the branch. The velocities become slightly negative in the lower region opposite the
iling edge of the bifurcation and re-develop to parabolic profiles again downstream at
exit of the main duct.

In the branch, however, some discrepancies are found both in comparison with the
merical results and with the measurements. The velocity profiles show an asymmetry
th higher values towards the trailing edge of the bifurcation. The reverse flow region
more pronounced along the upstream branch wall than in the main tube. Close to the
anch inlet all the upwind schemes overshoot the maximum velocity and undershoot the
gative velocities. The discrepancies between simulated and experimental results may in
rt be due to the fact that the experimental flow is not truly 2D at the branch inlet and
at the presence of secondary velocities in the experimental data reduce the magnitude
the streamwise velocity components. However, Collins and Xu's results seem to agree
mewhat better with the measurements at these locations. The discrepancies between
eir simulations and those in the present study may be partly ascribed to numerical
ffusion associated with the choice of upwind scheme in conjunction with the truncated
ometry. The effect of the geometry on the different upwind schemes of the present study
illustrated in Fig. 5, where the axial velocity profiles in the branch of the truncated and
e extended model are compared. From the left and right panel it is seen that the
pact of the extended geometry is marginal for higher order upwind schemes, whereas
bstantial discrepancies are observed in the middle panel for the power law scheme, which
known to produce more numerical diffusion than higher order schemes such as second
der and Quick. Such a change in geometry would probably yield similar effects for
e results of Collins and Xu. Probably more important, however, is that we learned
om private communications with Collins and Xu that the real Reynolds number in their
nulations was approximately 20% higher than the one reported. This explains, then, why
e fully developed flow pattern appears at a shorter distance from the branch inlet in our
nulations than for those of Collins and Xu. Furthermore, the numerical results of Liepsch
al. for the extended model, discretized with a hybrid differencing scheme (Spalding,
72) and a power law upwind scheme, show the same qualitative behavior as in the
esent study, i.e. they overshoot the maximum velocities and undershoot the negative
locities. The results are not included here.

In conclusion, the numerical and experimental velocity profiles in the MT agree well
all locations. In the branch, however, discrepancies are present at the inlet, both
tween the numerical results of Collins and Xu and those in the present study, and the
perimental results. Three-dimensional effects in the experiments carried out by Liepsch
al. are probably the most likely explanation for the discrepancies with the present
nulations. The discrepancies between the two numerical approaches are most likely due

to the short branch length and the higher Reynolds number in the numerical simulations of Collins and Xu. However, at about 6D both numerical approaches seem to agree well with the measurements.

4.2 3D validation

To validate the FVM-code for 3D bifurcations, comparisons were made with a study by Yung et al. for steady, incompressible, Newtonian flow through a rigid-walled, symmetric Y-bifurcation (Yung et al., 1990). The area ratio of the daughter-to-mother tube was 2.0 and the branching angle was 60°. Symmetry with respect to both the horizontal and the vertical center plane was assumed, and thus the analyses were confined to only one quarter of the flow region.

Yung et al. discretized the governing mass and momentum equations by a finite volume formulation, incorporating the SIMPLE solution algorithm (Patankar, 1980) for the pressure velocity coupling, a hybrid difference scheme for the convective and diffusive flux terms and a body fitted coordinate transformation. Their computational grid was generated by solving a set of Poisson equations subject to Dirichlet boundary conditions. For a 3D grid, the boundary points are normally specified on the surface constraining the flow domain. In this study, however, Yung et al. employed a simplified method such that the x-coordinates of the grid points were fixed beforehand, leaving only a 2D grid to be computed for each x-plane. This grid strategy and the choice of coordinate system yield a mesh with constant skewness in the daughter vessel. However, grid independent solutions are reported for a grid solution $31 \times 9 \times 13$ (31 control volumes in x-direction, 9 in y-direction and 13 in z-direction).

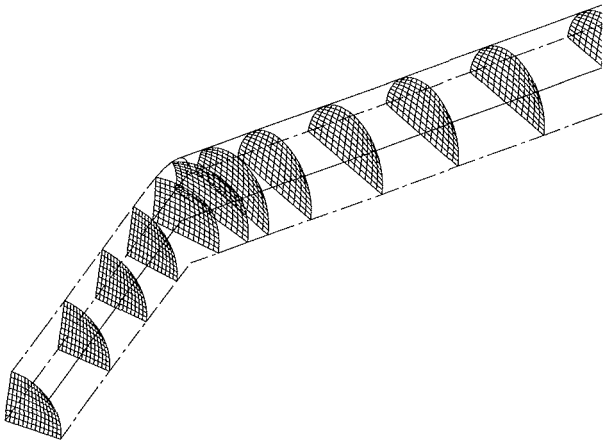

Figure 6: An outline of the Y-bifurcation geometry with the grid-distribution in the present study at selected cross-sections in streamwise direction.

In the present study an analogous model was established with a grid resolution equal

that of Yung et al., using the geometry and mesh generation preprocessor (Geomesh,)4) and the FVM-code. An outline of our geometry is given in Fig. 6, along with the grid tribution at selected cross-sections in streamwise direction. The validation simulations

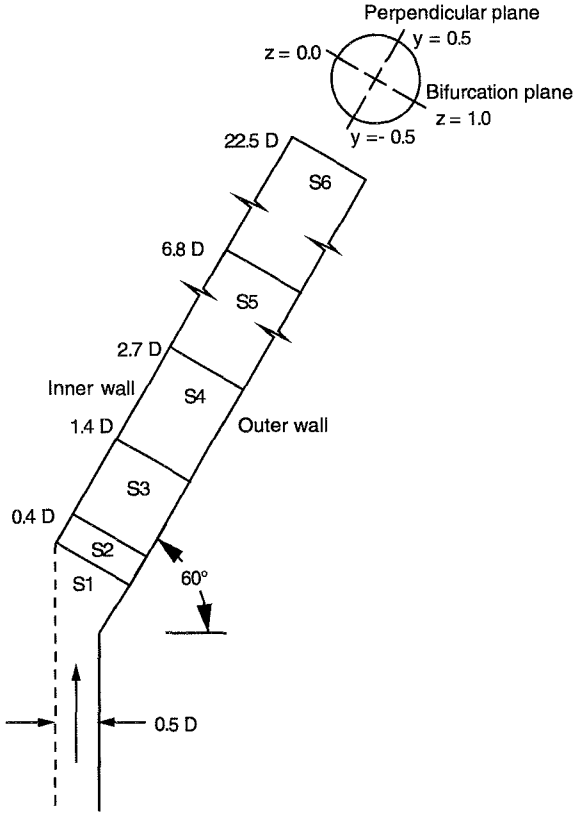

gure 7: An illustration of the bifurcation plane (BP), the perpendicular plane (PP), and the cations where the velocity profiles are presented.

ere performed for two upstream Reynolds numbers $Re = 100$ and $Re = 500$. For these nulations the SIMPLE algorithm and a second order upwind scheme were used for the essure velocity coupling and the advection terms, respectively.

Yung et al. presented axial velocity profiles in the bifurcation (BP) and the perpendicular planes (PP) at different axial positions. These planes and the locations where the locity profiles are presented and compared are illustrated in Fig. 7. The BP is located $y = 0$, extending from the inner wall ($z = 0$) to the outer wall ($z = 1$), whereas PP is ented vertically to the BP at the center of the branch, ranging from $y = -0.5$ to $y = 0.5$. Fig. 8 our axial velocity profiles at the stations S1-S6 are compared with the results Yung et al. for $Re = 100$ and $Re = 500$. The velocities are scaled by the maximum tlet velocity. Note that only half of the profile is computed for the velocities in the per-

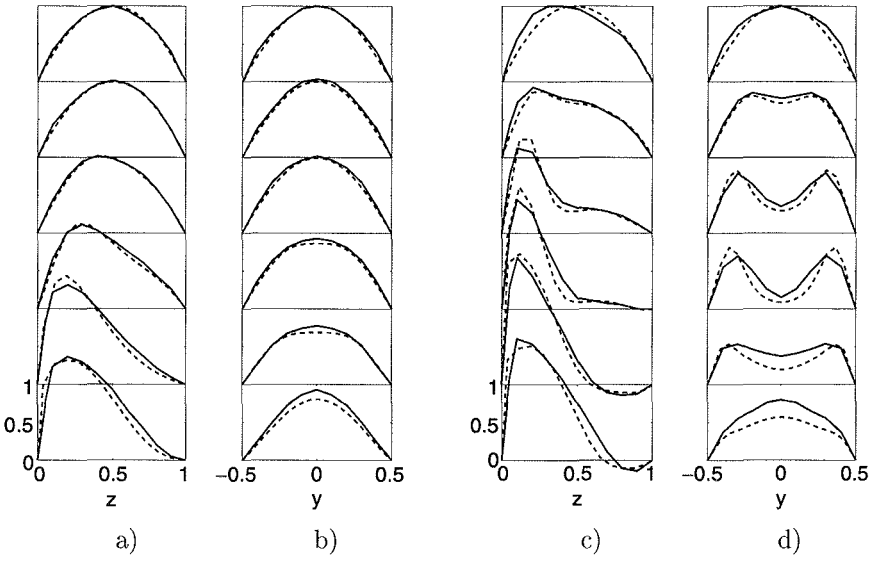

Figure 8: The axial velocity profiles for the present study (dashed line) and the those of Yung et al. (solid-line), in the bifurcation plane (BP) and the perpendicular plane (PP). In panel a) and b) the results are given for $Re = 100$ in the BP and the PP, respectively. The corresponding results for $Re = 500$ are shown in panel c) and d), respectively. The profiles are plotted in increasing consecutive order, i.e. S1-S6, starting at the bottom of the figure. The velocities are scaled by the maximum outlet velocity.

pendicular plane, whereas the other half is mirrored about the branching plane according to the *a priori* symmetry assumption. At station S1, the velocity profile in the BP is deflected at the inner wall due to the presence of the apex and the axial momentum of the fluid as it leaves the mother tube. Close to the outer wall, the velocity almost vanishes for $Re = 100$ after passing the sharp corner, whereas negative velocities (i.e. separation) occur in the case of $Re = 500$. At S5, approximately 7 diameters away from the apex, the flow appears to be fully developed for $Re = 100$. The results of the present study and those of Yung et al. agree well at all locations for $Re = 100$. The centrifugal forces induce a secondary flow which moves in a spiral from the inner corner to the outer edge along the upper wall and turns back along the center of the BP. With a strong centrifugal force, the velocity profile in both the BP and the PP will exhibit a trough in the middle. Such a trough appears for $Re = 500$ for both numerical approaches. However, for $Re = 500$ the discrepancies between the velocity profiles of the present study and that of Yung et al. are more pronounced. In conclusion, despite the differences in skewness between the two meshes, the simulations show qualitative agreement.

Summary of papers

This thesis consists of an introduction and five papers. Four of the papers are related to fetal hemodynamics and therefore grouped together (papers I-IV). The fifth paper relates to the hemodynamics in pulmonary veins.

paper I **Simulation of pressure drop and energy dissipation for blood flow in a human fetal bifurcation**
Based on physiological measurements, a 3D computational model of the umbilical vein and ductus venosus bifurcation for stationary flow conditions is established. The energy dissipation at the bifurcation inlet was estimated to constitute 24% to 31% of the pressure drop, depending on the Reynolds number and the curvature ratio.
J Biomech Eng 1998, **120**(4), 455–462.

paper II **Mechanical properties of the fetal ductus venosus and the umbilical vein**
The pressure-area relationship of the umbilical vein and the ductus venosus is studied in vitro. Each data set is fitted to an exponential function to determine the stiffness parameter and the area at a standard pressure.
Heart Vessels 1999, In press.

paper III **A mathematical model of umbilical venous pulsation**
A mathematical model is presented to identify the mechanical factors that influence pulsation in the umbilical vein. The umbilical vein is modeled as a compliant reservoir and the umbilical vein pressure is assumed to be equal to the stagnation pressure at the ductus venosus inlet.
Submitted for publication.

paper IV **Wave propagation in the human fetal ductus venosus-umbilical vein bifurcation**
The effect of ductus venosus tapering on the reflection coefficient is investigated with a mathematical model incorporating wave propagation. The results of this model are compared with those of paper III.
Submitted for publication

paper V **Mechanism of pulmonary venous pressure and flow waves**
A mathematical model of the pulmonary vein and the pulmonary bed is developed, where the pulmonary vein is modeled as a lossless transmission line and the pulmonary bed by a 3-element lumped parameter model. All pulsations are assumed to originate in the left atrium, the pressure in the pulmonary bed being constant.
Heart Vessels 1999, In press.

References

Anliker, M., Rockwell, R., Ogden, E., 1971. Nonlinear analysis of flow pulses and shock waves in arteries, part I: derivation and properties of mathematical model. Z ang Math Phys 22, 217–246.

Avolio, A., 1980. Multi-branched model of the human arterial system. Med Biol Eng Comput 18, 709–718.

Behrman, R. E., Lees, M. H., Peterson, E. N., de Lannoy, C. W., Seeds, A. E., 1970. Distribution of the circulation in the normal and asphyxiated fetal primate. Am J Obstet Gynecol 108, 956–9.

Bergel, D. H., 1972. The properties of blood vessels. In Fung, Y. C., Perrone, N., Anliker, M. (eds.), *Biomechanics : its foundations and objectives*. Prentice-Hall, Englewood Cliffs, NJ, 105–139.

Blanc, W., 1960. Premature closure of the ductus venosus. Am J Dis Child 100, 572.

Chako, A., Reynolds, S., 1953. Embryonic development in the human of the sphincter of the ductus venosus. Anat Rec 151, 151–173.

Chang, C., Atabek, H., 1961. The inlet length for oscillatory flow and its effects on the determination of the rate of flow in arteries. Phys Med Biol 6, 303–317.

Collins, M., Xu, X., 1990. A predictive scheme for flow in arterial bifurcations: comparison with laboratory measurements. In Mosora, F., Caro, C. G., Krause, E., Baquey, C., Pelissier, R. (eds.), *Biomechanical Transport Processes*. New York, 125–133.

Edelstone, D. I., Rudolph, A. M., 1979. Preferential streaming of ductus venosus blood to the brain and heart in fetal lambs. Am J Physiol 237, H724–H729.

Edelstone, D. I., Rudolph, A. M., Heymann, M. A., 1978. Liver and ductus venosus blood flows in fetal lambs in utero. Circ Res 42, 426–433.

Fluent, 1991. Fluent user's guide, version 4.0. Fluent Incorporated, 10 Cavendish Court Lebanon, NH 03766.

Fung, Y., 1984. Biodynamics. Circulation. Springer-Verlag New York Inc, New York.

Fung, Y., Fronek, K., Patitucci, P., 1979. Pseudoelasticity of arteries and the choice of its mathematical expression. Am J Physiol 237, H620–H631.

Gembruch, U., Krapp, M., Baumann, P., 1995. Changes of venous blood flow velocity

waveforms in fetuses with supraventricular tachycardia. Ultrasound Obstet Gynecol 5, 392–399.

omesh, 1994. GeoMesh^{TM}, User's guide. Fluent Incorporated, 10 Cavendish Court Lebanon, NH 03766.

dmundsson, S., Huhta, J. C., Wood, D. C., Tulzer, G., Cohen, A. W., Weiner, S., 1991. Venous doppler ultrasonography in the fetus with nonimmune hydrops. Am J Obstet Gynecol 164, 33–37.

nson, M. A., Kiserud, T., 1999. Circulation, Cambridge University Press, Cambridge, chap. Fetal development. in press.

saart, T., de Haan, J., 1986. Phasic blood flow patterns in the common umbilical vein of fetal sheep during umbilical cord occlusion and the influence of autonomic nervous system blockade. J Perinat Med 14, 19–26.

yashi, K., 1993. Experimental approaches on measuring the mechanical properties and constitutive laws of arterial walls. J Biomech Eng 115, 481–488.

cher, K., Campbell, S., Doyle, P., Harrington, K., Nicolaides, K., 1995a. Assessment of fetal compromise by Doppler ultrasound investigation of the fetal circulation. Circulation 91, 129–138.

cher, K., Ville, Y., Snijders, R., Nicolaides, K., 1995b. Doppler studies of the fetal circulation in twin-twin transfusion syndrome. Ultrasound Obstet Gynecol 5, 318–324.

lenstein, R., Niederer, P., Anliker, M., 1980. A viscoelastic model for use in predicting arterial pulse waves. J Biomech Eng 102, 318–25.

isman, T., Stewart, P., Wladimiroff, J., 1992. Ductus venosus blood flow velocity waveforms in the human fetus - a doppler study. Ultrasound Med Biomed 18, 33–37.

nes, C. J., Sugawara, M., Davies, R. H., Kondoh, Y., Uchida, K., Parker, K. H., 1994. Arterial wave intensity: physical meaning and physiological significance, Harwood Publishers, chap. 8. 129–148. Tokyo Symposium on Cardiovascular Mechanics, 1991. Recent progress in cardiovascular mechanics.

serud, T., Crowe, C., Hanson, M., 1998a. Ductus venosus agenesis prevents transmission of central venous pulsation to the umbilical vein in fetal sheep. Ultrasound Obstet Gynecol 11, 190–194.

serud, T., Eik-Nes, S. H., Blaas, H. G., Hellevik, L. R., 1991. Ultrasonographic velocimetry in the fetal ductus venosus. Lancet 388, 1412–1414.

serud, T., Eik-Nes, S. H., Blaas, H. G., Hellevik, L. R., Simensen, B., 1994a. Ductus venosus blood velocity and the umbilical circulation in the seriously growth retarded fetus. Ultrasound Obstet Gynecol 4, 109–114.

serud, T., Eik-Nes, S. H., Hellevik, L. R., Blaas, H. G., 1992. Ductus venosus — a longitudinal doppler velocimetric study of the human fetus. J Maternal Fetal Invest 2, 5–11.

serud, T., Eik-Nes, S. H., Hellevik, L. R., Blaas, H.-G., 1993. Ductus venosus blood

velocity changes in fetal cardiac diseases. J Matern Fetal Invest 3, 15–20.

Kiserud, T., Hellevik, L. R., Eik-Nes, S. H., Angelsen, B. A. J., Blaas, H. G., 1994b. Estimation of the pressure gradient across the fetal ductus venosus based on doppler velocimetry. Ultrasound Med Biomed 20, 225–232.

Kiserud, T., Rasmussen, S., Skulstad, S. M., 1998b. Distribution of umbilical blood through the ductus venosus. J Soc Gynecol Invest 5, 156–157.

Kücherer, H. F., Schiller, N. B., 1993. Cardiovascular imaging by ultrasound, Kluwer Academic Publishers, Netherlands, chap. What does pulmonary vein flow analysis add to the assessment of left ventricular hemodynamics? 23–36.

Langewouters, G., Wesseling, K., Goedhard, W., 1985a. The pressure dependent dynamic elasticity of 35 thoracic and 16 abdominal human aortas in vitro described by a five component model. J Biomech 18, 613–620.

Langewouters, G., Wesseling, K., Goedhard, W., 1985b. The static elastic properties of 45 human thoracic and 20 abdominal aortas in vitro and the parameters of a new model. J Biomech 17, 425–435.

Lassau, J. P., Bastian, D., 1983. Organogenesis of the venous structures of the human liver: a hemodynamic theory. Anat Clin 5, 97–102.

Liepsch, D., Moravec, S., Rastogi, A., Vlachos, N., 1982. Measurement and calculations of laminar flow in a ninety degree bifurcation. J Biomech 15, 473.

Lighthill, J., 1978. Waves in fluids, Cambridge University Press, Cambridge, chap. 2.

Lingman, G., Laurin, J., Maršál, K., 1986. Circulatory changes in fetuses with imminent asphyxia. Biol Neonate 49, 66–73.

Lonsdale, R., 1988. An algorithm for solving thermalhydraulic equations in complex geometries: the ASTEC code. UKAEA Report.

McDonald, D. A., 1973. Blood Flow in Arteries. The Camelot Press, Southampton, second edn.

Moore, K. L., Persaud, T. V. N., 1993. The Developing Human. Clinically Oriented Embryology. W.B. Saunders Company, Philadelphia.

Nakai, Y., Imanaka, M., Nishio, J., Ogita, S., 1995. Umbilical cord venous pulsation in normal fetuses and its incidence after 13 weeks of gestation. Ultrasound Med Biomed 21, 443–6.

Oepkes, D., Vandenbussche, F., Kanhai, H., 1993. Fetal ductus venosus blood flow velocities before and after transfusion in red-cell alloimmunized pregnancies. Obstet Gynecol 82, 237–241.

Parker, K., Jones, C., 1990. Forward and backward running waves in the arteries: analysis using the method of characteristics. J Biomech Eng 112, 322–326.

Parker, K., Jones, C., Dawson, J., Gibson, D., 1988. What stops the flow of blood from the heart? Heart Vessels 4, 241–5.

Patankar, S. V., 1980. Numerical heat transfer and fluid flow. Hemisphere Publishing

Corporation, Washington.

dley, T., 1980. The fluid mechanics of large blood vessels. Cambridge University Press, Oxford.

thoud, F., 1996. Analysis of wave reflections in the arterial system. Ph.D. thesis, École Polytechnique Fédérale de Lausanne.

thoud, F., Stergiopulos, N., Meister, J.-J., 1996. Separation of arterial pressure waves into their forward and backward running components. J Biomech Eng 118.

ines, J., Jaffrin, M., Shapiro, A., 1974. A computer simulation of arterial dynamics in the human leg. J Biomech 7, 77–91.

uss, M., Rudolph, A., Dae, M., 1983. Phasic blood flow patterns in the superior and inferior venae cavae and umbilical vein of fetal sheep. Am J Obstet Gynecol 145.

zzi, A. W., Inouye, M., 1973. Time split finite volume method for three-dimensional blunt-body flows. AIAA Journal 11, 1478–85.

zzo, G., Arduini, D., Romanini, C., 1992. Umbilical vein pulsations: a physiologic finding in early gestation. Am J Obstet Gynecol 167, 675–677.

idolph, A. M., 1985. Distribution and regulation of blood flow in the fetal and neonatal lamb. Circ Res 57, 811–821.

haaf, B. W., Abbrecht, P. H., 1972. Digital computer simulation of human systemic arterial pulse wave transmission: a nonlinear model. J Biomech 5, 345–64.

hiller, L., 1922. Die entwicklung der laminaren geschwindigkeitsverteilung und ihre bedeutung für zahigkeitsmessungen. Z Angew Math Mech 2, 96–106.

hlichting, H., 1934. Laminare kanaleinlaufströmung. ZAMM 14, 368–373.

hlichting, H., 1968. Boundary-Layer Theory. McGraw-Hill Book Company, New York, sixth edn.

gers, P., Stergiopulos, N., Verdonck, P., Verhoeven, R., 1997. Assessment of distributed arterial network models. Med Biol Eng Comput 35, 729–736.

ah, R., London, A., 1978. Laminar Flow Forced Convection in Ducts. Academic, New York.

alding, D. B., 1972. A novel finite differences formulation for differential expessions involving both first and second derivatives. Int J Num Meth Engng 4, 551–559.

ergiopulos, N., Young, D., Rogge, T., 1992. Computer simulation of arterial flow with applications to arterial and aortic stenoses. J Biomech 25, 1477–1488.

arg, S., 1951. Basic problems of the theory of laminar flows. In Russian, Moscow.

norburn, G. D., Harding, R. (eds.), 1994. Textbook of Fetal Physiology. Oxford Medical Publications. Oxford University Press, Oxford.

aishnav, R., Young, J., Patel, D., 1973. Distribution of stresses and strain-energy density through the wall thickness in a canine aortic segment. Circ Res 32, 577–583.

n Doormaal, J., Raithby, G., 1984. Enhancements of the simple method for predicting

incompressible fluid flow. Num Heat Transf 7, 147–163.

van Splunder, I., Stijnen, T., Wladimiroff, J., 1995. Fetal pressure-gradient estimations across the ductus venosus in early-pregnancy using doppler ultrasonography. Ultrasound Obstet Gynecol 6, 334–339.

van Splunder, I. P., Huisman, T. W. A., Stijnen, T., Wladimiroff, J. W., 1994. Presence of pulsations and reproducibility of waveform recording in the umbilical and left portal vein in normal pregnancies. Ultrasound Obstet Gynecol 4.

Westerhof, N., Bosman, F., De Vries, C., Noordergraaf, A., 1969. Analog studies of the human systemic arterial tree. J Biomech 2, 121–143.

Westerhof, N., Sipkema, P., Van den Bos, C., Elzinga, G., 1972. Forward and backward waves in the arterial system. Cardiovasc Res 6, 648–656a.

White, F. M., 1988. Fluid Mechanics, McGraw-Hill International Editions, New York, chap. 6.9. Mechanical Engineering Series. Second edn.

Womersley, J., 1957. An elastic tube theory of pulse transmission and oscillatory flow in mammalian arteries. Tech. Rep. WADC Technical Report TR 56-614, Wright Air Development Center, Wright Patterson Air Force Base, Ohio.

Young, D., Tsai, F., 1973. Flow characteristics in models of arterial stenoses-II. unsteady flow. J Biomech 6, 547–559.

Yung, C. N., De Witt, K. J., Keith, T. G., J., 1990. Three-dimensional steady flow through a bifurcation. J Biomech Eng 112, 189–97.

Zagzoule, M., Marc-Vergnes, J., 1986. A global mathematical model of the cerebral circulation in man. J Biomech 19, 1015–22.

Paper I

Simulation of Pressure Drop and Energy Dissipation for Blood Flow in a Human Fetal Bifurcation

Hellevik L.R.[1,3], Kiserud T.[2], Irgens F.[1],
Ytrehus T.[1], Eik-Nes S.H.[3]

[1]MTF/Div. Applied Mechanics, NTNU, Trondheim, Norway

[2]Dept. Obstetrics and Gynecology, Univ. Hosp. Bergen, Norway

[3]National Center for Fetal Medicine, Trondheim, Norway

Abstract

The pressure drop from the umbilical vein to the heart plays a vital part in human fetal circulation. The bulk of the pressure drop is believed to take place at the inlet of the ductus venosus, a short narrow branch of the umbilical vein. In this study a generalized Bernoulli formulation was deduced to estimate this pressure drop. The model contains an energy dissipation term and flow scaled velocities and pressures. The flow scaled variables are related to their corresponding spatial mean velocities and pressures by certain shape factors. Further, based on physiological measurements, we established a simplified, rigid-walled, 3D computational model of the umbilical vein and ductus venosus bifurcation for stationary flow conditions. Simulations were carried out for Reynolds numbers and umbilical vein curvature ratios in their respective physiological ranges. The shape factors in the Bernoulli formulation were then estimated for our computational models. They showed no significant Reynolds number or curvature ratio dependency. Further, the energy dissipation in our models was estimated to constitute 24% to 31% of the pressure drop, depending on the Reynolds number and the curvature ratio. The energy dissipation should therefore be taken into account in pressure drop estimates.

Published in *J Biomech Eng* 1998, **120**(4), 455–462.

Introduction

The advent of ultrasound techniques has opened a new era in fetal medicine by giving access to information about fetal hemodynamics non-invasively. Additional information may be deduced from measurements by means of physical/mathematical models, such as in cardiology where Doppler velocimetry is used to estimate pressure gradients by employing a simple Bernoulli formulation (Holen et al., 1976; Hatle et al., 1978).

Access to quantitative information has spurred the development of mathematical models aimed at describing functional relations, such as the circulation in the placenta (Guiot et al., 1992), and the resistance and velocity waveforms in the arterial system (Trudinger et al., 1985; Thompson and Stevens, 1989). However, the venous part of the fetal circulation still remains to be examined by means of mathematical models. Especially models that give quantitative information about the pressure drop from the umbilical vein (UV) to the left heart would be helpful to improve the physician's understanding of fetal cardiac function.

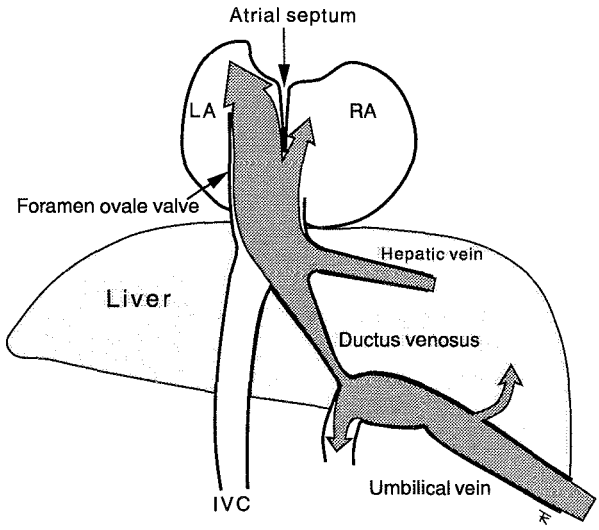

Figure 1: Oxygenated blood from the placenta may leave the umbilical vein and enter the ductus venosus. This blood is accelerated and directed towards the left atrium (LA) through the foramen ovale. RA denotes the right atrium and IVC the inferior vena cava.

The oxygenated placental blood that returns to the fetus through the UV enters the liver tissue or is shunted through the ductus venosus (DV), to reach the heart directly (Fig. 1). In animals, 50% of the oxygenated blood is directed through the DV, but the proportion increases to 70% during reduced oxygen content or reduced blood volume (Behrman et al., 1970; Edelstone and Rudolph, 1979; Edelstone et al., 1978). In the human fetus, a similar mechanism of preferential streaming (Fig. 1) is described from the UV through the DV and the foramen ovale (the atrial hole) towards the left atrium

Kiserud et al., 1991).

The high velocity in the DV, both in normal (Huisman et al., 1992; Kiserud et al., 992) and diseased (Oepkes et al., 1993) conditions, has been suggested to reflect a ajor portion of the pressure drop from the UV to the fetal heart. Attempts to lculate the UV-DV pressure drop by means of a simple Bernoulli equation have been ported (Kiserud et al., 1994; van Splunder et al., 1995). By employing such a method conjunction with measurements of the UV pressure, gained by needling, one may otain an estimate of the pressure in the fetal heart. However, until the methodological nitations are controlled, the formulation cannot reliably be used in clinical practice.

The study of blood flow in bifurcating vessels has been an important topic in biofluid echanics for several decades. Extensive monographs on the theoretical and experiental foundation of blood flow in arteries (McDonald, 1973; Pedley, 1980), have ovided a sound basis for the more recent numerical approaches (Power, 1995; Liepsh, 1994). As atherosclerosis is often found near bifurcations, much attention has een given, both numerically and experimentally, to understand the role of fluid dyamics in the development and progression of the disease (Lou and Yang, 1992; Xu nd Collins, 1990). The numerical models have evolved from 2D stationary, Newtoan, T-bifurcation models (Liepsch et al., 1982; Collins and Xu, 1990), via transient D-models for more realistic geometries, with both Newtonian (Perktold et al., 1991c) nd non-Newtonian (Perktold et al., 1991b) constitutive laws, to models incorporatg the fluid-structure interaction for blood and vessel wall in complex 3D-geometries adeghipour and Hajari, 1995; Perktold et al., 1994; Power, 1995).

The aim of the present study is twofold: a) to deduce a generalized Bernoulli rmulation applicable to pressure drop estimates in a general bifurcation, and b) to tablish a simple 3D computational model of the fetal UV-DV bifurcation and to vestigate the errors associated with the Bernoulli formulation for this model.

Method

Mathematical Formulation

a bifurcation, the energy dissipation varies from streamline to streamline and the ressure may vary as much over the tube cross-section as in the stream-wise direction 'edley, 1980, page 246). An ordinary Bernoulli approach, valid only for inviscid flow ong a streamline, might not suffice for estimating pressure drop in bifurcations. We ill therefore resort to an energy formulation and develop it in a form suitable for our udy.

The basic principles of conservation of mass and balance of linear momentum for compressible flow may be presented as:

$$\nabla \cdot \mathbf{v} = 0 \tag{1}$$

$$\rho \frac{\mathrm{D}\mathbf{v}}{\mathrm{D}t} = \mathrm{div}\mathbf{T} + \rho\mathbf{b} \tag{2}$$

here $\mathbf{v}$ denotes the fluid velocity, ρ the density, $\mathbf{T}$ the stress tensor, and $\mathbf{b}$ body

forces per unit mass. By multiplying (2) with the velocity vector, employing the Gauss theorem, using well known identities from tensor calculus, and integrating over a general control volume V we obtain the *mechanical energy equation*:

$$\int_V \rho \frac{\mathrm{D}\mathbf{v}}{\mathrm{Dt}} \cdot \mathbf{v} \, \mathrm{dV} = \int_V \mathrm{div}\,(\mathbf{v} \cdot \mathbf{T}) \, \mathrm{dV} - \int_V \mathbf{T} : \mathbf{D} \, \mathrm{dV} + \int_V \rho \mathbf{b} \cdot \mathbf{v} \, \mathrm{dV}$$

where the rate of strain tensor is denoted by $\mathbf{D}$. The stress tensor may be decomposed into isotropic and deviatoric parts $\mathbf{T} = -p\mathbf{I} + \mathbf{T}'$, which in conjunction with the incompressibility assumption implies: $\mathbf{T} : \mathbf{D} = \mathbf{T}' : \mathbf{D}$. Here p denotes the pressure. Further, we define *total rate of viscous energy dissipation* Δ, which is equal to the stress power in the case of incompressible flow, and the term Δ' as:

$$\Delta = \int_V \mathbf{T} : \mathbf{D} \, \mathrm{dV} = \int_V \mathbf{T}' : \mathbf{D} \, \mathrm{dV}, \qquad \Delta' = \int_{\partial V} \mathbf{v} \cdot \mathbf{T}' \cdot \mathbf{n} \, \mathrm{dA}$$

where ∂V denotes the surface of the control volume V and $\mathbf{n}$ the outward unit normal vector. Further, we introduce $\Delta_t = \Delta - \Delta'$ and $q^2 = \mathbf{v} \cdot \mathbf{v}$ for convenience. For stationary flow without body forces we then employ the Gauss theorem, the incompressibility assumption, a vector identity, and obtain:

$$\int_{\partial V} \rho \frac{q^2}{2} \, (\mathbf{v} \cdot \mathbf{n}) \, \mathrm{dA} = -\int_{\partial V} p \, \mathbf{v} \cdot \mathbf{n} \, \mathrm{dA} - \Delta_t \tag{3}$$

We let the control volume take the form of a general bifurcation as shown in Fig. 2, and let A_n denote the n-th cross section. Then, by introducing the following conventions:

$$\begin{aligned} w_n &= |\mathbf{v} \cdot \mathbf{n}|, & Q &= \int_{A1} \mathbf{v} \cdot \mathbf{n} \, \mathrm{dA} \\ \frac{1}{2}\hat{q_n^2} &= \frac{1}{Q} \int_{An} \frac{1}{2} q^2 w_n \, \mathrm{dA}, & \hat{p}_n &= \frac{1}{Q} \int_{An} p w_n \, \mathrm{dA} \end{aligned} \tag{4}$$

we get the relation between pressure, velocity and energy loss from (3) and (4):

$$\left(\hat{p}_1 + \frac{1}{2}\rho \hat{q_1^2}\right) - \left(\hat{p}_2 + \frac{1}{2}\rho \hat{q_2^2}\right) - \left(\hat{p}_3 + \frac{1}{2}\rho \hat{q_3^2}\right) = \frac{\Delta_t}{Q} \tag{5}$$

Further, we let p_t denote the total pressure:

$$p_t = p + \frac{1}{2}\rho q^2$$

Then, by following the same conventions as in (4) we obtain:

$$\hat{p}_{t1} - \hat{p}_{t2} - \hat{p}_{t3} = \frac{\Delta_t}{Q} \tag{6}$$

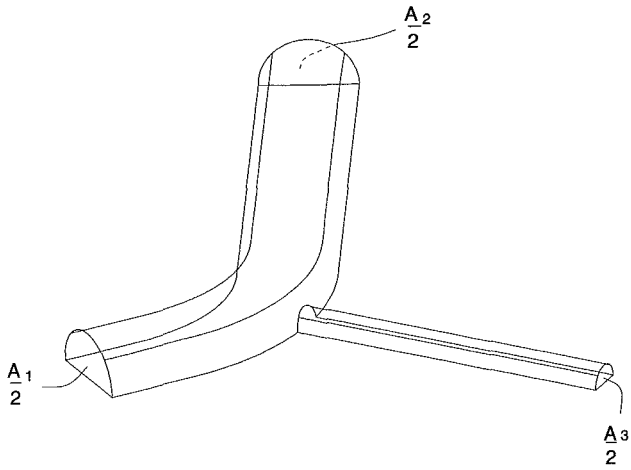

Figure 2: Upper half of the bifurcation control volume.

he term on the right hand side in (6) may be understood as the total loss of energy r the whole bifurcation. However, a further physical interpretation is not readily ailable as the inlet pressure is related to two outlet pressures. A clinically relevant pression should relate the main tube (MT) inlet pressure to the branch pressure only. e assume therefore that it is possible to divide the former control volume into two bcontrol volumes: V_2 and V_3, where the V_2 volume holds the fluid that finally will ach the MT outlet with flow rate Q_2, while V_3 is the branch counterpart with flow te Q_3. Further, we let A_{12} and A_{13} denote the sub-cross-sectional areas of V_2 and , respectively, at the MT inlet cross-section A_1. For these control volumes we then tain from (3) and (4):

$$\begin{aligned} \hat{p}_{t12} = \frac{1}{Q}\int_{A_{12}} p_t\, w_n \,\mathrm{dA} &= \hat{p}_{t2} + \frac{\Delta_{t12}}{Q} \\ \hat{p}_{t13} = \frac{1}{Q}\int_{A_{13}} p_t\, w_n \,\mathrm{dA} &= \hat{p}_{t3} + \frac{\Delta_{t13}}{Q} \end{aligned} \tag{7}$$

ere $\hat{p}_{t1i}$ represents the flow scaled total pressure at cross-section A_{1i} at the MT inlet, d Δ_{t1i} represents the dissipative terms for control volume V_i. These definitions imply e relation: $\hat{p}_{t1} = \hat{p}_{t12} + \hat{p}_{t13}$. Further, by substitution into (6) we also get the expected lation:

$$\Delta_t = \Delta_{t12} + \Delta_{t13}$$

Thus, the sum of the energy losses in the subcontrol volumes equals the total loss of mechanical energy in the whole bifurcation. If the pressure p_1 is constant and the velocity is a function of the radial coordinate only at the MT inlet, it can be shown that:

$$\hat{p}_{t13} = \frac{Q_3}{Q}\,\hat{p}_{t1}, \quad \hat{p}_{t12} = \frac{Q_2}{Q}\,\hat{p}_{t1} \tag{8}$$

From (7) and (8) a relation between the MT inlet pressure and the branch pressure is obtained:

$$\hat{p}_{t1} - \frac{Q}{Q_3}\,\hat{p}_{t3} = \frac{\Delta_{t13}}{Q_3} \tag{9}$$

By splitting the total pressures into pressure and kinetic energy terms we may formulate a generalized Bernoulli equation:

$$\hat{p}_1 + \frac{1}{2}\,\rho\,\hat{q_1^2} = \left(\hat{p}_3 + \frac{1}{2}\,\rho\,\hat{q_3^2}\right)\frac{Q}{Q_3} + \frac{\Delta_{t13}}{Q_3} \tag{10}$$

The inviscid form of this equation will be referred to as the simplified Bernoulli equation. Note that the terms involved are not physical quantities that can be obtained by pressure manometers or flowmeters. However, they may be related to their spatial mean counterparts, i.e. the spatial mean velocity v_m and the spatial mean pressure p_m in the following manner:

$$\hat{q^2} = \alpha\, v_m^2, \quad \hat{p} = \beta\, p_m \tag{11}$$

where α is velocity shape factor and β a shape factor for the pressure. A constant pressure yields $\beta = 1$, and a uniform velocity profile implies $\alpha = 1$, whereas a parabolic velocity profile corresponds to $\alpha = 2$.

By assuming a uniform pressure $p_1 = p_{m1}$, and a parabolic velocity profile at the MT inlet we get from (10) and (11):

$$p_1 - \beta\, p_{m3} = \frac{1}{2}\,\rho\alpha v_{m3}^2 - \rho v_{m1}^2 + \frac{\Delta_{t13}}{Q_3} \tag{12}$$

Geometry and reference bifurcation

A reference bifurcation for our computational models of the UV-DV bifurcation, was taken as a 3D T-bifurcation (Fig. 3). The diameters were taken as the mean values of the UV and the DV in human fetus at the 26-th week of gestation (Kiserud et al., 1994). Thus, as the UV is represented by the MT in the models, the MT diameter was taken as $D_{mt} = 4.3 \cdot 10^{-3}\ m$. The trumpet-shape of the DV (Chako and Reynolds, 1953; Blanc, 1960) was neglected and a constant diameter $D_b = 1.65 \cdot 10^{-3}\ m$ in the branch of our models was adopted. As curvatures will be imposed on the MT in the simulation section, the MT was segmented into four different regions. For a complete geometrical description, see Table 1 and Fig. 3.

Dimensionless parameter	Value
L_{u1}/D_{mt}	0.9
L_{u2}/D_{mt}	1.3
L_{d1}/D_{mt}	1.0
L_{d2}/D_{mt}	4.4
L_b/D_b	10.0

able 1: Geometrical parameters for the T-bifurcation. $D_{mt} = 4.3 \cdot 10^{-3}$ m and $D_b = 65 \cdot 10^{-3}$ m

urvature ratio

ne of the main geometrical features of the junction between the UV and the DV the human fetus, is the curvature of the UV. Thus, it is of importance to exploit d enhance the understanding of curvature impact on both the energy loss and the ape parameters. By introducing proper scales and orthogonal curvilinear toroidal ordinates for the governing mass and momentum equations (1) and (2), an important n-dimensional quantity is found for flow in curved tubes (Ward-Smith, 1980), namely e curvature ratio:

$$\delta = \frac{D}{2R} \tag{13}$$

here R is the radius of curvature, D the diameter of the tube.

To have an impression of the physiological range of the curvature ratio δ of the UV, neteen healthy pregnant women were recruited from the low risk antenatal clinic. he participants were non-smokers, had a normal obstetrical history and their present ngleton pregnancy was uneventful. The gestational age of the fetuses was assessed ultrasonography. The radius of curvature R of the UV, was estimated with a ir of compasses from 2D-ultrasonographic images. Subsequently the curvature ratio $= D_{mt}/2R$, was estimated by taking the umbilical vein diameter as $D_{mt} = 4.3{\cdot}10^{-3}m$, . the mean diameter at the 26th week of gestation.

omputational Method

e employed an finite volume method (FVM) using a commercially available package luent, 1991) running on an HP 9000/755 workstation to solve the governing mass and omentum equations. The SIMPLE algorithm (Patankar, 1980) was utilized for the essure-velocity coupling, and a second order upwind scheme was used to discretize the nvective terms. The walls were assumed to be rigid, and the flow regime was assumed be plane symmetric in order to reduce memory requirements and computational sts. Further, the fluid was assumed to be incompressible and Newtonian with density $= 1.05 \cdot 10^3$ kg/m^3 and dynamic viscosity $\mu = 4.2 \cdot 10^{-3}$ kg/ms.

The dynamic viscosity corresponded to human fetal whole blood at delivery (Joupla et al., 1986), and the density corresponded to human whole blood (Perktold et al., 91a; Fernandez et al., 1976). The imposed boundary conditions were intended to

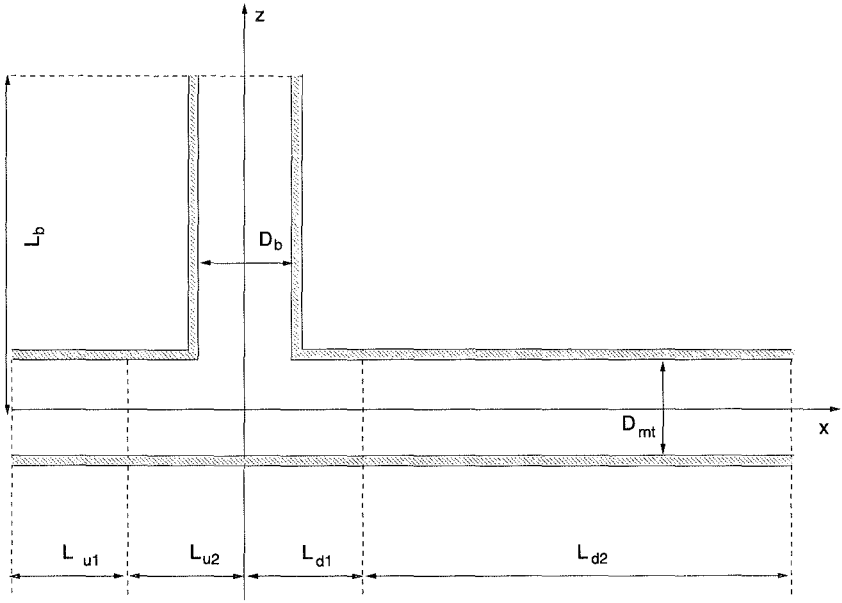

Figure 3: Sketch of the 3D T-bifurcation.

reflect the physiological values obtained by Doppler ultrasonography (Kiserud et al., 1994), where approximately 45% of the blood is directed into the branch. For the mean flow at 26 weeks of gestation, this corresponds to the following Reynolds numbers: $Re \approx 109$, $Re_o \approx 60$, $Re_b \approx 128$, for MT inlet/outlet and branch, respectively. The Reynolds numbers are based on the hydraulic diameters, a convention which will be followed throughout the paper.

To obtain a branch volume fraction of approximately 45%, with pressure boundary conditions at the MT and branch outlets for a given Reynolds number, we established the following procedure: At first a preliminary simulation was performed for the reference bifurcation; stationary parabolic velocity profiles were the boundary conditions at the MT boundaries, and a zero velocity gradient was the boundary condition at the branch outlet. Secondly, the pressure values at the MT and branch outlets from the preliminary simulations were taken as boundary conditions for the models with MT-curvature.

Results

Reference bifurcation

Preliminary simulations for various branch lengths were performed to ensure that the imposed boundary conditions at the branch outlet did not yield upstream effects on the

elocity profiles. The structured reference grid, which constituted $99 \times 15 \times 52$ control olumes, was constructed with decreasing control volumes towards the bifurcation for better resolution in the branch. Two additional grids were constructed for grid-dependency tests; a coarse grid ($50 \times 9 \times 30$) and a refined grid ($119 \times 22 \times 72$). As ressure drop and pressure distribution are some of the main features of interest in this aper, we focused on the mean pressure distribution in the MT in our grid tests. The ean spatial pressure in each MT cross-section is plotted versus the normalized MT ngth in Fig. 4. It is seen that the coarse grid overpredicts the sudden pressure drop the bifurcation, whereas the overall pressure drop is well represented. The reference id solution follows the refined grid solution rather well at all locations.

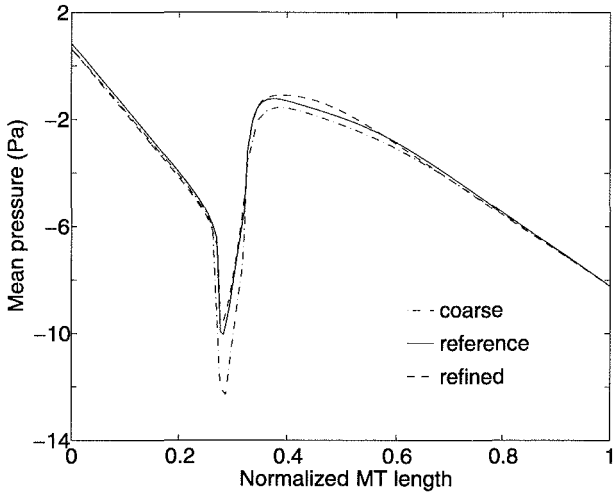

igure 4: Spatial mean pressure in the MT versus normalized MT length. Coarse grid lash-dot), reference grid (solid line), refined grid (dashed).

hysiological curvature ratios

he mean gestational age of the fetuses was 30 weeks (range 19-39), and the mean ysiological curvature ratio $\delta_m = 0.19$ (range 0.12-0.35).

imulations

ine different grids with varying MT curvature were constructed, each with a constant dius of curvature R, starting at L_{u1}/D_{mt} MT diameters and ending at $(L_{u1} + L_{u2} + L_{u3})/D_{mt}$ diameters, see Table 1 and Fig. 3.

All grids had resolutions equal to the reference T-bifurcation. The curvature ratios ere held approximately in the physiological range, ranging from $\delta = 0.15$ to $\delta = 0.35$.

For all these geometrical configurations the axial center line lengths ($L_{u1} + L_{u2} + L_{d1} + L_{d2}$) of the MT were kept constant. A typical grid is depicted in Fig. 5.

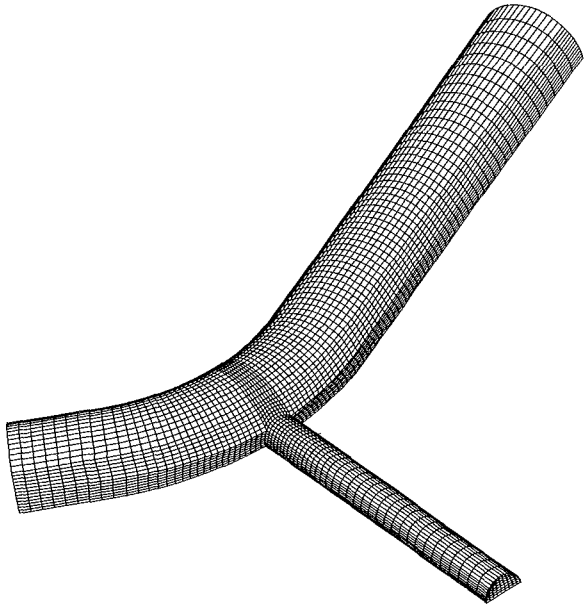

Figure 5: A typical grid configuration for a bifurcation with MT curvature.

Simulations were carried out for two inlet Reynolds numbers per configuration, corresponding to the mean and maximum umbilical venous flow at the 26th week of gestation: $Re \approx 109$ ($Q \approx 88$ ml/min) and $Re \approx 163$ ($Q \approx 132$ ml/min).

Filled, interpolated pressure contours in the symmetry-plane for a representative curvature ratio are shown in Fig. 6. A pronounced pressure drop at the bifurcation inlet is clearly seen, and immediately after the inlet at the MT wall facing the bifurcation, the pressure builds up again to oppose the centrifugal forces due to the change in direction of the fluid.

In Figs. 7 and 8, the cross-sectional mean pressure and the center-line pressure in the MT are plotted versus the normalized MT length for the various curvature ratios, and for Reynolds numbers $Re \approx 163$ and $Re \approx 109$, respectively. The imposed boundary conditions imply that the pressure at the MT outlet remains constant for all configurations, and that the overall pressure drop is changed by variations in the inlet pressure. The graphs show monotonous curvature ratio dependence in the pressure, i.e. the higher curvature ratio the higher pressure drop is required to force the fluid through the bifurcation. The relative difference in the mean pressure drop at $\delta = 0.15$ and $\delta = 0.35$ is approximately 35% for $Re \approx 163$. For $Re \approx 109$ the relative difference is approximately 26%. For brevity these results are not depicted here. A prominent feature of the mean pressure distribution is the sudden pressure drop and recovery

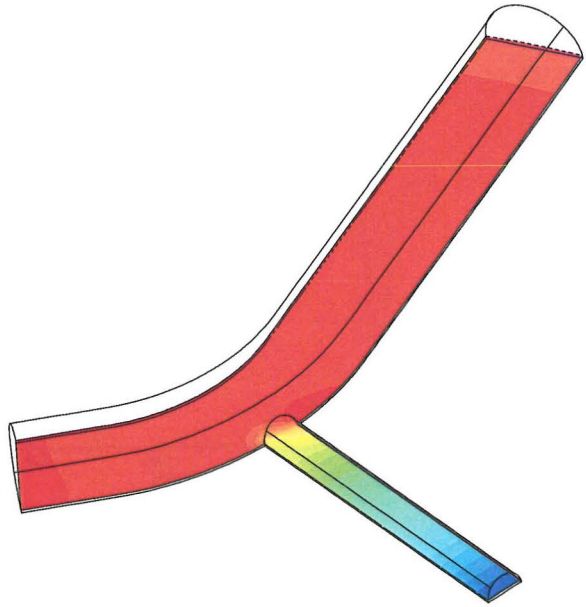

Figure 6: The pressure distribution in symmetry-plane for a representative curvature ratio. Flow from left to right.

t the MT-branch junction. For convenience we denote this feature as a pressure ssure. The qualitative difference in the pressure fissures for the mean pressures and he center line pressures is caused by the large cross-sectional variation in pressure, ttributed to the centrifugal forces (Fig. 6). However, distal to the branch inlet these ifferences vanish , thus the center line pressure and the spatial mean pressure may be sed interchangeably.

The cross-sectional mean pressure in the branch is plotted versus the normalized ranch length in Fig. 9, starting at the MT wall furthermost from the branch inlet. egardless of the curvature ratio, the pressure is rather constant in the MT, and then hows a rapid drop at the branch inlet, after which it merges to a linear Poiseuille ehavior. The pressure drop at the branch inlet of approximately 200 Pa (1.5 mmHg) iffers from the MT pressure drop by an order of magnitude (Figs. 7 and 9), whereas he changes caused by the variation in curvature are of the same order of magnitude s the corresponding changes in the MT.

Further, the volume fraction at the MT outlet was calculated (Fig. 10). A monotonous ependency of curvature may be observed. However, the relative variation in volume raction is less than 2% for both Reynolds numbers.

The energy dissipation from the MT to the branch inlet was also computed. The nlet station was located at $0.7D_{mt}$ upstream from the bifurcation center in the MT, here the pressure drop starts to deviate from the linear Poiseuille drop. This corresponds

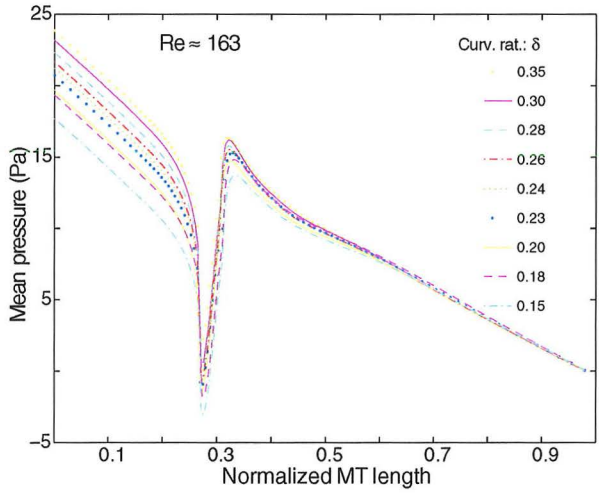

Figure 7: Mean pressure in MT for $Re \approx 163$.

to a normalized MT length of 0.2 (Fig. 7).

Further, a station in the branch at $1.6D_b$ from the bifurcation center, close to the branch inlet at $1.3D_b$, was chosen as the outlet station in the branch. At this station the rapid pressure drop is over and a linear Poiseuille pressure drop has been established (Fig. 9). The lengths $1.6D_b$ and $1.3D_b$ corresponds to normalized branch lengths of 0.26 and 0.23, respectively. We define *the energy dissipation factor* λ as the the ratio of the energy dissipation to the flow scaled pressure drop ratio, i.e. :

$$\lambda = \frac{\Delta_{t13}}{Q_3} / (\hat{p_1} - \frac{Q}{Q_3}\hat{p_3})$$

This factor expresses the relative error obtained by using the simplified Bernoulli equation to estimate the flow scaled pressure drop. From Fig. 11 we see that λ, ranges from 24% to 31% for all simulation configurations. A weak impact of both Reynolds numbers and curvature ratio is observed. For the lower Reynolds number $Re \approx 109$, the energy dissipation is approximately 5% higher than for $Re \approx 163$, regardless of curvature ratio. This is reasonable as viscous effects are expected to be more prominent at low Reynolds numbers.

The λ-factor decreases slightly as δ increases. If we take into account that the flow distribution is almost unaffected by changes in δ, the decrease in λ may be ascribed to a decrease in $\hat{p_1} - \hat{p_3}$, i.e. a slight reduction in the resistance from the MT to the branch inlet as δ increases.

The computed shape factors α and β are plotted in Figs. 12 and 13. From the scale of the ordinate we see that regardless of the Reynolds number, the correlation between the α-factor the curvature ratio is only marginal. The α-factor may thus be

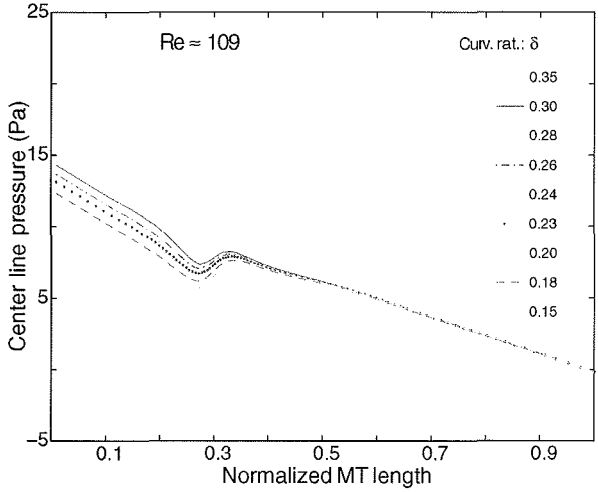

Figure 8: Center line pressure in MT for $Re \approx 109$.

aken as a constant, given by the mean value $\alpha_m = 1.5$. The apparent non-monotonous -dependency of the curvature ratio may, also due to the small scale, most probably e ascribed to numerical errors. The β-variation in the Reynolds number is also only aarginal, and we may take it as its constant mean value $\beta_m = 0.94$

Conclusions and discussion

n this study we deduced a generalized Bernoulli formulation applicable for pressure rop estimates in a general bifurcation.

In the results from the computational model of the fetal UV/DV-bifurcation, the ressure profiles (Figs. 7 and 8) show significant curvature ratio impact on the overall IT pressure drop. But as the pressure drop in the branch differs from the MT pressure rop by an order of magnitude (Fig. 9), the curvature ratio impact on the branch ressure drop is only modest. Note also that this overall pressure drop is in the rder of 20 Pa, corresponding to 0.15 mmHg, and therefore would not be measurable. lowever, pressure fissures similar to the ones in the present study have been reported n experimental investigations for arterial branch models. These measurements were onducted for flow regimes with higher Reynolds numbers than in the present study for oth steady (Cho et al., 1985) and unsteady (Back et al., 1986) flow. In these works ne pressure rise was attributed to inertial effects associated with momentum losses in ne MT due to the flow through the branch. Further, Back et al. (1986) also measured me averaged pressure drops for the branch pulsatile flow at a lower time averaged eynolds number ($Re_{osc} \approx 115$).

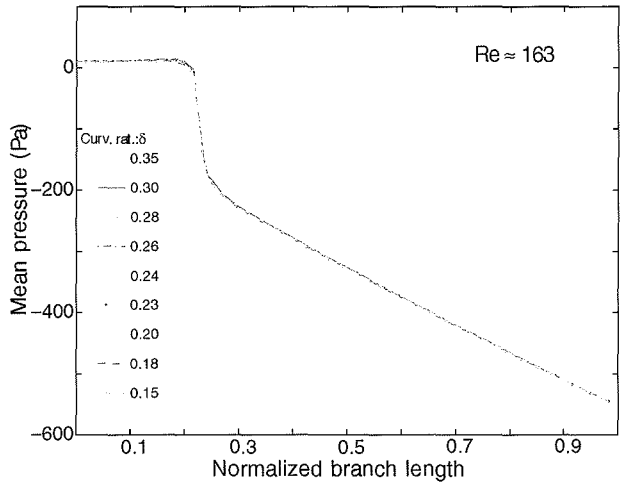

Figure 9: Mean branch pressure for $Re \approx 163$.

The relative variation in volume fraction at the MT outlet is less than 2%; hence the importance of the curvature ratio as a volume distributor is minor for our models.

Further, the simulation results indicate that the shape factors α and β should be included for pressure drop estimates in bifurcations. For the geometries in our simulations, they may be taken as $\alpha = 1.5$ and $\beta = 0.94$, i.e. independent of Reynolds number and curvature ratio. Further, the dissipation appeared to constitute about 30% of the pressure drop from the MT to the branch inlet and to have a modest Reynolds number and curvature ratio dependency. We therefore conclude that the energy dissipation also should be taken into account in pressure drop estimates for bifurcation geometries similar to the ones in this study.

In our simulations we have assumed the blood to be Newtonian, even though it is known that it has viscoplastic rheological properties. However, significant non-Newtonian effects appear only at low shear rates (Chang and Tarbell, 1988). Numerical studies of arterial bifurcations with the Casson model show that the effect of non-Newtonian rheology on the fluid dynamics is not dramatic (Lou and Yang, 1993; Perktold et al., 1991b). It is therefore assumed that the inclusion of non-Newtonian rheological models would not change the results significantly.

Further, we have also made a rigid wall assumption. Numerical comparisons have been made between rigid wall and compliant wall solutions for the carotid artery bifurcation (Reuderink, 1991; Perktold et al., 1994). The compliant models show that the velocity-magnitudes and wall shear stresses are significantly reduced in the reversed flow area. Reduced wall shear stress is associated with a parabolic-like velocity profile, and thus a possible consequence in our simulations might be that the velocity profile at the branch inlet would be more parabolic, i.e. α closer to 2.

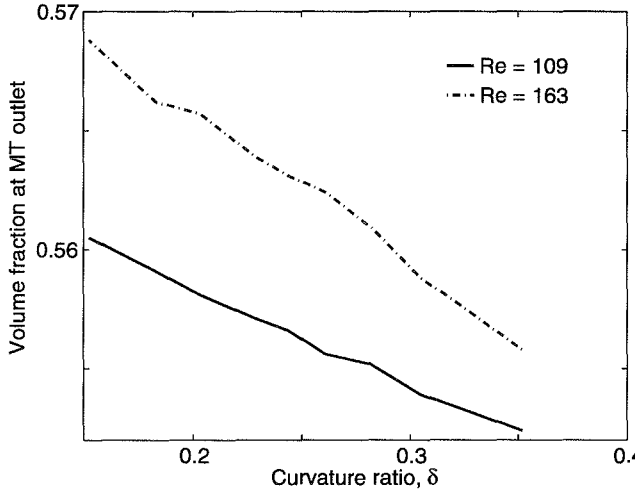

Figure 10: Volume fraction at MT outlet versus curvature ratio δ.

The pressures in the fetal heart oscillates during the heart cycle, and this yields a ılsatile flow in the DV. The normal DV velocity pattern is triphasic; A peak during ɛntricular systole, a second peak during early ventricular diastole and a nadir during ɾrial contraction. The velocity waveform ranges from 0.4-0.85 m/s during the last half normal pregnancies (Huisman et al., 1992; Kiserud et al., 1992) and is altered during tal diseases with an increased pulsatility (Kiserud et al., 1993). In our simulations ıe velocities are taken as steady, and in general velocity profiles for steady flow are ore or less parabolic, whereas in a pulsatile flow the profile tends to a flat one for high omersley numbers. Numerical simulations for the aortic bifurcation have shown that r steady flow with an average Re, the shear stresses are less than 10% of those for an ısteady flow. Even with peak Re, the steady solution still underestimates the shear resses in most places (Lou and Yang, 1991). However, physiological measurements ow that the UV-flow is steady; this indicates that the pressure-pulse propagating ɔstream in the DV is subject to significant reflection and/or damping in the UV. hus, the UV-DV flow regime may be of a less pulsatile character than the flow at e aortic bifurcation. Still, our steady simulations might be insufficient, therefore ılsatile simulations should be performed in the future.

As stated previously, the DV has a more trumpet-like shape, i.e. a narrow inlet ction with a wider outlet section, whereas in our simulations it has been given a nstant diameter for simplicity. Thus in a more physiological model the branch will ve a narrower inlet section. This will probably affect the velocity profile and we erefore assume that the numerical values of the shape factors and the dissipation ould be modified for a more physiological relevant model.

Further, it should be noted that we have only estimated the pressure drop from

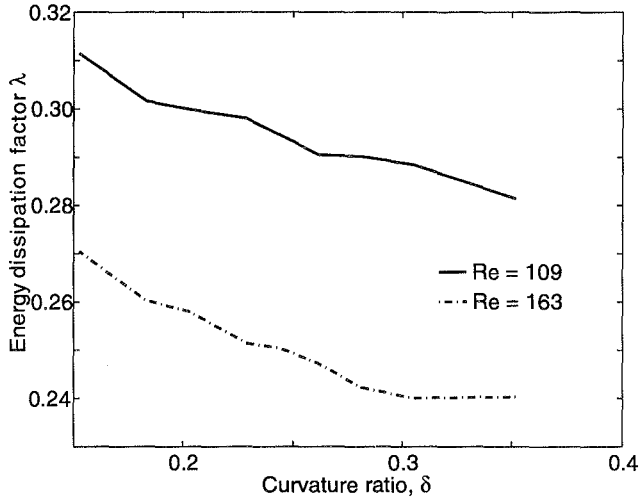

Figure 11: The energy dissipation factor λ versus curvature ratio δ.

the MT to the branch inlet. Thus, the effects of pressure recovery due to the change of cross-section and the pressure drop due to viscous forces in the branch are not addressed in the present study. To obtain an estimate of these effects we make the following assumptions for the DV: local Poiseuille flow, a linearly diverging branch with an expansion factor of 2, the DV inlet diameter is $D_b = 1.65^{-3}m$, and the DV length as $8.4D_b$ (the length from just downstream of the branch junction $1.6D_b$, to the outlet at $10D_b$). Then for $Re \approx 163$ a rough estimate of the viscous and cross-sectional effects may be obtained by application of the mean flow momentum equation along the branch axis, yielding a pressure recovery estimate of approximately 0.4 mmHg. However, these estimates are sensitive to the branch inlet diameter and to the expansion factor. Furthermore, the assumption of Poiseuille flow is inaccurate. Therefore we suggest that a parametric study should be performed in the future.

From the discussion above, it is clear that the estimates of the shape-factors and the energy-dissipation should be taken as indicative only. However, we would maintain that the suggested mathematical formulation (12) for pressure drop estimates could be useful. Thus, to improve the estimates of the shape-factors and the energy dissipation, computational models that better mimic the physiological reality should be established.

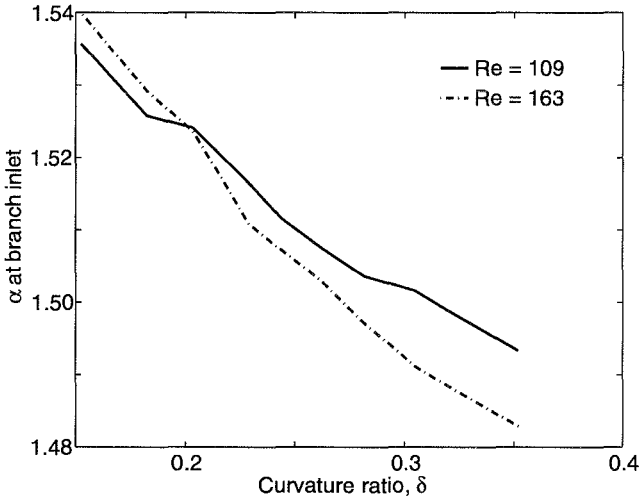

Figure 12: The shape factor α versus curvature ratio δ.

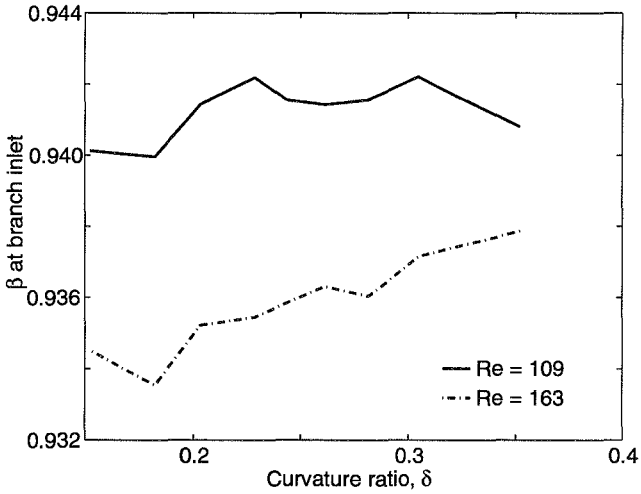

Figure 13: The shape factor β versus curvature ratio δ.

Acknowledgments

The English text was revised by Mrs. Nancy Lea Eik-Nes. The authors would also like to thank Reidar Kristoffersen, Stein Inge Rabben, Knut V. Høyland, Gaute Stokkan and Sevald Berg for reading through the manuscript.

References

Back, L., Cho, Y., Crawford, D., 1986. Phasic and spatial pressure measurements in a femoral artery branch model for pulsatile flow. J Biomech Eng 108, 251–258.

Behrman, R. E., Lees, M. H., Peterson, E. N., de Lannoy, C. W., Seeds, A. E., 1970. Distribution of the circulation in the normal and asphyxiated fetal primate. Am J Obstet Gynecol 108, 956–9.

Blanc, W., 1960. Premature closure of the ductus venosus. Am J Dis Child 100, 572.

Chako, A., Reynolds, S., 1953. Embryonic development in the human of the sphincter of the ductus venosus. Anat Rec 151, 151–173.

Chang, L., Tarbell, J., 1988. A numerical study of flow in curved tubes simulating coronary arteries. J Biomech 27, 927.

Cho, Y., Back, L., Crawford, D., 1985. Experimental investigation of branch flow ratio, angle and Reynolds number effects of the pressure and flow fields in arterial branch models. J Biomech Eng 107, 257–267.

Collins, M., Xu, X., 1990. A predictive scheme for flow in arterial bifurcations: comparison with laboratory measurements. In Mosora, F., Caro, C. G., Krause, E., Baquey, C., Pelissier, R. (eds.), *Biomechanical Transport Processes*. New York, 125–133.

Edelstone, D. I., Rudolph, A. M., 1979. Preferential streaming of ductus venosus blood to the brain and heart in fetal lambs. Am J Physiol 237, H724–H729.

Edelstone, D. I., Rudolph, A. M., Heymann, M. A., 1978. Liver and ductus venosus blood flows in fetal lambs in utero. Circ Res 42, 426–433.

Fernandez, R., De Witt, K., Botwin, M., 1976. Pulsatile flow through a bifurcation with applications to arterial disease. J Biomech 9, 575.

Fluent, 1991. Fluent user's guide, version 4.0. Fluent Incorporated, 10 Cavendish Court Lebanon, NH 03766.

Guiot, C., Pianta, P. G., Todros, T., 1992. Modelling the feto-placental circulation: I. A distributed network predicting umbilical haemodynamics throughout pregnancy. Ultrasound Med Biomed 18, 535–44.

Hatle, L., Brubakk, A., Tromsdal, A., Angelsen, B., 1978. Non-invasive assessment of pressure drop in mitral stenosis by doppler ultrasound. Br Heart J 40, 131–140.

Holen, J., Aaslid, R., Landmark, K., Simonsen, S., 1976. Determination of pressure

gradient in mitral stenosis with a non-invasive ultrasound doppler technique. Acta Med Scand 199, 455–460.

uisman, T., Stewart, P., Wladimiroff, J., 1992. Ductus venosus blood flow velocity waveforms in the human fetus - a doppler study. Ultrasound Med Biomed 18, 33–37.

ɔuppila, P., Kirkinen, P., Puukka, R., 1986. Correlation between umbilical vein blood flow and umbilical blood viscosity in normal and complicated pregnancies. Arch Gynecol 237, 191–197.

iserud, T., Eik-Nes, S. H., Blaas, H. G., Hellevik, L. R., 1991. Ultrasonographic velocimetry in the fetal ductus venosus. Lancet 388, 1412–1414.

iserud, T., Eik-Nes, S. H., Hellevik, L. R., Blaas, H. G., 1992. Ductus venosus — a longitudinal doppler velocimetric study of the human fetus. J Maternal Fetal Invest 2, 5–11.

iserud, T., Eik-Nes, S. H., Hellevik, L. R., Blaas, H. G., 1993. Ductus venosus blood velocity changes in fetal cardiac diseases. J Maternal Invest 3, 15–20.

iserud, T., Hellevik, L. R., Eik-Nes, S. H., Angelsen, B. A. J., Blaas, H. G., 1994. Estimation of the pressure gradient across the fetal ductus venosus based on doppler velocimetry. Ultrasound Med Biomed 20, 225–232.

epsch, D. (ed.), 1994. Biofluid Mechanics. Proceedings of the 3rd International Symposium. VDI verlag.

epsch, D., Moravec, S., Rastogi, A., Vlachos, N., 1982. Measurement and calculations of laminar flow in a ninety degree bifurcation. J Biomech 15, 473.

ɔu, Z., Yang, W., 1991. A computer simulation of the blood flow at the aortic bifurcation. Bio Med Mater Eng 173.

ɔu, Z., Yang, W., 1992. Biofluid dynamics at arterial bifurcations. Crit Rev Biomed Eng 19, 455–493.

ɔu, Z., Yang, W., 1993. A computer simulation of the non-Newtonian blood flow at the aortic bifurcation. J Biomech 173.

cDonald, D. A., 1973. Blood Flow in Arteries. The Camelot Press, Southampton, second edn.

ɐpkes, D., Vandenbussche, F., Kanhai, H., 1993. Fetal ductus venosus blood flow velocities before and after transfusion in red-cell alloimmunized pregnancies. Obstet Gynecol 82, 237–241.

ɪtankar, S. V., 1980. Numerical heat transfer and fluid flow. Hemisphere Publishing Corporation, Washington.

ɛdley, T., 1980. The fluid mechanics of large blood vessels. Cambridge University Press, Oxford.

ɛrktold, K., Nerem, R., Peter, R., 1991a. A numerical calculation of flow in a curved tube model of the left main coronary artery. J Biomech 24, 175–189.

Perktold, K., Peter, R., Resch, M., Langs, G., 1991b. Pulsatile non-Newtonian blood flow in three-dimensional carotid bifurcation models: a numerical study of flow phenomena under different bifurcation angles. J Biomed Eng 13, 507–515.

Perktold, K., Resch, M., Peter, R., 1991c. Three-dimensional numerical analysis of pulsatile flow and all shear stress in the carotid artery bifurcation. J Biomech 24, 409–420.

Perktold, K., Thurner, E., Kenner, T., 1994. Flow and stress characteristics in rigid walled and compliant carotid artery bifurcation models. Med Biol Eng Comp 32, 19–26.

Power, H. (ed.), 1995. Bio-fluid Mechanics. Computational Mechanics Publications, Southampton.

Reuderink, P., 1991. Analysis of the flow in a 3d distensible model of the carotid artery bifurcation. Ph.D. thesis, The Eindhoven Institute of Technology, The Netherlands.

Sadeghipour, M., Hajari, B., 1995. Pulsatile blood flow in deformable vessels - non-Newtonian behavior. In *Proceedings of the 1995 Bioengineering Conference.* ASME, Bioeng Div, Beever Creek, CO, USA, vol. 29, 345–346.

Thompson, R., Stevens, R., 1989. Mathematical model for interpretation of doppler velocity waveform indices. Med Biol Eng Comput 27, 269–276.

Trudinger, B., Giles, W., Cook, C., Bomardieri, J., Collins, L., 1985. Fetal umbilical artery flow velocity waveform and placental resistance: clinical significance. Br J Obstet Gynaecol 92, 23–30.

van Splunder, I., Stijnen, T., Wladimiroff, J., 1995. Fetal pressure-gradient estimations across the ductus venosus in early-pregnancy using doppler ultrasonography. Ultrasound Obstet Gynecol 6, 334–339.

Ward-Smith, A., 1980. Internal fluid flow. The fluid dynamics of flow in pipes and ducts. Clarendon press, Oxford.

Xu, X., Collins, M., 1990. A review of the numerical analysis of blood flow in arterial bifurcations. J Eng Med 204, 205–216.

Paper II

Mechanical properties of the fetal ductus venosus and umbilical vein

Hellevik L.R.[1], Kiserud T.[2], Irgens F.[1],
Stergiopulos N.[3], Hanson M.[2].

[1]MTF/Div. Applied Mechanics, NTNU, Trondheim, Norway
[2]Dept. Obstetrics and Gynaecology, Univ. College, London, UK
[3]Biomedical Engineering Laboratory, EPFL, Lausanne, Switzerland

Abstract

During fetal circulatory compromise, velocity pulsations in the precordial veins increase and are commonly transmitted through the ductus venosus into the umbilical vein, indicating a serious prognosis. The nature of the pulsations and their transmission into the periphery, specifically the umbilical vein, is poorly understood. We present information on the mechanical properties of fetal veins as a basis for describing the pulse wave propagation. Five fetal sheep livers with connecting veins (gestational age 0.8–0.9) were studied in vitro. The transmural pressure, obtained with a fluid-filled catheter, was reduced stepwise from 10.3 to 0 mmHg, and the diameter determined by ultrasonography. Each data set was fitted to an exponential function to determine the stiffness parameter and the area at a standard pressure, which we proposed to be 5 mmHg for the fetal venous circulation. The stiffness parameter was 6.2 ± 1.8 at the ductus venosus outlet, 3.4 ± 1.3 at the ductus venosus inlet, and 4.0 ± 1.0 in the umbilical vein. Correspondingly, values for compliance and pulse wave velocity for the three venous sections were established for a physiological pressure range. The estimated pulse wave velocity of 1–3 m/s is comparable with values estimated for veins in adults. The mechanical properties of fetal veins are comparable with those described for veins later in life. The stiffness parameter represents the elastic properties at all pressure levels and conveniently permits inference of compliance and pulse wave velocity.

To appear in *Heart and Vessels* 1999

Introduction

In 1979 Gill (Gill, 1979) described the fetal umbilical vein (UV) dimension and velocity in utero by applying combined ultrasound imaging and Doppler velocimetry. The umbilical vein is a sizeable vessel in the fetus and was accessible with the equipment available at the time. In addition, Doppler velocity waveforms for fetal arteries were the focus of interest at that time. Later studies focused on the pulsating flow in the precordial veins which was found to be a useful method to evaluate fetal cardiac function (Reed et al., 1990; Kanzaki and Chiba, 1990; Wladimiroff et al., 1991; Respondek et al., 1996). Another vein, the ductus venosus (DV) was shown to play a key role in shunting oxygenated umbilical blood in the human fetus (Kiserud et al., 1991; Huisman et al., 1992). During congestive heart disease or abnormal atrial contractions, augmented pulsation of the precordial veins is increasingly transmitted to peripheral sections of the veins as the fetus deteriorates, and may reach the umbilical vein mainly through the ductus venosus (Lingman et al., 1986; Kiserud et al., 1993, 1994, 1998). Such pulsatile changes in the umbilical vein are regarded as a sign of poor prognosis (Gudmundsson et al., 1991; Nakai et al., 1994). In the fetal sheep, injection of saline expands the venous system, increases the venous pressure, reduces the transmission time for wave travel and leads to umbilical venous velocity pulsations (Reed et al., 1996, 1997). However, the occurrence and pattern of pulsations show individual variations and the way they are transmitted is not well understood.

Mathematical models of the UV/DV junction have been applied to describe the hemodynamic characteristics more precisely. In a computational model with steady flow and rigid walls, the velocity profile was found to be partially blunted and skewed (Pennati et al., 1996). Energy dissipation up to 30% of the UV DV-inlet pressure drop has been reported (Hellevik et al., 1998). The mechanical properties of fetal veins are not known, and computations with elastic walls and pulsatile flow have so far not been attempted. Once information on the mechanical properties of the UV and DV is available, the wave propagation can be addressed in a mathematical model, and a more meaningful interpretation of various clinical findings can be expected.

Thus, the aim of the present study was to estimate the mechanical properties, i.e., the stiffness parameter, the compliance, and the pulse wave velocity, of the intra-abdominal UV, the DV inlet, and the DV outlet in the fetal sheep.

Methods

Experimental methods

All procedures were conducted in accordance with UK Home Office regulations and the Guidance for the Operation of Animals (Science Procedures) Act (1986). Immediately after sacrifice of five mule cross ewes of median gestational age of 130 days (range 124–138), term being 147 days, the fetal lambs were delivered through a uterotomy. The intra-abdominal UV was catheterized and flushed with heparin-saline solution (10 IU/ml saline). The inferior vena cava was divided below the atria and at the level of

ıe renal veins, the portal vein was ligated close to the pancreas, and the liver excised om the posterior abdominal wall and the peripheral parts of the diaphragm. A tube ore 4 mm) connected the UV to the input reservoir which was filled with saline. Care as taken to avoid introduction of air into the system. The preparation was rinsed ith saline until all portions of the liver tissue were equally pale and no more blood uld be detected at the outflow from the inferior vena cava. The inferior vena cava was ıen ligated at both ends. The preparation was submersed to a depth of 11–14 cm in line at 37°C (Fig. 1) to achieve similar pressure and temperature to the intrauterine nditions but with the influence of flow, neural activity, and endogenous vasoactive gents eliminated or kept at a low activity.

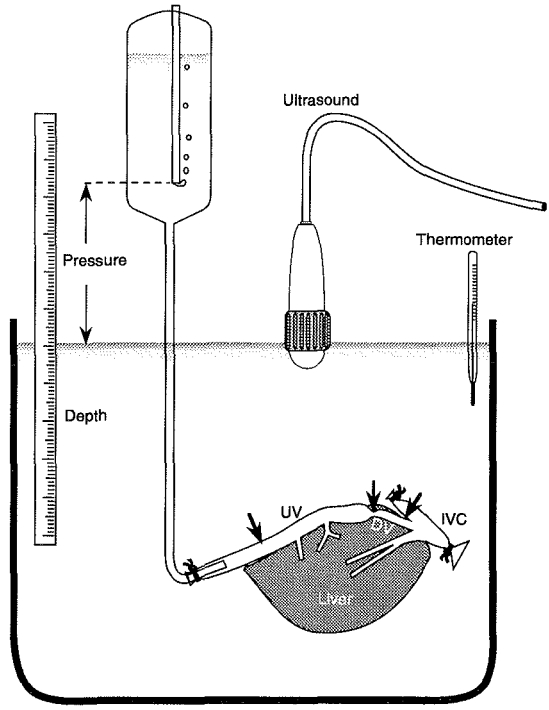

gure 1: Experimental setup. The liver of the fetal sheep was submersed in saline. The ferior vena cava (IVC) and the portal vein were ligated, and the umbilical vein (UV) was nnected to a pressure regulated input tube. The preparation was placed with the UV and e ductus venosus facing upwards to facilitate the ultrasound measurements. The sites of easurement are marked with arrows.

The saline level in the basin was kept constant by means of an overflow. The ansmural pressure in the UV and the DV was determined from the distance between

the meniscus in the air inflow tube in the input reservoir and that of the basin (Fig. 1). The pressure was changed by varying the level in the input reservoir. The venous system was filled up to a pressure of maximum 10.3 mmHg and measurements of the dimensions were then done at stepwise reductions in pressure.

The vessel diameters were measured with a Vingmed CFM 800 ultrasound scanner with a 7.5 MHz multifrequency annular array sector transducer (Vingmed, Horten, Norway). The axial resolution was $\leq$ 0.6 mm, according to the manufacturer, and the upper 95% confidence limit for the diameter, based on repeat measurements ($\geq$ 5 times), was $\leq$ 0.06 mm (Kiserud et al., 1999). The inner diameter, D, of the intra-abdominal portion of the UV (Fig. 1) was measured at the entrance to the liver by averaging five or more measurements. Subsequently, the area A, was calculated by assuming a circular cross section ($A = \pi D^2/4$). The same technique was applied for the inlet of the ductus venosus (at the junction with the UV) and its outlet (at the junction with the inferior vena cava). The measurements were performed when the pressure and the vessel wall had reached stability. Each experiment was completed within 3–5 h.

Parametric expression for pressure-area relation and compliance

Since the pressure and area seemed to be exponentially related by visual inspection of the measurements, we use the constitutive equation:

$$p = p_s \, e^{\beta \left(\frac{A}{A_s} - 1\right)} \tag{1}$$

where p_s is a standard pressure, β the stiffness parameter, and A_s the cross-sectional area of the vessel at the standard pressure. The standard pressure was taken as p_s = 5 mmHg, and for each data set a least square fit was performed to determine β and A_s. Umbilical venous pressures are reported to be between 2–12 mmHg (Ville et al., 1994; Weiner et al., 1989; Castle and Mackenzie, 1986; Nicolini et al., 1989). Our equation is similar to that which has been suggested for the arterial vessel walls (Hayashi et al., 1980; Hayashi, 1993), the only difference being that we have used area as the primary variable to represent the vessel dimension, whereas in the equation for arteries the diameter was employed. The dimensionless quantity β represents the structural stiffness of the vessel wall and is called the *stiffness parameter* in the arterial wall studies. It has been useful in the evaluation of the elastic properties of arteries, not only in fundamental studies, but also in clinical medicine (Hayashi, 1993).

From Eq. 1 parameters such as compliance C and pulse wave velocity c may be derived:

$$C = \frac{\partial A}{\partial p} = C_s \, \frac{p_s}{p} = \frac{A_s}{\beta p}, \qquad c^2 = \frac{\partial p}{\partial A} \, \frac{A}{\rho} = \frac{p}{\rho} \, (\beta + \ln \frac{p}{p_s}) \tag{2}$$

where the compliance at standard pressure is:

$$C_s = \frac{A_s}{p_s} \, \frac{1}{\beta} \tag{3}$$

and ρ is the density of the blood.

Results

ı the five preparations it was possible to determine the pressure-area relationship for ıe UV (n = 4), DV inlet (n = 5), and DV outlet (n = 5). The pressure and area ere found to be exponentially related at all locations and to be fitted well by the ast-squares method. The experimental and fitted pressure-area curves for DV inlet, V outlet, and UV are depicted in Fig. 2.

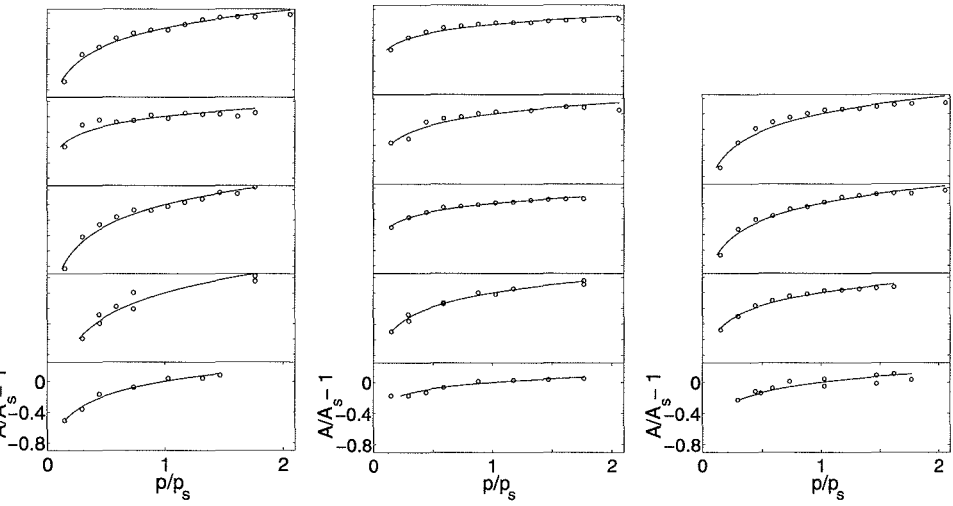

igure 2: Nondimensional area $A/A_s - 1$ vs nondimensional pressure p/p_s for experiments pen circles) and exponential fits (solid lines), at the inlet (left panel) and the outlet (middle anel) of the ductus venosus. The data for the intra-abdominal umbilical vein are presented the right panel. A_s corresponds to the area at the standard pressure $p_s = 5$ mmHg.

The estimated parameters, β and A_s, for each data set at each location are summarized in Table 1.

	β	SD	range	A_s	SD	range
DV inlet	3.4	1.3	2.2, 5.6	4.4	0.7	3.6, 5.3
DV outlet	6.2	1.8	3.8, 8.6	21.0	10.6	8.1, 35.4
UV	4.0	1.0	3.1, 5.3	28.3	9.4	20.1, 41.7

able 1: The mean stiffness-parameter β of the inlet and outlet of the ductus venosus (DV) ıd the intra-abdominal portion of the umbilical vein (UV) determined *in vitro* in the fetal eep. The mean cross-sectional areas A_s in mm^2 at standard pressure $p_s = 5$ mmHg.

The β-value ranges are quite wide, especially for the DV outlet. From Table 1 ə can see that the mean β value at DV outlet is larger than that at both DV inlet ıd UV, and that the mean β value in the UV is larger than that at the DV inlet.

Correspondingly, the pulse wave velocity, calculated with mean β values (Eq. 2), was found to be largest at the DV outlet, smallest at the DV inlet, and intermediate in the UV (see Fig. 3). Representative values for the compliance at the standard pressure

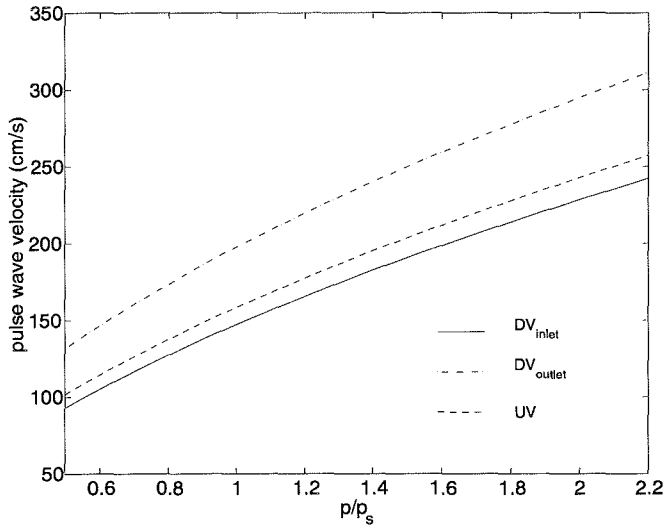

Figure 3: Estimated pulse wave velocity for the ductus venosus inlet (DV_{inlet}), outlet (DV_{outlet}), and the intra-abdominal umbilical vein (UV), based on averaged β- and A_s-values.

p_s, were obtained from Eq. 2 and the averaged β and A_s values from Table 1. Their values were found to be: $C_s^i = 2.6 \cdot 10^{-3}\text{cm}^2/\text{mmHg}$, $C_s^o = 6.8 \cdot 10^{-3}\text{cm}^2/\text{mmHg}$, and $C_s^u = 1.4 \cdot 10^{-2}\text{cm}^2/\text{mmHg}$ at the DV inlet, DV outlet, and UV, respectively. The pressure dependency of the compliance at these locations is depicted in Fig 4. These values are also based on averaged β- and A_s-values. From the data it is seen that the compliance was largest in the UV, intermediate at the DV outlet, and smallest at the DV inlet.

Discussion

The stiffness parameter, β was 6.2 ± 1.8 at the DV outlet, 3.4 ± 1.3 at the DV inlet, and 4.0 ± 1.0 in the UV (Table 1). The pulse wave velocity varied correspondingly (Fig. 3). However, the compliance at the three locations was not inversely related to the stiffness parameter (Fig. 4). The reason for this is that compliance does not represent mechanical properties alone, but also includes geometry (see Eq. 2). Since the cross-sectional area at the DV inlet is relatively small, the corresponding compliance turns out to be lower than that observed at the two other locations.

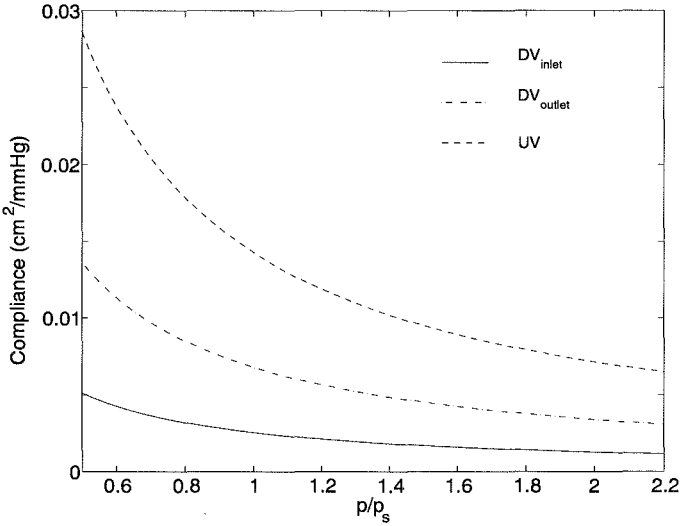

igure 4: Estimated compliance for the ductus venosus inlet (DV_{inlet}), outlet (DV_{outlet}), ıd the intra-abdominal umbilical vein (UV), based on averaged β- and A_s-values.

Hayashi (Hayashi, 1993) reviewed recent studies on the elastic properties of arterial alls, and argued that a simple constitutive relation, such as an exponential or logathmic one, is more advantageous than the more elaborated relations based on strain ıergy functions (Vaishnav et al., 1973; Fung et al., 1979). In these simple formulations ıe number of coefficients are reduced, while their physical meaning is retained.

From a practical point of view, expressing the elastic properties by a single paramter is more useful than a thorough but more composite expression based on several ıarameters. However, the pulse wave velocity depends on pressure; the compliance on ɔth pressure and area. Thus, neither pulse wave velocity or compliance rigorously ·present the elastic properties of the vessel wall. On the contrary, once a reference ·essure has been agreed upon, the β-value will describe the elastic properties of the all material at all physiological pressure levels. Hayashi suggested a reference pres-ıre in the arterial system of adults of $p_s = 100$ mmHg. Since the umbilical venous ·essure is reported to be 2–12 mmHg (Ville et al., 1994; Weiner et al., 1989; Castle ıd Mackenzie, 1986; Nicolini et al., 1989), we propose $p_s = 5$ mmHg as the reference ılue for the fetal venous circulation.

A three-parameter arc-tangent model was suggested to capture the S-shape, i.e. ıe presence of an inflection point, of the arterial pressure-area relation better than ı exponential function (Langewouters et al., 1985a,b). However, our pressure-area easurements in the UV and the DV showed no inflection point (i.e. S-shape), most ·obably because the pressure variation is much smaller in fetal veins than in adult teries. Thus, we preferred the simplest regression model that gave a statistically

satisfying representation of the data, i.e., the exponential model.

Hayashi related pressure and diameter, whereas the present approach relates pressure and area. This convention is motivated from the fact that a constitutive relation should readily be included in mathematical models for wave propagation. In such models, the conservation laws and the constitutive laws are often formulated with area, not diameter, as one of the primary variables (Raines et al., 1974; Stergiopulos et al., 1992).

In the human fetus, foot-to-foot estimates of pulse wave velocities have been reported to be 2.5 m/s in the umbilical artery (Stale et al., 1991), and 1.4–2.9 m/s in the abdominal aorta (Sindberg Eriksen et al., 1984). However, data on elastic properties in the fetal venous tree are scarce. In a study by Azuma and Masamitsu (Azuma and Masamitsu, 1973), stress-strain curves are given for some veins in the adult. By assuming that $1.5 \cdot 10^{-2}$ is a representative wall-thickness diameter ratio (Fung, 1984), we can estimate pulse wave velocities in the range of 0.5–3 m/s as a function of strain in the jugular, axillary and femoral veins. Estimates from data in the human saphenous vein (Wesley et al., 1975) and in the abdominal vena cava (Anliker et al., 1969) of a dog yield pulse wave velocities ranges of 0.6–6 m/s and 2–6 m/s, respectively. The pulse wave velocity estimates in Fig. 3 for fetal veins, the DV and UV, are thus within the range of pulse wave velocities in both human fetal arteries and in human veins in adults. We performed static pressure measurements, and thus our experiments do not account for viscoelastic effects such as hysteresis, creep, and relaxation. These effects should be dealt with in future studies.

By studying the UV and DV as an explant with the liver, the influence of neural influences and endogenous vasoactive substances and the shear stress of flow is eliminated or low. Adrenergic stimulation influences the DV in vitro (Coceani et al., 1984), and prostaglandin seems to act on the DV in much the same way as on the ductus arteriosus (Coceani and Olley, 1988), but probably produces a weaker response (Momma et al., 1984). The extent of such regulation is not known for the fetus in utero. By excluding such possible modifying effects on the stiffness parameter, we believe that the present results give a fair picture of the mechanical properties of the DV and UV, and, furthermore, we suggest that the same preparation should be used to quantify these modifying effects.

It is known that in postnatal life veins can collapse when subjected to a negative transmural pressure. This is probably a rare event for the UV/DV in fetal life and has not been addressed in the present study.

The similarity between the venous circulation of the human fetus and the fetal sheep is well documented (Rudolph, 1985; Kiserud et al., 1992), suggesting that equivalent mechanical properties also can be expected for the UV and DV. Hence, we suggest that the present results of stiffness parameters can be used for calculating pulse velocity and compliance in the human UV and DV until corresponding human data are available.

The stiffness parameter cannot be derived during conventional evaluation of the sick fetus with the currently available noninvasive techniques, but is an important determinant of compliance. In fetal congestive heart failure, reduced compliance due to an elevated venous pressure is believed to promote UV pulsations. On the other hand, in the early stages of pregnancy, pulsations in the UV are present under physiological

onditions. We believe that such pulsations can be ascribed to a low compliance due to ne small dimensions of the DV and UV in the first trimester. Much in the same way as coustic waves are attenuated, reflected, and transmitted when hitting a medium with different density, the atrial wave is expected to be modified according to changes in ne mechanical properties and geometry (i.e., changes in impedance) along the DV and ne UV. In the present study we demonstrate and quantify the mechanical properties nd dimensions of the DV and the UV, and show that these factors, together with the ressure, determine the compliance (see Eq. 2). Based on the information presented in nis paper, the stiffness parameter and dimension of the DV and UV, the underlying nechanisms for pulsations in the UV can be studied (e.g., in computer simulations).

In conclusion, the information about the mechanical properties of the UV and DV resented in this paper can be used to investigate wave transmission and reflection henomena in the UV/DV bifurcation. A better understanding of these phenomena nay be helpful in the interpretation of the pulsatile changes recorded in the DV and V during fetal diseases.

Acknowledgments

he help of Atle Kleven with post-script conversion is gratefully appreciated. Torvid iserud was supported by the British Heart Foundation and the Norwegian Research ouncil.

References

Anliker, M., Wells, M., Ogden, E., 1969. The transmission characteristics of large and small pressure waves in the abdominal vena cava. IEEE Trans Biomed Eng 16, 262–273.

Azuma, T., Masamitsu, H., 1973. Distensibility of the vein: from the architectural point of view. Biorheology 10, 469–479.

Castle, B., Mackenzie, I., 1986. In vivo observations on intravascular blood pressure in the fetus during mid-pregnancy. In Rolfe, P. (ed.), *Fetal physiological measurements.* Wellington: Butterworths, London, Boston, Durban, Singapore, Toronto, 65–69.

Coceani, F., Adeagbo, A., Cutz, E., Olley, P., 1984. Autonomic mechanisms in the ductus venosus of the lamb. Am J Physiol 247, H17–H24.

Coceani, F., Olley, P., 1988. The control of cardiovascular shunts in the fetal and perinatal period. Can J Pharmacol 66, 1129–1134.

Fung, Y., 1984. Biodynamics. Circulation. Springer-Verlag New York Inc, New York.

Fung, Y., Fronek, K., Patitucci, P., 1979. Pseudoelasticity of arteries and the choice of its mathematical expression. Am J Physiol 237, H620–H631.

Gill, R. W., 1979. Pulsed doppler with B-mode imaging for quantitative blood flow measurement. Ultrasound Med Biomed 5, 223–235.

Gudmundsson, S., Huhta, J. C., Wood, D. C., Tulzer, G., Cohen, A. W., Weiner, S., 1991. Venous doppler ultrasonography in the fetus with nonimmune hydrops. Am J Obstet Gynecol 164, 33–37.

Hayashi, K., 1993. Experimental approaches on measuring the mechanical properties and constitutive laws of arterial walls. J Biomech Eng 115, 481–488.

Hayashi, K., Handa, H., Nagasawa, S., Okumura, A., Moritake, K., 1980. Stiffness and elastic behavior of human intracranial and extracranial arteries. J Biomech 13, 185–184.

Hellevik, L. R., Kiserud, T., Irgens, F., Ytrehus, T., Eik-Nes, S. H., 1998. Simulation of pressure drop and energy dissipation for blood flow in a human fetal bifurcation. J Biomech Eng 120, 455–462.

Huisman, T. W. A., Stewart, P. A., Wladimiroff, J. W., 1992. Ductus venosus blood flow velocity waveforms in the human fetus - a doppler study. Ultrasound Med Biomed 18, 33–37.

Kanzaki, T., Chiba, Y., 1990. Evaluation of the preload condition of the fetus by inferior vena caval blood flow pattern. Fetal Diagn Ther 5, 168–174.

Kiserud, T., Crowe, C., Hanson, M., 1998. Ductus venosus agenesis prevents transmission of central venous pulsation to the umbilical vein in fetal sheep. Ultrasound Obstet Gynecol 11, 190–194.

Kiserud, T., Eik-Nes, S. H., Blaas, H.-G., Hellevik, L. R., 1991. Ultrasonographic

velocimetry of the fetal ductus venosus. Lancet 338, 1412–1414.

iserud, T., Eik-Nes, S. H., Blaas, H. G., Hellevik, L. R., 1992. Foramen ovale-an ultrasonographic study of its relation to the inferior vena cava, ductus venosus and hepatic veins. Ultrasound Obstet Gynecol 2, 389–396.

iserud, T., Eik-Nes, S. H., Blaas, H. G., Hellevik, L. R., Simensen, B., 1994. Ductus venosus blood velocity and the umbilical circulation in the seriously growth retarded fetus. Ultrasound Obstet Gynecol 4, 109–114.

iserud, T., Eik-Nes, S. H., Hellevik, L. R., Blaas, H.-G., 1993. Ductus venosus blood velocity changes in fetal cardiac diseases. J Matern Fetal Invest 3, 15–20.

iserud, T., Saito, T., Ozaki, T., Rasmussen, S., Hanson, M., 1999. Validation of diameter measurements by ultrasound. Intra-observer and inter-observer variation assessed *in vitro* and in fetal sheep. Ultrasound Obstet Gynecol , in press.

ngewouters, G., Wesseling, K., Goedhard, W., 1985a. The pressure dependent dynamic elasticity of 35 thoracic and 16 abdominal human aortas in vitro described by a five component model. J Biomech 18, 613–620.

ngewouters, G., Wesseling, K., Goedhard, W., 1985b. The static elastic properties of 45 human thoracic and 20 abdominal aortas in vitro and the parameters of a new model. J Biomech 17, 425–435.

ngman, G., Laurin, J., Maršál, K., 1986. Circulatory changes in fetuses with imminent asphyxia. Biol Neonate 49, 66–73.

omma, K., Takeuchi, H., Hagiwara, H., 1984. Pharmacological constriction of the ductus arteriosus and ductus venosus in fetal rats. In Nora, J., Takao, A. (eds.), *Congenital heart disease. Causes and processes.* Futura, Mount Kisco, 313–327.

akai, Y., Imanaka, M., Nishio, J., Ogita, S., 1994. Umbilical cord venous pulsation in normal fetuses and its incidence after 13 weeks gestation. Ultrasound Med Biomed 21, 443–446.

colini, U., Fisk, N., Talbert, D., Rodeck, C., Kochenour, N., 1989. Intrauterine manometry: technique and application to fetal pathology. Prenat Diagn 1989 , 243–254.

nnati, G., Redaelli, A., Bellotti, M., Ferrazzi, E., 1996. Computational analysis of the ductus venosus fluid dynamics based on doppler measurements. Ultrasound Med Biomed 22, 1017–1029.

ines, J., Jaffrin, M., Shapiro, A., 1974. A computer simulation of arterial dynamics in the human leg. J Biomech 7, 77–91.

ed, K. L., Appleton, C. P., Anderson, C. F., Shenker, L., Sahn, D. J., 1990. Doppler studies of vena cava flows in human fetuses; insights into normal and abnormal cardiac physiology. Circulation 81, 498–505.

ed, K. L., Chaffin, D. G., Anderson, C. F., 1996. Umbilical venous doppler velocity pulsations and inferior vena cava pressure elevations in fetal lambs. Obstet Gynecol

87, 617–620.

Reed, K. L., Chaffin, D. G., Anderson, C. F., Newman, A. T., 1997. Umbilical venous velocity pulsations are related to atrial contraction pressure waveforms in fetal lambs. Obstet Gynecol 89, 953–956.

Respondek, M., Kaczmarek, P., Pertynski, T., 1996. Fetal echocardiography guidelines to predict survival of fetuses with ascites. Ultrasound Obstet Gynecol 7, 256–261.

Rudolph, A. M., 1985. Distribution and regulation of blood flow in the fetal and neonatal lamb. Circ Res 57, 811–821.

Sindberg Eriksen, P., Gennser, G., Linström, K., 1984. Physiological characteristics of diameter pulses in the fetal descending aorta. Acta Obstet Gynecol Scand 63, 355–363.

Stale, H., Maršál, K., Gennser, G., Benthin, M., Dahl, P., Linström, K., 1991. Aortic diameter pulse waves and blood flow velocity in the small, for gestational age, fetus. Ultrasound Med Biomed 17, 471–478.

Stergiopulos, N., Young, D., Rogge, T., 1992. Computer simulation of arterial flow with applications to arterial and aortic stenoses. J Biomech 25, 1477–1488.

Vaishnav, R., Young, J., Patel, D., 1973. Distribution of stresses and strain-energy density through the wall thickness in a canine aortic segment. Circ Res 32, 577–583.

Ville, Y., Sideris, I., Hecher, K., Snijders, R., Nicolaides, K., 1994. Umbilical venous pressure in normal, growth-retarded, and anemic fetuses. Am J Obstet Gynecol 170, 487–494.

Weiner, C., Heilskov, J., Pelzer, G., Grant, S., Wenstrom, K., Williamson, R., 1989. Normal values for human umbilical venous and amniotic fluid pressures and their alteration by fetal disease. Am J Obstet Gynecol 161, 714–717.

Wesley, R., Vaishnav, R., Fuchs, J., Patel, D., Greenfield Jr., J., 1975. Static linear and nonlinear elastic properties of normal and arterialized venous tissue in dog and man. Circ Res 37, 509–520.

Wladimiroff, J. W., Huisman, T. W. A., Stewart, P. A., 1991. Normal fetal doppler inferior vena cava, transtricuspid, and umbilical artery flow velocity waveforms between 11 and 16 weeks' gestation. Am J Obstet Gynecol 166, 921–924.

Paper III

A mathematical model of umbilical venous pulsation

Hellevik L.R.[1], Stergiopulos N.[2], Kiserud T.[3],
Rabben S.I.[4], Eik-Nes S.H.[5], Irgens F.[1]

[1]MTF/Div. Applied Mechanics, NTNU, Trondheim, Norway
[2]Biomedical Engineering Laboratory EPFL, Switzerland
[3]Dept. Obstetrics and Gynecology, Univ. Hosp. Bergen, Norway
[4]Dept. Physiology and Biomedical Engineering, NTNU, Trondheim, Norway
[5] Dept. Obstetrics and Gynecology, National Center for Fetal Medicine, Norway

Abstract

Pulsations in the fetal heart propagate through the precordial vein and the ductus venosus but are normally not transmitted into the umbilical vein. Pulsations in the umbilical vein do occur, however, in early pregnancy and in pathological conditions. Such transmission into the umbilical vein is poorly understood. We present a mathematical model to identify the mechanical factors that influence pulsation in the umbilical vein. The umbilical vein was modeled as a compliant reservoir and the umbilical vein pressure was assumed to be equal to the stagnation pressure at the ductus venosus inlet. We calculated the index of pulsation of the umbilical vein pressure ((max-min)/mean), the reflection and transmission factors at the ductus venosus inlet, numerically and with estimates. Typical dimensions in the physiological range for the human fetus were used, while stiffness parameters were taken from fetal sheep. We found that wave transmission and reflection in the umbilical vein ductus venosus bifurcation depend on the impedance ratio between the umbilical vein and the ductus venosus, as well as the ratio of the mean velocity and the pulse wave velocity in the ductus venosus. The impedances, in turn, depend on the mechanical properties of the veins, the pressure level, and their dimensions. Thus, we believe that the mathematical model is suitable for analyzing the factors involved in the occurrence of umbilical venous pulsations.

Submitted for publication

Introduction

Doppler velocimetry of the fetal venous system is increasingly used in the hemodynamic evaluation of the sick fetus. In contrast to the pulsatile flow in precordial veins, the blood flow in the umbilical vein (UV) is usually stationary. In 1986, Lingman et al. described a pulsatile velocity in the UV in fetuses with imminent asphyxia (Lingman et al., 1986); Gudmundsson et al., who found the same pulsations in fetuses with congestive heart disease, suggested this sign as a marker of poor prognosis (Gudmundsson et al., 1991). Similarly, such pulsations were found in cases with fetal cardiac malformations (Kiserud et al., 1993), arrhythmias (Gembruch et al., 1995), serious growth restriction (Kiserud et al., 1994a) and twin-twin transfusion syndrome (Hecher et al., 1995).

However, UV pulsation is a normal phenomenon in fetuses of a gestational age of 13 weeks and younger (Rizzo et al., 1992; Nakai et al., 1995), and its occurrence is described even in normal fetuses during late pregnancy, particularly in the deep intra-abdominal portion of the vein (van Splunder et al., 1994).

There are probably several sources and types of pulsation (Huhta, 1997; Kiserud, 1997). The pulsation commonly occurring in the sick fetus (and in the normal fetus during early pregnancy) appears as a short deflection linked to the cardiac cycle. It is believed that an augmented atrial contraction is transmitted mainly through the ductus venosus to the umbilical vein (Kiserud et al., 1993; Kiserud, 1997).

Fetal sheep experiments have shown that such waves are transmitted to the UV during adrenergic stimulation and hypoxic challenge (Reuss et al., 1983; Hasaart and de Haan, 1986), and that the transmission of such waves is blocked by the agenesis of the ductus venosus (Kiserud et al., 1998). The complete waveform of the precordial venous velocity may be transmitted into the UV in cases of gross placental compromise, or during the extreme afterload seen in twin-twin transfusion syndrome (Fig. 1). The local mechanisms that govern the transmission and occurrence of pulsations in the UV are not well understood.

The aim of the present study was to identify the mechanical factors that influence pulsation in the intra abdominal UV using a mathematical model.

Method

The DV acts as a direct communication that shunts blood from the UV to the fetal heart (Fig. 2). Downstream from the DV, the fetal heart contracts periodically and generates pressure and flow waves that propagate in the negative flow direction into the DV and thereby give rise to the characteristic pulsatile DV velocity pattern. In this study the positive flow directions were taken as shown in Fig. 2. The UV flow *before* the bifurcation was denoted Q^b; the UV flow *after* the bifurcation, Q^a; the flow in the DV, Q. To account for a non-zero and timevarying net inflow into the UV, $(Q^b - Q^a - Q)$, we were led to introduce a compliance of the UV to ensure mass conservation.

In the following section we develop the mathematical model to calculate pulsations in the UV pressure p^{uv} from an imposed DV flow pattern. Subsequently, the DV

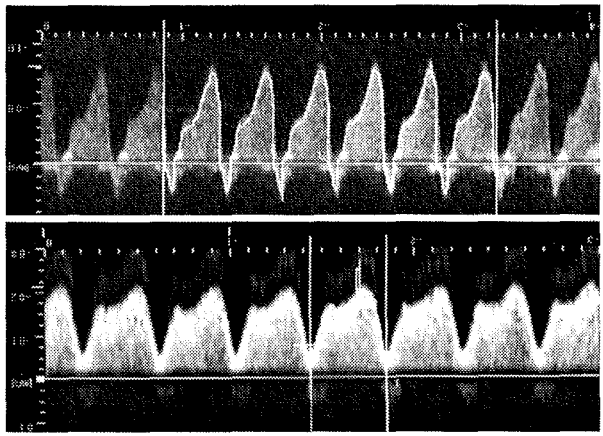

igure 1: Venous Doppler velocity recordings for twin-twin transfusion syndrome. Upper anel: DV velocity pattern. Lower panel: UV velocity pattern.

ressure p is estimated. In the next step approximate analytical expressions are devel- oed for the reflection and transmission factors at the DV inlet. Further, we introduce n index of pulsation to quantify pulsatility, and provide computational details.

Iathematical model

onservation of mass at the bifurcation is expressed as:

$$\frac{\partial V}{\partial t} = C^{uv}\frac{\partial p^{uv}}{\partial t} = Q^b - Q^a - Q \tag{1}$$

here V and $C^{uv} = \partial V/\partial p$ are the UV volume and volume compliance, respectively. o ensure no accumulation of mass over a cycle, the pulsatile DV flow is assumed to e:

$$Q(t) = Q^b - Q^a + \sum_{n=1}^{N} Q_n\, e^{j\omega_n t} \tag{2}$$

nere $j = \sqrt{-1}$ and ω_n is the n-th harmonic angular frequency. In what follows, a bscript n of a primary variable denotes its corresponding Fourier-coefficient. For a nstant C^{uv} Eq. (1) is integrable, and with an imposed flow as given by Eq. (2) the V pressure is:

$$p^{uv}(t) = p_0^{uv} - \sum_{n=1}^{N} \frac{Q_n}{\omega_n C^{uv}}\, e^{j(\omega_n t - \pi/2)} \tag{3}$$

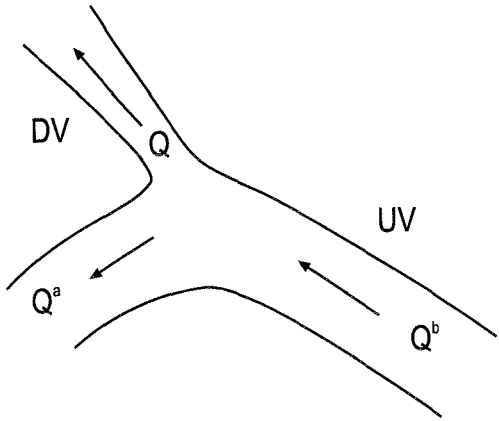

Figure 2: Diagram of flows in the mathematical model of the umbilical vein (UV) and ductus venosus (DV). The flows in the UV before and after the bifurcation are denoted by Q^b and Q^a, respectively, and the flow in the DV by Q.

From this solution we see that there will always be a phase shift between the UV pressure and the DV flow of 90°, and that the larger the UV compliance C^{uv}, and/or angular frequency ω_n, the smaller the pulsations in the UV pressure p^{uv}.

We have previously shown (Hellevik et al., 1999) that the pressure-area relationship in both the UV and the DV is nonlinear and can be described by the following relation:

$$p(A) = p_s \, e^{\beta \, (A/A_s - 1)} \tag{4}$$

where A is the cross-sectional area and β the stiffness parameter. The subscript s denote the area at the reference pressure $p_s = 5$ mmHg. By assuming that the UV length, L_{uv}, is constant, i.e. the UV is tethered, an estimate of the UV volume compliance may be obtained:

$$C^{uv} = \frac{A_s^{uv} \, L_{uv}}{\beta_{uv} \, p^{uv}} \tag{5}$$

where A_s^{uv} is the reference cross-sectional area and β_{uv} the stiffness parameter of the UV. With the introduction of a nonlinear C^{uv} Eq. (1) does not yield an analytical solution, but may readily be solved numerically by an explicit, one-step Runge-Kutta method.

The pressures in the merging vessels of a bifurcation have frequently been assumed to be equal (Fung, 1984; Avolio, 1980; Stergiopulos et al., 1992). However, compared to the UV, the DV is a small vessel, with a UV/DV diameter ratio g in the range of 2 to 6 (Kiserud, 1999). This change in diameter is accompanied by a convective acceleration and, consequently, a pressure drop; this pressure drop has been approximated by a Bernoulli formulation (Kiserud et al., 1994b; Pennati et al., 1996; Hellevik et al., 1998).

hus, we refrained from the assumption of equal pressures in the merging branches in ıe present study to incorporate the dynamic pressure p^d:

$$p^{uv} = p + p^d, \qquad p^d = \frac{1}{2}\,\rho \left(\frac{Q}{A}\right)^2 \tag{6}$$

here ρ denotes the fluid density. To close the system of equations (Eq. (6)) a consti-ıtive equation from our experiments, expressed by Eq. (4) was introduced (Hellevik al., 1999). For an imposed flow Q and a calculated UV pressure p^{uv}, the DV pres-ıre p may thus be obtained numerically from the nonlinear Eqs. (4) and (6) by a ewton-Raphson approach.

eflection and transmission factors

ı this section, approximate analytical solutions for the reflection factor Γ and the ansmission factor T will be outlined to obtain a qualitative understanding of how the ırameters involved influence reflection and transmission at the DV inlet.

For simplicity we assumed: $Q = Q_0 + Q_n\, e^{j\omega_n t}$, $A = A_0 + A_n\, e^{j\omega_n t}$, and $A_n = C\, p_n$, here C is the area compliance of the DV. From Eq. (6) and multivariate Taylor-xpansion:

$$p_n^d \approx \rho u_0^2\ (Q_n/Q_0 - C p_n/A_0) \tag{7}$$

here $u_0 = Q_0/A_0$, i.e. the mean DV velocity. As the incident waves travel in the egative flow direction we defined: $Z_{uv} = p_n^{uv}/(-Q_n)$ and then from Eqs. (6) and (7):

$$p_n \approx -Q_n\, \frac{Z_{uv} + \rho u_0/A_0}{1 - (u_0/c)^2} \tag{8}$$

owever, when $u_0 \ll c$ the denominator of Eq. (8) will be close to one and:

$$p_n \approx -Q_n\ (Z_{uv} + \rho u_0/A_0) \tag{9}$$

hus, an estimate of the DV inlet impedance Z_{dv} was found to be:

$$Z_{dv} = \frac{p_n}{-Q_n} \approx Z_{uv} + Z_c\, u_0/c \tag{10}$$

ırther, the incident (p^i) and reflected (p^r) pressure components at the DV inlet may be timated by the linear splitting purposed by Westerhof et al. (1972): $p^i = (p - Z_c\, Q)/2$, $= (p + Z_c\, Q)/2$, where $Z_c = \rho c/A_0$ is the characteristic impedance of the DV and c e pulse wave velocity in the DV: $c^2 = A_0/\rho\, C$.

Finally, the estimates of the reflection factor $\Gamma = p_n^r/p_n^i = (Z_{dv} - Z_c)/(Z_{dv} + Z_c)$ ıd the transmission factor $T = p_n^{uv}/p_n^i$ was obtained:

$$\Gamma \approx \frac{1 - (1 - u_0/c)\ Z_c/Z_{uv}}{1 + (1 + u_0/c)\ Z_c/Z_{uv}} \tag{11}$$

$$T \approx \frac{2}{1 + (1 + u_0/c)\, Z_c/Z_{uv}} \tag{12}$$

From the estimates in Eqs. (10), (11), and (12) we see, qualitatively, how the nonlinear term in Eq.(6) influences the DV impedance, reflection factor, and transmission factor at the DV inlet. Observe that when $u_0 \to 0$ these estimates degenerate to the expressions for a pure reservoir termination, and thus $\Gamma \to |\Gamma_0|\, e^{-j\,2\theta_0}$, and $T \to |T_0|\, e^{-j\,\theta_0}$, with $\theta_0 = \arctan(Z_c/|Z_{uv}|)$, $|T_0| = 2/\sqrt{1 + (Z_c/|Z_{uv}|)^2}$, and $|\Gamma_0| = 1$. For perfectly matched impedances $\theta_0 = 45°$ and $|T_0| = 1$, i.e. this corresponds to full transmission with no reflection. On the contrary, when $Z_c/|Z_{uv}| \to \infty$, the phase angle $\theta_0 \to 90°$, $|T_0| \to 0$, i.e. there is no transmission and a phase lag between incident and reflected pressure waves of 180°, corresponding to a complete cancellation of pressure pulsations in the DV. Note that as $Z_{uv} = 1/(j\omega\, C^{uv})$ (see Eq. (3)), the modulus of the impedance ratio $Z_c/|Z_{uv}|$ is proportional to g^2. From our estimates we deduced that the mean velocity u_0 related to the dynamic pressure term, reduces the modulus of both Γ and T. Further, the phase angle of T increases slightly, whereas counteracting effects in the numerator and denominator in Eq. (11) tends to cancel and leaves the phase angle of Γ relatively unaffected.

Index of pulsation

To quantify pulsations we introduced an index of pulsation (IP):

$$IP(\cdot) = \frac{\max(\cdot) - \min(\cdot)}{\text{mean}(\cdot)} \tag{13}$$

For a constant C^{uv} and with "small" changes in p^{uv} an approximation of the index of pulsation of the UV pressure was obtained from Eq. (3):

$$IP(p^{uv}) = \sum_{n=1}^{N} \frac{2\, Q_n\, \beta_{uv}}{\omega_n\, A_s^{uv}\, L_{uv}} \tag{14}$$

Thus, subject to the assumptions above, $IP(p^{uv})$ is a linear function of the stiffness parameter β_{uv} and the flow component Q_n, whereas it is a nonlinear function of the reference area A_s^{uv}.

The UV velocity does not occur in our model explicitly. However, pressure and flow waves are related through the characteristic impedance in the absence of reflections. Thus, by assuming that reflections are negligible in the UV, the index of pulsation of UV pressure can be shown to be related to the index of pulsation of the UV velocity $IP(u^{uv})$ in the following manner:

$$IP(u^{uv}) \approx \kappa\, IP(p^{uv}) \tag{15}$$

with $\kappa = p_0^{uv}/(\rho\, c_{uv}\, u_0^{uv})$, where c_{uv} and u_0^{uv} denote the pulse wave velocity and the mean velocity in the UV, respectively. Note that although $IP(p^{uv})$ is independent of pressure (Eq. (14)) this is not the case for $IP(u^{uv})$, due to the pressure dependence of κ.

Computational details

nless otherwise stated, stiffness parameters from fetal sheep experiments were used r the calculations (Hellevik et al., 1999). The β-value at the DV inlet has a mean of 4 and ranges from 2.2 to 5.5, whereas the UV stiffness parameter β_{uv} has a mean of 0 and ranges from 3.1 to 5.3.

To obtain a typical flow pattern for the DV (Fig.3) recordings were made of Doppler elocity measurements of fetuses in the low-risk antenatal clinic. A typical Doppler elocity measurement was multiplied with a typical cross-sectional area corresponding a DV diameter of $D_{dv} = 0.8$ mm. The DV inlet diameter ranges from 0.4 mm to 2.2 m, while the UV/DV diameter ratio g ranges from 2 to 6 (Kiserud, 1999). The flow as averaged over four cycles and low-pass filtered, keeping only the six first harmonics .e. N=6) of Eq. (2). Further, all UV pressures were calculated numerically using the ressure dependent compliance C^{uv} (see Eq. (5)) and $L_{uv} = 7$ cm, unless otherwise ated.

Results

he results from two parameter configurations illustrate how the index of pulsation of ie UV pressure is affected by extreme, but physiological, UV parameter values (Fig. 3). he DV parameters were kept constant and taken as: $\beta = 3.4$, and $A_s = 0.63\,\mathrm{mm}^2$

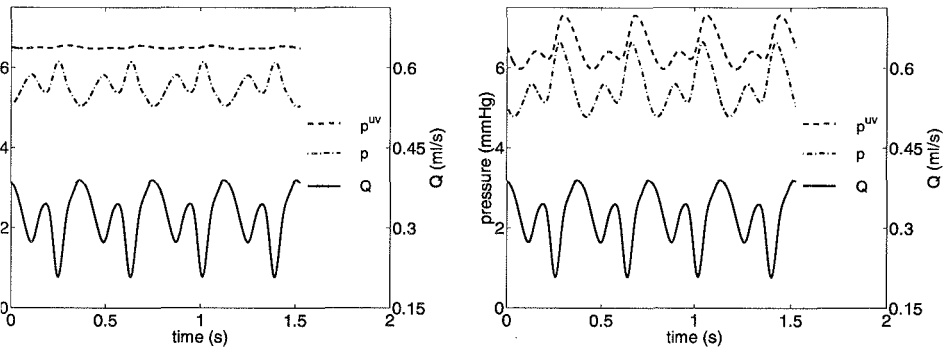

igure 3: Calculated UV pressure p^{uv} and DV pressure p for the imposed flow pattern Q in e DV. Left panel: compliant UV. Right panel: less compliant UV.

$)_{dv} = 0.9$ mm), i.e. typical values within the physiological range. The results in the ft panel correspond to a relatively compliant UV ($C^{uv} = 8.0 \cdot 10^{-2}$ ml/mmHg) at ean pressure $p_0^{uv} = 6.5$ mmHg with parameter values: $\beta_{uv} = 3.1$ and $A_s^{uv} = 23\,\mathrm{mm}^2$ $)_{uv} = 5.4$ mm, $g = 6$). The right panel shows the results corresponding to a less mpliant UV ($C^{uv} = 5.2 \cdot 10^{-3}$ ml/mmHg) at mean pressure $p_0^{uv} = 6.5$ mmHg with ırameter values: $\beta_{uv} = 5.3$ and $A_s^{uv} = 2.6\,\mathrm{mm}^2$ ($D_{uv} = 1.8$ mm, $g = 2$). Relatively odest pulsations in p^{uv} were observed for the compliant case ($IP = 0.02$), whereas rge pulsations were obtained for the less compliant case ($IP = 0.21$).

The IP of the UV pressure was calculated for parameter configurations where only one parameter was changed. In the left panel of Fig. 4 the IP is plotted as a function of the UV stiffness parameter β_{uv} for three UV/DV ratios: g=2, g=4, and g=6, i.e. the minimum, mean, and maximum in the physiological range. The index of pulsation was largest for the series with the smallest g, i.e. the smallest impedance ratio, and smallest for the series with the largest g, i.e. the highest impedance ratio. For each g the IP showed linear behavior as a function of β_{uv}. Likewise, the IP is plotted in the right

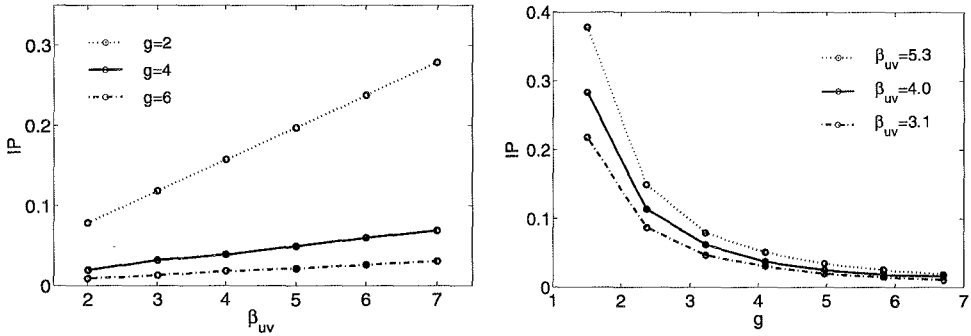

Figure 4: Left panel: index of pulsation IP of the UV pressure plotted versus UV stiffness parameters β_{uv} for three different values of UV/DV diameter ratios g. Right panel: IP of the UV pressure plotted versus the UV/DV diameter ratio g for extreme and mean values of the UV stiffness parameters β_{uv}.

panel of Fig. 4 as a function of the of the UV/DV diameter g for extreme and mean values of the stiffness parameter of the UV: $\beta_{uv} = 3.1$, $\beta_{uv} = 4.0$, $\beta_{uv} = 5.3$. The index of pulsation was largest for the series with the largest β_{uv}, i.e. the smallest impedance ratio, and smallest for the series with the smallest β_{uv}, i.e. the highest impedance ratio. For each β_{uv} the IP showed nonlinear behavior as a function of A_s^{uv}.

The impact of the dynamic pressure term on the reflection factor Γ is illustrated in Fig. 5, where the first harmonic, corresponding to the heart rate, of the modulus $|\Gamma|$, and phase $\angle\Gamma$, are plotted against the UV/DV diameter ratio g. The stiffness parameters were taken as $\beta = 2.2$ and $\beta_{uv} = 5.3$, as this parameter configuration (i.e. minimal β and maximal β_{uv}) showed the largest change in $\angle\Gamma$ as a function of g. The DV diameter was kept constant at $D_{dv} = 0.9$ mm to maintain a constant mean velocity $u_0 = 0.4$ m/s for all simulations. The moduli of both the analytical estimate in Eq. (11) and the numerical simulations were both found to be lower than 1, i.e. lower than for a pure reservoir, and only a mild g-dependence of the moduli was observed. Nevertheless, the analytical estimate consistently overestimates the modulus (mean difference 15%). The phase angles vary from approximately $-90°$ to $-170°$. Although the analytical estimate overpredicts the magnitude of the phase angle for small g and underpredicts for large g, only minor discrepancies were observed for the phase angles (mean difference of 1%).

The IP of the DV pressure was also found to decrease with increasing g (Fig. 6), i.e.

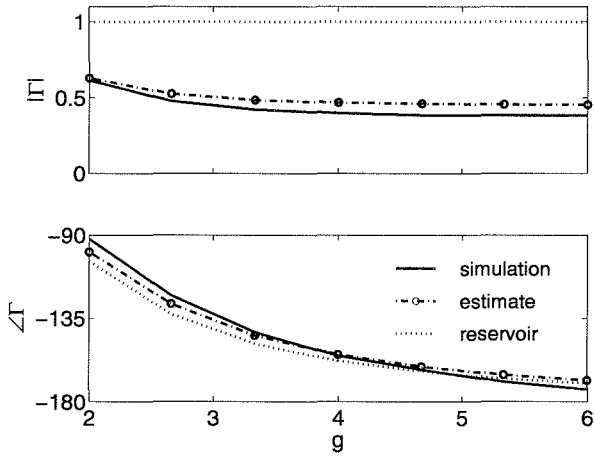

igure 5: The first harmonic modulus (upper panel) and phase (lower panel) of the reflection ctor Γ for a pure reservoir (dots), analytical estimate in Eq. (11) (dash-dots), and numerical mulation (solid).

ıe phase angle of Γ becomes more negative. This is due to the fact that the reflected ressure wave tends to cancel the incident pressure wave for phase angle of Γ close $-180°$; when the phase angle approaches $-90°$, the cancellation diminishes. This illustrated in Fig. 7 where the incident and the reflected pressure components are esented for $g = 6$ (i.e. $\angle\Gamma \approx -170°$) and for $g = 2$ (i.e. $\angle\Gamma \approx -90°$). For the UV/DV ameter ratio $g = 2$ the index of pulsation of the DV pressure was $IP(p) = 0.35$. The 's of the incident and reflected pressures were 0.76 and 0.38, respectively. Conversely, r $g = 6$ the $IP(p)$ decreased to IP=0.21, accompanied by IPs of 0.70 and 0.29 for the cident and reflected pressure components, respectively.

Further, the corresponding first harmonic of the transmission factor T, was also cal-ılated (Fig. 8). The p^d-impact on the modulus of T was found to be less pronounced an for Γ; the analytical estimate of T was somewhat better than for Γ (mean differ-ıce 1%). By contrast, the g-dependence is stronger for $|T|$ than for $|\Gamma|$, as it ranges ɔm approximately 1 for small values of g to approximately 0.1 for lager values of g. ɔrrespondingly, this is accompanied by a stronger reduction in the IP of p^{uv} than for e p (Fig. 6). The mean difference between the analytical estimate and the simulated lue for $|T|$ was 6%. The phase angles of T range from approximately $-60°$ to $-90°$. agreement with what was predicted from the estimates, the magnitude of the phase ıgles from the analytical estimates and the simulations are consistently larger than e "pure reservoir" value. The mean difference between the analytical estimate and e simulated value was 1%.

To illustrate the impact of both the mean velocity u_0 and the UV/DV ratio g on $|\Gamma|$, nulations were carried out for g ranging from 2 to 6, and DV diameters from 0.9 mm

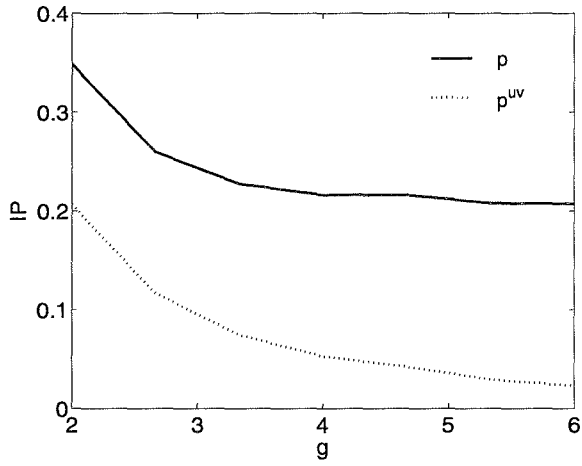

Figure 6: The index of pulsation IP for the UV pressure (dots) and DV pressure (solid) as a function of the UV/DV ratio g.

to 2 mm (Fig. 9). The imposed flow was the same for all simulations and the stiffness parameters were the same as for the previous simulations. Thus, the simulations with the smallest DV diameter had the highest mean velocity ($u_0 \approx 0.4$ m/s), while the simulations with the highest diameter had the lowest mean velocity ($u_0 \approx 0.1$ m/s). The behavior of $|\Gamma|$ corresponds well with our theoretical predictions; the lower the u_0 the higher the Γ regardless of g.

Finally, to assess the impact of a pressure dependent UV compliance C^{uv}, the UV pressure was calculated both numerically and analytically from Eq. (3), with a pressure dependent C^{uv} given by Eq. (5), and a constant UV compliance evaluated at the mean UV pressure from Eq. (5), respectively. Only modest root-mean-square (RMS) differences (RMS = 0.24 mmHg) between the analytical and the numerical solution were observed for a low compliant UV ($C^{uv} = 7.6 \cdot 10^{-3}$ ml/mmHg). For a more compliant UV ($C^{uv} = 2.1 \cdot 10^{-2}$ ml/mmHg), the RMS-value reduced to RMS = 0.03 mmHg. Parameter settings corresponding to higher UV compliance gave consistently lower RMS-values.

Discussion

In this paper we have developed a mathematical model to study the factors influencing pulsations in the UV.

We have demonstrated that both the stiffness parameter, i.e. the mechanical properties, and the size, i.e. the UV cross-sectional area, influence the index of pulsation IP of the pressure in the UV. In our model, the IP increases linearly with the stiffness factor of the UV, whereas the IP shows a nonlinear dependency with respect to the

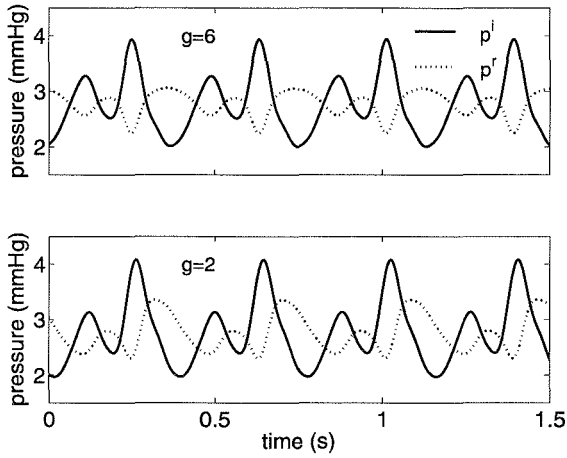

igure 7: The incident p^i and reflected p^r pressure waves for $g = 6$ (upper panel) and $g = 2$ ower panel).

V cross-sectional area (see Fig.4).

We have shown that a low compliant UV yielded an index of pulsation for the UV essure $IP = 0.21$, which is relatively high. Conversely, a compliant UV yielded a latively small index of pulsation: $IP = 0.02$ (see Fig. 3). Thus, our simulations show at although both flow and pressure in the DV were highly pulsatile, the UV pressure ay show little pulsatility, due to a relatively high UV compliance. This agrees well ith the pattern of pulsatile DV velocity concurrent with a more or less constant UV elocity in a normal pregnancy. During the first trimester however, pulsations in the V are present under normal physiological conditions (Rizzo et al., 1992; Nakai et al., 995; van Splunder et al., 1996). Based on the present model (Fig. 4) we believe that art of the reason for these pulsations is the low compliance due to the small dimensions the UV during the first part of the pregnancy.

UV pulsations have been associated with various pathological situations: hypoxic allenge (Lingman et al., 1986), asphyxial cardiomyopathy, congenital heart lesions Nakai et al., 1992), and elevated venous pressure (Reed et al., 1996). However, future arametric studies are needed to assess the relations between the parameters of Eqs. 4) and (15) and the various pathological situations. Nevertheless, our results are in greement with the findings of Reed et al., as an increase in the pressure may result in increased $IP(u^{uv})$, in spite of a constant $IP(p^{uv})$ due to the pressure dependency of (see Eq. (15)). Only pressure *differences* influence the mean velocity, thus a general crease in the pressure level does not affect the mean velocity. Consequently, for a nstant $u_0^{uv} = 0.2$ m/s and $\beta_{uv} = 4$, a UV pressure change from 2 to 12 mmHg will use changes in κ from 1.4 to 2.8.

UV pulsations have also been found late in the pregnancy in fetuses with no heart

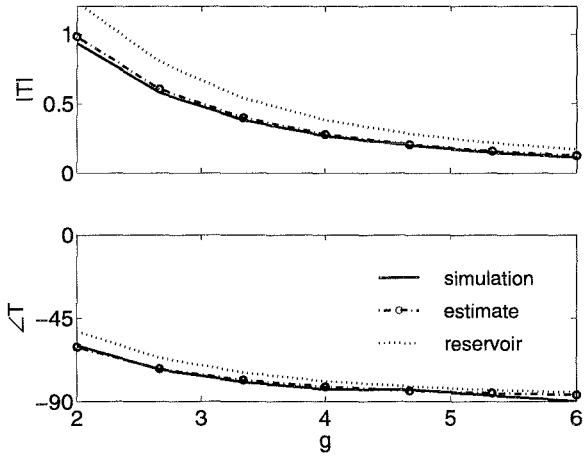

Figure 8: The first harmonic modulus (upper panel) and phase (lower panel) of the transmission factor T for a pure reservoir (dots), analytical estimate in Eq. (12) (dash-dots), and numerical simulation (solid).

anomalies, and with no sign of increased preload (Nakai et al., 1997a,b). In these cases the umbilical cord was either hypercoiled or compressed. Thus, we believe that the UV pulsations might be explained as a result of a reduced UV compliance as our results suggest.

By introducing the dynamic pressure term p^d in Eq. (6) we have shown that the mean velocity in the DV causes the reflection factor modulus $|\Gamma|$ to decrease(Fig 9). Only minor changes were observed for $\angle\Gamma$ and T. The analytical estimates of $|\Gamma|$ and $|T|$ differ from the simulated by 15% and 6% in mean, respectively. These estimates can be improved to 3% and 0.24% respectively, by including the $(u_0/c)^2$-term in the denominator of Eq. (8). The p^d-term, however, has little effect on the phase angle of Γ, and the phase angle for the "pure reservoir" and the analytical estimate both agree well with the simulated values. This was also the case for the phase angle of the transmission factor, whereas somewhat larger discrepancies were found for the $|T|$.

The impedance ratio Z_c/Z_{uv} influences how incident and reflected pressure components interact in the DV. For a large g (i.e. large $Z_c/|Z_{uv}|$) the phase angle of the reflection factor $\angle\Gamma \to -180°$ (Fig. 5), and thus decreases the IP of the DV pressure (Fig. 6). However, as the mean velocity u_0 reduces the $|\Gamma|$, there will be *no complete* cancellation of pulsations in the DV pressure even if $\angle\Gamma \to -180°$ (Fig. 7 upper panel). Further, the transmission factor is affected by changes in the impedance ratio; A large g-value (i.e. large $Z_c/|Z_{uv}|$) corresponds to a low $|T|$, and will yield a small IP of the UV pressure and vice versa. Thus, the Γ and the T factors should be regarded as important determinants of pulsation in the DV and the UV, respectively.

The model incorporates a pressure dependent compliance for the UV. However,

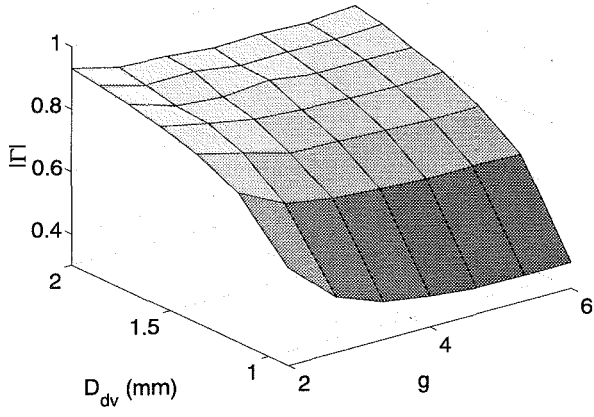

igure 9: The modulus of $|\Gamma|$ versus the UV/DV diameter ratio g and DV diameter D_{dv}.

ıe simulations with constant and pressure dependent UV compliance C^{uv}, showed ıat the UV pressure was estimated well with a constant C^{uv}. Thus, the analytical xpression of the pulsatility of the UV pressure IP in Eq. (14) served as a good and mple approximation.

In our model the DV flow was imposed in the UV without incorporating wave ropagation in the DV. The pulse wave velocity in the DV has been estimated to be in ıe range 1.0-3 m/s (Hellevik et al., 1999), and for a fundamental frequency of 2.5 Hz, ıis corresponds to wave lengths ranging from 0.4 m to 1.2 m, which is much larger than ıe physiological length of the DV of only a few centimeters (Kiserud et al., 1994b). hus, waves propagate within the DV almost instantaneously and the assumption that ıe flow along the DV equals the flow at the inlet is therefore reasonable. The c_{uv} of ıe UV was estimated to be in the same range as for the DV (Hellevik et al., 1999). particular, at a mean pressure of 6.5 mmHg, the pulse wave velocity $c_{uv} \approx 1.9$ m/s. or a characteristic UV length of $L_{uv} = 7$ cm, this corresponds to a transit time $\approx L_{uv}/c_{uv} \approx 37$ ms, which is relatively short compared to a physiological period of $= 0.4$ s. Thus, we believe that a lumped approach gives a fair description of the ıysics involved.

In conclusion, by means of a mathematical model we have shown that wave transission and reflection in the UV/DV bifurcation depend on the impedance ratio $/Z_{uv}$, as well as the ratio of the mean velocity and the pulse wave velocity in the V. The impedances depend, in turn, on the mechanical properties of the veins, the essure level, and the dimensions. Thus, we believe that the mathematical model esented in this paper is suitable for analyzing the factors involved in the occurrence pulsations in the UV.

Acknowledgments

Special thanks to Drs. Patrick Segers and Jan Vierendeels for comments and discussions. The text was revised by Nancy Lea Eik-Nes.

References

Avolio, A., 1980. Multi-branched model of the human arterial system. Med Biol Eng Comput 18, 709–718.

Fung, Y., 1984. Biodynamics. Circulation. Springer-Verlag New York Inc, New York.

Gembruch, U., Krapp, M., Baumann, P., 1995. Changes of venous blood flow velocity waveforms in fetuses with supraventricular tachycardia. Ultrasound Obstet Gynecol 5, 392–399.

Gudmundsson, S., Huhta, J. C., Wood, D. C., Tulzer, G., Cohen, A. W., Weiner, S., 1991. Venous doppler ultrasonography in the fetus with nonimmune hydrops. Am J Obstet Gynecol 164, 33–37.

Hasaart, T., de Haan, J., 1986. Phasic blood flow patterns in the common umbilical vein of fetal sheep during umbilical cord occlusion and the influence of autonomic nervous system blockade. J Perinat Med 14, 19–26.

Hecher, K., Ville, Y., Snijders, R., Nicolaides, K., 1995. Doppler studies of the fetal circulation in twin-twin transfusion syndrome. Ultrasound Obstet Gynecol 5, 318–324.

Hellevik, L. R., Kiserud, T., Irgens, F., Stergiopulos, N., Hanson, M., 1999. Mechanical properties of the fetal ductus venosus and the umbilical vein. Heart Vessels , in press.

Hellevik, L. R., Kiserud, T., Irgens, F., Ytrehus, T., Eik-Nes, S. H., 1998. Simulation of pressure drop and energy dissipation for blood flow in a human fetal bifurcation. J Biomech Eng 120, 455–462.

Huhta, J., 1997. Deciphering the hieroglyphics of venous doppler velocities. Ultrasound Obstet Gynecol 9.

Kiserud, T., 1997. In a different vein: the ductus venosus could yield much valuable information. Ultrasound Obstet Gynecol 9, 369–372.

Kiserud, T., 1999. Hemodynamics of the ductus venosus. Eur J Obstet Gynecol Reprod Biol , in press.

Kiserud, T., Crowe, C., Hanson, M., 1998. Ductus venosus agenesis prevents transmission of central venous pulsation to the umbilical vein in fetal sheep. Ultrasound Obstet Gynecol 11, 190–194.

Kiserud, T., Eik-Nes, S. H., Blaas, H. G., Hellevik, L. R., Simensen, B., 1994a. Ductus venosus blood velocity and the umbilical circulation in the seriously growth retarded fetus. Ultrasound Obstet Gynecol 4, 109–114.

iserud, T., Eik-Nes, S. H., Hellevik, L. R., Blaas, H.-G., 1993. Ductus venosus blood velocity changes in fetal cardiac diseases. J Matern Fetal Invest 3, 15–20.

iserud, T., Hellevik, L. R., Eik-Nes, S. H., Angelsen, B. A. J., Blaas, H. G., 1994b. Estimation of the pressure gradient across the fetal ductus venosus based on doppler velocimetry. Ultrasound Med Biomed 20, 225–232.

ngman, G., Laurin, J., Maršál, K., 1986. Circulatory changes in fetuses with imminent asphyxia. Biol Neonate 49, 66–73.

akai, Y., Imanaka, M., Nishio, J., Ogita, S., 1995. Umbilical cord venous pulsation in normal fetuses and its incidence after 13 weeks of gestation. Ultrasound Med Biomed 21, 443–6.

akai, Y., Imanaka, M., Nishio, J., Ogita, S., 1997a. Umbilical venous pulsation and regional circulatory disturbance. Ultrasound Med Biomed 23, 1165–9.

akai, Y., Imanaka, M., Nishio, J., Ogita, S., 1997b. Umbilical venous pulsation associated with hypercoiled cord in growth-retarded fetuses. Gynecol Obstet Invest 43, 6–7.

akai, Y., Miyazaki, Y., Matsuoka, Y., Matsumoto, M., Imanaka, M., Ogita, S., 1992. Pulsatile umbilical venous flow and its clinical significance. Br J Obstet Gynaecol 99, 977–80.

ennati, G., Redaelli, A., Bellotti, M., Ferrazzi, E., 1996. Computational analysis of the ductus venosus fluid dynamics based on doppler measurements. Ultrasound Med Biomed 22, 1017–1029.

eed, K. L., Chaffin, D. G., Anderson, C. F., 1996. Umbilical venous doppler velocity pulsations and inferior vena cava pressure elevations in fetal lambs. Obstet Gynecol 87, 617–620.

euss, M., Rudolph, A., Dae, M., 1983. Phasic blood flow patterns in the superior and inferior venae cavae and umbilical vein of fetal sheep. Am J Obstet Gynecol 145.

izzo, G., Arduini, D., Romanini, C., 1992. Umbilical vein pulsations: a physiologic finding in early gestation. Am J Obstet Gynecol 167, 675–677.

ergiopulos, N., Young, D., Rogge, T., 1992. Computer simulation of arterial flow with applications to arterial and aortic stenoses. J Biomech 25, 1477–1488.

n Splunder, I. P., Huisman, T. W., DeRidder, M. A., Wladimiroff, J. W., 1996. Fetal venous and arterial flow velocity wave forms between eight and twenty weeks of gestation. Pediatr Res 1996 40, 158–62.

n Splunder, I. P., Huisman, T. W. A., Stijnen, T., Wladimiroff, J. W., 1994. Presence of pulsations and reproducibility of waveform recording in the umbilical and left portal vein in normal pregnancies. Ultrasound Obstet Gynecol 4.

esterhof, N., Sipkema, P., Van den Bos, C., Elzinga, G., 1972. Forward and backward waves in the arterial system. Cardiovasc Res 6, 648–656a.

Paper IV

Wave propagation in the human fetal ductus venosus-umbilical vein bifurcation

Hellevik L.R.[1], Vierendeels J.[2], Kiserud T.[3],
Stergiopulos N.[4], Irgens F.[1], Dick E.[2],
Riemslagh K.[2], Verdonck P.[2]

[1]MTF/Div. Applied Mechanics,NTNU, Trondheim, Norway
[2]IBITECH, Univ. Gent, Belgium
[3]Dept. Obstetrics and Gynecology, Univ. Hosp. Bergen, Norway
[4]Biomedical Engineering Laboratory EPFL, Switzerland

Abstract

Pressure and flow pulsations in the fetal heart propagate through the precordial vein and the ductus venosus but are normally not transmitted into the umbilical vein. Pulsations in the umbilical vein do occur, however, in early pregnancy and in pathological conditions. Such transmission into the umbilical vein is not well understood. In this paper we developed a mathematical model to study the effect of ductus venosus tapering on the reflection factor. The one-dimensional mass and momentum equations were solved for the ductus venosus, whereas the umbilical vein was imposed as an upstream boundary condition. Further, the results of the present model were compared with those of a previously proposed lumped model. We found that the results of the previous lumped model agree well, both quantitatively and qualitatively, with the present model of the ductus venosus-umbilical vein bifurcation. The only effective reflection site in the ductus venosus was found to be the ductus venosus inlet. The tapered geometry of the ductus venosus was of minor importance. Differences between the ductus venosus inlet and outlet flow were also found to be minor for medium to large umbilical vein-ductus venosus diameter ratios.

Submitted for publication

Introduction

Pulsations in the fetal heart propagate through the precordial vein and the ductus venosus (DV) but are normally not transmitted into the umbilical vein (UV). Pulsations in the UV do occur, however, in early pregnancy and in pathological conditions (Lingman et al., 1986; Gudmundsson et al., 1991; Kiserud et al., 1993; Gembruch et al., 1995; Kiserud et al., 1994; Hecher et al., 1995). The DV is regarded as the main transmission line of pulsations between the fetal heart and the UV (Kiserud et al., 1998). However, the transmission of pulsations into the UV is still not well understood. We have previously proposed a lumped mathematical model aimed at describing the mechanical factors influencing UV pulsation (Hellevik et al., 1999b). In that paper the UV was modeled as a compliant reservoir and linked to the DV by assuming that the UV pressure was equal to the stagnation pressure at the DV inlet. We found that wave transmission and reflection in the DV depend on the impedance ratio between the UV and the DV, as well as on the ratio of the mean velocity and the pulse wave velocity in the DV. However, in this lumped model the DV inlet flow was imposed directly at the inlet of the DV, i.e. the wave propagation in the DV was not dealt with properly.

The aim of the present study was threefold: a) to develop a mathematical model for wave propagation in the UV/DV bifurcation based on the one-dimensional mass and momentum equations where the UV is imposed as a boundary condition (BC) in a characteristic manner; b) to study the effect of DV tapering on the reflection factor; c) to compare the results and analytical approximations of the previous lumped model with those of the present model.

Methods

The DV acts as a direct communication that shunts blood from the UV to the fetal heart (Fig. 1). Downstream from the DV, the fetal heart contracts periodically and generates pressure and flow waves that propagate in the negative flow direction into the DV and thereby give rise to the characteristic pulsatile DV velocity pattern. In analogy with our previous paper, the positive flow directions were taken as shown in Fig. 1. The UV flow *before* the bifurcation was denoted Q^b; the UV flow *after* the bifurcation, Q^a; the flow in the DV, Q.

The ductus venosus

The mathematical model for the DV was based on the one-dimensional equations obtained by integration of the governing mass and momentum equations over the cross-section of the vessel lumen (Raines et al., 1974):

$$\frac{\partial A}{\partial t} + \frac{\partial Q}{\partial x} = 0 \tag{1}$$

$$\frac{\partial Q}{\partial t} + \frac{\partial}{\partial x}\left(\frac{Q^2}{A}\right) = -\frac{A}{\rho}\frac{\partial p}{\partial x} + \frac{\pi D \tau_0}{\rho} \tag{2}$$

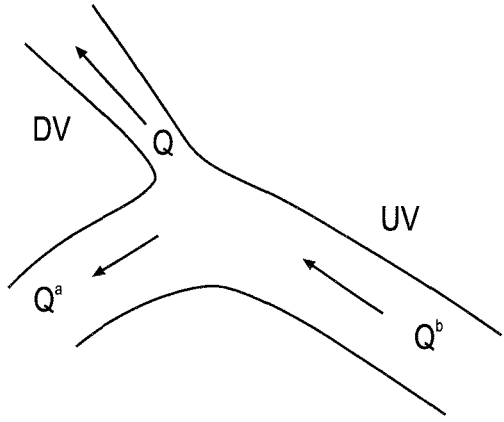

igure 1: Diagram of flows in the mathematical model of the umbilical vein (UV) and ductus nosus (DV). The flows in the UV before and after the bifurcation are denoted by Q^b and ^{a}, respectively, and the flow in the DV by Q.

here p is the pressure, A the cross-sectional area at the DV inlet, ρ the fluid density, the vessel diameter, and τ_0 the shear stress at the wall. The shear stress may be proximated by (Young and Tsai, 1973):

$$\tau_0 = -\frac{\rho}{\pi D}\left[\frac{8\pi\nu c_v}{A}\,Q + (c_u - 1)\frac{\partial Q}{\partial t}\right] \tag{3}$$

here c_u and c_v are functions of the Womersley number $\alpha = (D/2)\sqrt{\omega/\nu}$ (see e.g. cDonald, 1973). The kinematic viscosity and the angular frequency are denoted by and ω, respectively. By substitution of Eq. (3) into Eq. (2), a modified momentum uation was obtained:

$$c_u\frac{\partial Q}{\partial t} + \frac{\partial}{\partial x}\left(\frac{Q^2}{A}\right) + \frac{A}{\rho}\frac{\partial p}{\partial x} + B\frac{Q}{A} = 0 \tag{4}$$

ith $B = 8\pi\nu c_v$.

To complete the system of equations, a linear constitutive relation for the vessel all was introduced:

$$p = p(A) = p_s\left[1 + \beta\,(\frac{A}{A_s} - 1)\right] \tag{5}$$

here A_s is the DV cross-sectional area at the DV inlet at the reference pressure = 5 mmHg and β is the stiffness parameter. This constitutive equation is a first der Taylor expansion of a constitutive equation by Hellevik et al. (1999a). The iffness parameter was taken from sheep experiments and typical human fetal cross-ctional areas were used for the DV. The tapering of the DV was expressed by the V expansion factor $f = D_o/D_i$, where D_o and D_i are the outlet and inlet diameters the DV, respectively.

The umbilical vein

To account for a non-zero and time varying net inflow into the UV, $(Q^b - Q^a - Q)$, we introduced a compliance of the UV (C^{uv}). Conservation of mass at the bifurcation is expressed as:

$$\frac{\partial V}{\partial t} = C^{uv}\frac{\partial p^{uv}}{\partial t} = Q^b - Q^a - Q \tag{6}$$

where V and $C^{uv} = \partial V/\partial p$ are the UV volume and volume compliance, respectively. In accordance with our previous paper the UV length, L_{uv}, was assumed to be constant: $L_{uv} = 7$ cm, and the UV volume compliance C^{uv}, to be:

$$C^{uv} = \frac{A_s^{uv}\, L_{uv}}{\beta_{uv}\, p^{uv}}$$

where A_s^{uv} is the UV reference cross-sectional area, β_{uv} the UV stiffness parameter, and p^{uv} the UV pressure. Accordingly we assumed that p^{uv} equals the stagnation pressure at the DV inlet:

$$p^{uv} = p + p^d, \qquad p^d = \frac{1}{2}\rho\left(\frac{Q}{A}\right)^2 \tag{7}$$

From Eq. (6) and (7):

$$\frac{\partial A}{\partial t} + \frac{1}{2}\rho C\frac{\partial}{\partial t}\left(\frac{Q}{A}\right)^2 = \frac{C}{C^{uv}}\left(Q^b - Q^a - Q\right) \tag{8}$$

where the area compliance C, of the DV has been introduced from Eq. (5) as:

$$C = \frac{\partial A}{\partial p} = \frac{A_s}{\beta p_s} \tag{9}$$

Eq. (8) was imposed as a BC for the DV. Note that this differential equation links the fluid dynamics at the DV inlet to the UV, while the UV pressure has been eliminated; the only "UV parameter" in Eq. (8) is C^{uv}. Finally, the UV diameter D_{uv} was related to the DV diameter through the UV/DV diameter ratio: $g = D_{uv}/D_i$.

Numerical implementation

An explicit, one-step MacCormack scheme was employed to solve the discretized equations (Eq. (1) and Eq. (4)) (MacCormack, 1969). The DV was taken as a linearly diverging branch with respect to diameter and was discretized with 21 equidistant nodes and a physiological length of $L = 10^{-2}$ m. For all simulations, the Courant-Friedrich-Lewy number (Courant et al., 1928) was close to 1. The linearized and discretized version of Eq. (8) was imposed as a BC in a characteristic manner at the DV inlet. To solve the nonlinear system of equations for the BC at the DV inlet, a fixed number of subiterations (3) were performed for each time step.

Only one harmonic component, corresponding to the fundamental frequency in our revious study (Hellevik et al., 1999b), was imposed in the BC at the DV outlet. The lood was assumed to have a density $\rho = 1.05 \cdot 10^3$ kg/m^3 (Fernandez et al., 1976) and dynamic viscosity of $\mu = 4.2 \cdot 10^{-3}$ kg/ms (Jouppila et al., 1986). Further details on ie numerical implementation may be found in the appendix.

Results

o compare the reflection factors for the present and the previous model, the stiffness arameters for the DV and the UV were taken as $\beta = 2.2$ and $\beta_{uv} = 5.3$ (i.e. minimal β nd maximal β_{uv}), as this parameter configuration showed the largest variation in the hase angle $\angle\Gamma$ as a function of g. Simulations were performed for expansion factors =1.25, 1.5, and 2, while the DV inlet diameter was kept constant, $D_i = 0.9$ mm, to aintain a constant cross-sectional mean velocity at the DV inlet (Fig. 2).

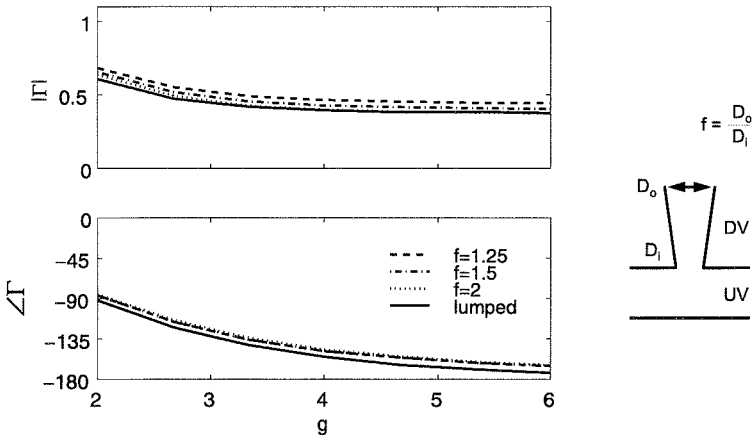

igure 2: Comparison between the previous lumped model (solid line) and the present model ith expansion factors f =1.25 (dashed-line), 1.5 (dash-dotted line), and 2 (dotted line) for ie first harmonic modulus $|\Gamma|$ (upper panel) and phase angle $\angle\Gamma$ (lower panel) of the reflection ctor as a function of the UV/DV diameter ratio g. For all simulations $D_i = 0.9$ mm.

The moduli $|\Gamma|$, for all simulation configurations were found to agree well with ie values from our previous lumped model; the RMS-values relative to the previous odel were all less than 0.08. Likewise, the phase angles $\angle\Gamma$, also corresponded well ith the previous results. However, the phase angles of the present model consistently nderestimated the absolute value of the phase angle, with RMS-values less than 10° r all configurations.

To illustrate the impact of the mean DV inlet velocity (u_0) and the UV/DV diameter atio g, simulations were carried out for g ranging from 2 to 6, with average stiffness

parameters for the UV and DV ($\beta_{uv} = 4.0$, $\beta = 3.4$), and with a fixed DV outlet diameter $D_o = 1.8$ mm (Fig. 3).

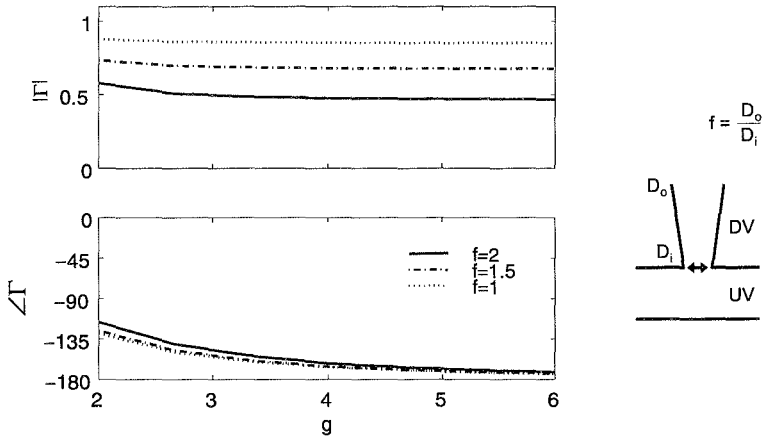

Figure 3: The first harmonic of the modulus $|\Gamma|$ (upper panel) and the phase angle $\angle\Gamma$ (lower panel) of the reflection factor as a function of the UV/DV diameter ratio g for three different expansion factors: $f = 1$ (dotted line), $f = 1.5$ (dash-dotted line), and $f = 2$ (solid line). For all simulations $D_o = 1.8$ mm.

For a fixed imposed flow and DV outlet diameter, the u_o was changed by employing the expansion factors: $f = 1, 1.5, 2$, i.e. by changing the DV inlet diameter. For these expansion factors the mean DV inlet velocities were: $u_0 \approx 0.1$ m/s, $u_0 \approx 0.3$ m/s, and $u_0 \approx 0.5$ m/s, respectively. The stiffness parameters were the same as for the previous set of simulations. From Fig. 3 we see that the lower the u_0 the larger the modulus of the reflection factor $|\Gamma|$, whereas the opposite was the case for the phase angle $\angle\Gamma$.

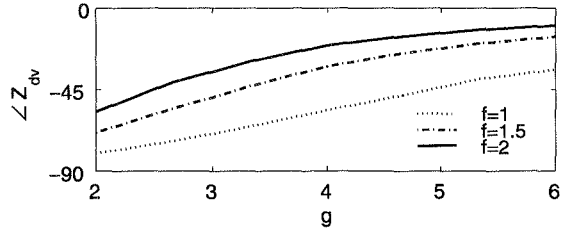

Figure 4: The phase angle $\angle Z_{dv}$ of the DV inlet impedance Z_{dv} as a function of the UV/DV diameter ratio g for three different expansion factors: $f = 1$ (solid line), $f = 1.5$ (dash-dotted line), and $f = 2$ (dotted line).

The corresponding phase angles $\angle Z_{dv}$ of the DV inlet impedance, are depicted in Fig. 4. For each expansion factor f we observe that $\angle Z_{dv}$ increases with increasing g.

ikewise, for a given UV/DV diameter ratio g, the $\angle Z_{dv}$ increases with increasing f. urther, the phase angles of the UV impedance $Z_{uv} = p_{uv}(\omega_1)/(-Q(\omega_1))$, were found be close to $-90°$, for all configurations, with a maximum RMS of 3.4°.

Finally, a range of simulations were performed, again with averaged stiffness parameters for the UV and DV, to investigate the differences between DV inlet and utlet flow (Fig. 5). The simulations were carried out for the three expansion factors: f=1.25, 1.5, 2, with the DV inlet diameter fixed: $D_i = 0.9$ mm. The upper panel of Fig. 5 shows the relative percentual difference of the flow amplitudes: $_{amp} = 100 \cdot (|Q_o| - |Q_i|)/|Q_i|$, as a function of g; the lower panel shows the corresponding angular difference: $d_{ang} = \angle Q_o - \angle Q_i$. The mean d_{amp} were 3.3%, 3.7%, and 0% for $f = 1.25$, 1.5, and 2, respectively. The corresponding mean values for d_{ang} ere 7.6°, 6.7°, and 5.8°, respectively.

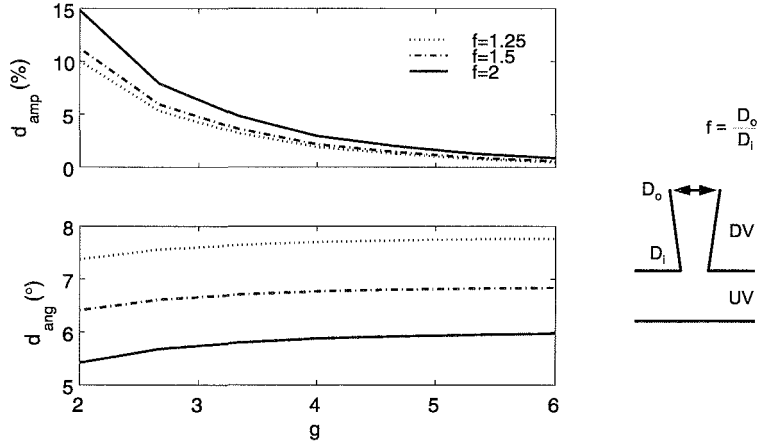

igure 5: The relative percentual difference d_{amp} between the amplitude of DV outlet and let flow (upper panel) as a function of the UV/DV diameter ratio g. The phase difference $_{ang}$ between DV outlet and inlet flow (lower panel).

The expansion factor was observed to have only a minor impact on the reflection ctor Γ, with maximum inter configuration RMS-values of 0.4% and 0.3° for $|\Gamma|$ and Γ, respectively.

Discussion

this study we have developed a mathematical model of wave propagation in the V/DV bifurcation. The model was developed to study the effect of DV tapering the reflection factor at the DV inlet and to compare the results and analytical proximations of a previous lumped model (Hellevik et al., 1999b) with those of the esent model.

For a wide range of UV/DV diameter ratios g and for various expansion factors f, only minor differences between the present and the previous model were found for the reflection factor Γ (Fig. 2). The differences for the reflection factor modulus $|\Gamma|$ had a maximum RMS-value of 0.08, whereas the RMS-value between the present and previous reflection factor phase angles $\angle\Gamma$ were less than 10° for all parameter configurations. The reason for these discrepancies may be due to the slightly different mathematical approach used to calculate the DV inlet pressure in the two methods: in the previous paper the DV inlet pressure is calculated from the UV pressure which occurs explicitly, whereas in the present paper the UV pressure is imposed implicitly with a differential equation (Eq. (8)) as the BC. Another factor that may have influenced the differences is that the mean DV inlet velocities for the present model configurations were slightly lower (u_0 = 0.43 m/s, 0.46 m/s, 0.47 m/s for f = 1.25, 1.5, 2, respectively) than that for the previous model (u_0 = 0.48 m/s). From the approximate analytical solution of Γ:

$$\Gamma = \frac{1 - (1 - u_0/c)\ Z_c/Z_{uv}}{1 + (1 + u_0/c)\ Z_c/Z_{uv}}$$

we may deduce that the lower the u_0 the higher the $|\Gamma|$; this agrees well with the fact that $|\Gamma|$ is highest for the lowest u_0, i.e. f = 1.25.

Further, we found that with the DV inlet diameter and imposed flow pattern fixed, changes in the expansion factor f do not influence the reflection factor at the DV inlet. This was found to be true for both extreme and normal stiffness parameters for the UV and DV. On the contrary, for a fixed DV outlet diameter, changes in the expansion factor, i.e. the DV inlet diameter, do influence the reflection factor significantly. These results correspond well with the approximate analytical solution for Γ in our previous paper, where it was shown that a reduced DV mean velocity will increase the $|\Gamma|$. From this we conclude: the only effective reflection site in the DV is located at the DV inlet; DV tapering *per se* is of minor importance for the DV inlet reflection factor.

Further, the calculations of the $\angle Z_{dv}$ (Fig. 4) also correspond well with the approximate analytical solution:

$$Z_{dv} \approx \frac{u_0}{c}\ Z_c + Z_{uv}$$

where Z_{uv} denotes the imaginary UV impedance and $Z_c/|Z_{uv}| \propto g^2$. From the approximation one may deduce that an increase in g yields an increase in $\angle Z_{dv}$ and that an increase in the DV inlet cross-sectional area, i.e. reduction in f, corresponds to a reduction in the $\angle Z_{dv}$.

For medium to large UV/DV diameter ratios g, the relative difference in flow amplitude d_{amp} was found to be less than 10%, while for small g the relative difference increased. Still, d_{amp} was always positive demonstrating larger flow pulsations at the outlet than at the inlet. Although not directly comparable, these findings agree with previous investigations in vivo where the *velocity pulsation* at the DV outlet was found to be larger than that at the DV inlet (Pennati et al., 1997; Acharya and Kiserud, 1999). In this case the differences between the indices of pulsation at the DV inlet and

ıe DV outlet may also be ascribed to changes in the respective velocity profiles. In articular the angle between the DV and the UV affect the DV inlet velocity profile Pennati et al., 1997), whereas the DV expansion factor f will influence the velocity rofile at the DV outlet through diffusor effects (White, 1988). Further, the results of ıe present study indicate that the larger the DV expansion factor f, the larger the elative amplitude difference d_{amp}. These effects can not be ascribed to viscous ef- cts, since the amplification increases with f and should thus have caused less viscous amping; the opposite, however, was observed. Furthermore, viscous effects should not epend upon the impedance ratio. Thus, the amplitude amplification effects must be scribed to wave propagation phenomena.

Likewise, the phase angle differences were found to be positive and less than 8° for l parameter configurations tested. This implies that the DV outlet flow pulsations ere just barely leading the DV inlet flow. The results indicate that the larger the xpansion factor the smaller the the phase lag. By contrast, in absence of reflections, larger expansion factor corresponds to an increased averaged DV cross-sectional area nd consequently to a reduced pulse wave velocity accompanied by an increased phase g. Thus, as we observed that an increase in expansion factor was accompanied by decrease in phase lag, this phenomenon has to be ascribed to reflections at the DV let. We therefore conclude that the differences between the DV inlet and outlet ows for both amplitude and phase were found to be minor for medium to large for V/DV diameter ratios. Consequently, we maintain the proposition from our previous aper: the lumped model the UV/DV bifurcation gives a fair description of the physics volved (Hellevik et al., 1999b).

The pressure-area relationship of the DV and the UV have recently been proven to e nonlinear (Hellevik et al., 1999a), i.e. pressure is a nonlinear function of area. In ıe present study we have, for simplicity, assumed a linear pressure-area relationship. owever, based on our previous study where no considerable impact of nonlinear con- itutive equations were found (Hellevik et al., 1999b), we believe that the influence f nonlinearity in the present model would be minor. Further, the results from the udy on mechanical properties indicate that the stiffness parameter at the DV outlet ay be different from that at the DV inlet. Such possible spatial variations in the echanical properties of the DV have not been incorporated in the present study and ıould therefore be accounted for in future studies.

In conclusion: we have shown that the results of the previous lumped model agree ell, both quantitatively and qualitatively, with the present model of the UV/DV ifurcation. Furthermore, the tapered geometry of the DV was found to be of minor nportance. Differences between the DV inlet and outlet flow were also found to be inor for medium to large UV/DV diameter ratios.

Acknowledgments

he help of Ir. Manuel Vandevoorde with BC implementation is gratefully appreciated. he text was revised by Nancy Lea Eik-Nes.

References

Acharya, G., Kiserud, T., 1999. Pulsations of the ductus venosus blood velocity and diameter are more pronounced at the outlet than at the inlet. Eur J Obstet Gynecol Reprod Biol , in press.

Anderson, D., Tannehill, H., Pletcher, R., 1984. Computational fluid mechanics and heat transfer. Hemisphere publishing Co., New York.

Courant, R., Friedrichs, K. O., Lewy, H., 1928. Über die Differenzengleichungen der Mathematischen Physik. Math Ann 100, 32.

Fernandez, R., De Witt, K., Botwin, M., 1976. Pulsatile flow through a bifurcation with applications to arterial disease. J Biomech 9, 575.

Gembruch, U., Krapp, M., Baumann, P., 1995. Changes of venous blood flow velocity waveforms in fetuses with supraventricular tachycardia. Ultrasound Obstet Gynecol 5, 392–399.

Gudmundsson, S., Huhta, J. C., Wood, D. C., Tulzer, G., Cohen, A. W., Weiner, S., 1991. Venous doppler ultrasonography in the fetus with nonimmune hydrops. Am J Obstet Gynecol 164, 33–37.

Hecher, K., Ville, Y., Snijders, R., Nicolaides, K., 1995. Doppler studies of the fetal circulation in twin-twin transfusion syndrome. Ultrasound Obstet Gynecol 5, 318–324.

Hellevik, L. R., Kiserud, T., Irgens, F., Stergiopulos, N., Hanson, M., 1999a. Mechanical properties of the fetal ductus venosus and the umbilical vein. Heart Vessels , in press.

Hellevik, L. R., Stergiopulos, N., Kiserud, T., Rabben, S., Eik-Nes, S. H., Irgens, F., 1999b. A mathematical model of umbilical venous pulsation. Submitted .

Jouppila, P., Kirkinen, P., Puukka, R., 1986. Correlation between umbilical vein blood flow and umbilical blood viscosity in normal and complicated pregnancies. Arch Gynecol 237, 191–197.

Kiserud, T., Crowe, C., Hanson, M., 1998. Ductus venosus agenesis prevents transmission of central venous pulsation to the umbilical vein in fetal sheep. Ultrasound Obstet Gynecol 11, 190–194.

Kiserud, T., Eik-Nes, S. H., Blaas, H. G., Hellevik, L. R., Simensen, B., 1994. Ductus venosus blood velocity and the umbilical circulation in the seriously growth retarded fetus. Ultrasound Obstet Gynecol 4, 109–114.

Kiserud, T., Eik-Nes, S. H., Hellevik, L. R., Blaas, H.-G., 1993. Ductus venosus blood velocity changes in fetal cardiac diseases. J Matern Fetal Invest 3, 15–20.

Lingman, G., Laurin, J., Maršál, K., 1986. Circulatory changes in fetuses with imminent asphyxia. Biol Neonate 49, 66–73.

MacCormack, R., 1969. The effect of viscosity in hypervelocity impact cratering. AIAA

paper , 69–354.

cDonald, D. A., 1973. Blood Flow in Arteries. The Camelot Press, Southampton, second edn.

ennati, G., Bellotti, M., Ferrazzi, E., Rigano, S., Garberi, A., 1997. Hemodynamic changes across the human ductus venosus: a comparison between clinical findings and mathematical calculations. Ultrasound Obstet Gynecol 9, 383–391.

aines, J., Jaffrin, M., Shapiro, A., 1974. A computer simulation of arterial dynamics in the human leg. J Biomech 7, 77–91.

hite, F. M., 1988. Fluid Mechanics, McGraw-Hill International Editions, New York, chap. 6.9. Mechanical Engineering Series. Second edn.

oung, D., Tsai, F., 1973. Flow characteristics in models of arterial stenoses-II. unsteady flow. J Biomech 6, 547–559.

ppendix

umerical implementation

ternal scheme

y introducing the compliance $C = \partial A/\partial p$, which is readily obtained from the conitutive Eq. (5), the pressure was eliminated from Eq. (4). Further, we adopted the ondensed notation:

$$\mathbf{M} = \begin{bmatrix} 0 & 1 \\ \dfrac{A}{c_u C \rho} - \dfrac{Q^2}{c_u A^2} & \dfrac{2Q}{c_u A} \end{bmatrix} = \begin{bmatrix} 0 & 1 \\ \dfrac{c^2 - u^2}{c_u} & \dfrac{2u}{c_u} \end{bmatrix}$$

ith $u = Q/A$ and $c^2 = A/(C\rho)$, and:

$$\mathbf{u} = \begin{bmatrix} A \\ Q \end{bmatrix}, \quad \frac{\partial \mathbf{F}}{\partial x} = \mathbf{M}\,\frac{\partial \mathbf{u}}{\partial x}, \quad \mathbf{b} = \begin{bmatrix} 0 \\ -f \end{bmatrix}$$

he governing equation system Eq. (1) and (4) may then be represented:

$$\frac{\partial \mathbf{u}}{\partial t} + \frac{\partial \mathbf{F}}{\partial x} = \mathbf{b} \tag{10}$$

which allows for a generic Forward-Backward MacCormack discretization (MacCorack, 1969) of the governing equation in a cell-vertex fashion with non-overlapping ontrol volumes (Fig: 6):

orward step

$$\mathbf{u}_i^{\overline{n+1}} = \mathbf{u}_i - \Delta t \left(\frac{\mathbf{F}_{i+1}^n - \mathbf{F}_i^n}{\Delta x} + \frac{\mathbf{b}_{i+1}^n + \mathbf{b}_i^n}{2} \right)$$

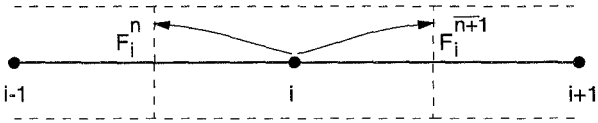

Figure 6: Vertex-centered MacCormack scheme formulation with non-overlapping control volumes.

Backward step

$$\mathbf{u}_i^{n+1} = \frac{1}{2}\left[\mathbf{u}_i^n + \overline{\mathbf{u}_i^{n+1}} - \Delta t\left(\frac{\overline{\mathbf{F}_i^{n+1}} - \overline{\mathbf{F}_{i-1}^{n+1}}}{\Delta x} + \frac{\overline{\mathbf{b}_i^{n+1}} + \overline{\mathbf{b}_{i-1}^{n+1}}}{2}\right)\right]$$

Riemann invariants

By using the Split Coefficient Matrix method (SCM) (Anderson et al., 1984) a splitting of $\mathbf{M} = \mathbf{R}\Lambda\mathbf{L}$ was obtained, where Λ is the diagonal eigenvalue matrix of $\mathbf{M}$, and $\mathbf{L}$ and $\mathbf{R}$ the left and right eigenmatrices, respectively. Finally, the right eigenmatrix was taken as $\mathbf{R} = \mathbf{L}^{-1}$, and the splitting was introduced into Eq. (10) yielding:

$$\mathbf{L}\,\frac{\partial \mathbf{u}}{\partial t} + \Lambda\,\mathbf{L}\,\frac{\partial \mathbf{u}}{\partial x} = \mathbf{L}\,\mathbf{b} \tag{11}$$

The eigenvalues of $\mathbf{M}$ were found to be:

$$\lambda_i = \frac{u \pm c^*}{c_u} \tag{12}$$

where the plus and minus signs are associated with subscript $i = 1, 2$, respectively, and $c^* = \sqrt{(1 - c_u)\,u^2 + c_u\,c^2}$. The corresponding eigenvectors were found to be:

$$\mathbf{l}_i = \begin{bmatrix} 1 \\ l_{i2} \end{bmatrix} \tag{13}$$

where $l_{i2} = (u \pm \sqrt{(1 - c_u)u^2 + c_u c^2})/(C(c^2 - u^2))$. The products $\mathbf{l}_i \cdot \mathbf{u}$ with $i = 1, 2$, are the Riemann invariants; the Eq. (11) is a system of the classical wave-equations, where the Riemann invariants propagate with wave speed λ_i. When the Riemann invariants are accounted for in the implementation of the BCs, they are said to be *imposed in a characteristic manner.*

Boundary conditions

To impose the BCs, the variables were advanced in time for the whole field, including the boundaries, to generate an update. The BCs were not included in this update but imposed afterwards in a characteristic manner for both the forward and the backward

tep at the DV inlet. That is, the convected Riemann invariant, which is a combination f A and Q, was filtered out simultaneously with the imposition of the BC.

In general, the BC may be given as a combination of the two primary variables: $(A,Q,t)\ A + b(A,Q,t)\ Q = g(t)$, where a, b and g are prescribed functions. The BC and the Riemann combination will then generally constitute a nonlinear equation ystem from which the new values A_N^{n+1} and Q_N^{n+1} may be obtained. Below we give a etailed description of how the inlet boundary was treated.

The BC at the outlet was imposed implicitly. Flow was imposed for inviscid simu-ations, whereas pressure was used for viscous simulations as imposition of flow in this ase lead to divergence.

nlet boundary

At the inlet, the DV model was coupled with the UV model represented by Eq. (8). A orward Euler discretization of Eq. (8) yielded:

$$A^{n+1} + \frac{\rho C}{2}\left(\frac{Q^{n+1}}{A^{n+1}}\right)^2 = A + \frac{\rho C}{2}\left(\frac{Q}{A}\right)^2 + \Delta t\,\frac{C}{C^{uv}}\left(Q^b - Q^a - Q\right) \tag{14}$$

here the superscript n for the present time step was omitted for clarity. This is a onlinear equation which we linearized in the following manner:

$$A^{n+1} + \frac{\rho C}{2}\frac{Q}{A^2}\,Q^{n+1} = A + \frac{\rho C}{2}\left(\frac{Q}{A}\right)^2 + \Delta t\,\frac{C}{C^{uv}}\left(Q^b - Q^a - Q\right) \tag{15}$$

r in a more compact form:

$$\tilde{m}_{11}\,A^{n+1} + \tilde{m}_{12}\,Q^{n+1} = k_1 \tag{16}$$

here:

$$\tilde{m}_{11} = 1, \quad \tilde{m}_{12} = \frac{\rho C}{2}\frac{Q}{A^2}$$

$$k_1 = A + \frac{\rho C}{2}\left(\frac{Q}{A}\right)^2 + \Delta t\,\frac{C}{C^{uv}}\left(Q^b - Q^a - Q\right)$$

The vertex at the DV inlet was located at the physical boundary and associated ith a half control volume. In the *forward step* we first generated an update, denoted y a star, for the half control volume at the inlet with contributions from both the flux nd source terms:

$$\mathbf{u}_0^{\overline{n+1}*} = \mathbf{u}_0^n - \frac{\Delta t}{\Delta x/2}(\mathbf{F}_1^n - \mathbf{F}_0^n) + \Delta t\,(\mathbf{b}_1^n + \mathbf{b}_0^n)$$

ubsequently, the left-traveling Riemann invariant was filtered out from the internal eld:

$$\mathbf{l}_2 \cdot \mathbf{u}_0^{\overline{n+1}} = \mathbf{l}_2 \cdot \mathbf{u}_0^{\overline{n+1}*} = k_2 \tag{17}$$

which on component form yields:

$$A_0^{\overline{n+1}} + l_{22}\, Q_0^{\overline{n+1}} = k_2 \tag{18}$$

Both Eq. (16) and Eq. (18) have to be satisfied simultaneously and thus form an equation system which we represented:

$$\tilde{\mathbf{M}}\mathbf{u}^{\overline{n+1}} = \mathbf{k} \tag{19}$$

where $\tilde{m}_{ij}$ and k_i denote the components of the matrix $\tilde{\mathbf{M}}$ and vector $\mathbf{k}$, respectively; $\tilde{m}_{21} = 1$ and $\tilde{m}_{22} = l_{22}$. Thus, the characteristic imposition of the BC at the DV inlet resulted in the nonlinear equation system Eq. (19). A fixed number of three subiterations were performed to solve the nonlinear system of equations. The nonlinear terms in $\tilde{\mathbf{M}}$ and the eigenvector were linearized by using the values of the primary variables at the previous subiteration level.

Finally, the procedure was repeated for the *backward step* where the source term was disregarded following the convention for the fluxes. First the update was generated:

$$\begin{aligned} \mathbf{u}_0^{n+1*} &= \frac{1}{2}\left[\mathbf{u}_0^n + \mathbf{u}_0^{\overline{n+1}} - \frac{\Delta t}{\Delta x/2}(\mathbf{F}_0^{\overline{n+1}} - \mathbf{F}_0^{\overline{n+1}})\right] \\ &= \frac{1}{2}\left[\mathbf{u}_0^n + \mathbf{u}_0^{\overline{n+1}}\right] \end{aligned}$$

This update was subsequently combined with the Riemann invariant in the same manner as for the forward step.

Paper V

Paper V

Mechanism of pulmonary venous pressure and flow waves

Hellevik L.R.[1], Segers P.[2], Stergiopulos N.[3],
Irgens F.[1], Verdonck P.[2], Thompson C.R.[4],
Lo K.[4], Miyagishima R.T.[4], Smiseth O.A.[5]

[1]MTF/Div. Applied Mechanics,NTNU, Trondheim, Norway
[2]IBITECH, Univ. Gent, Belgium
[3]Biomedical Engineering Laboratory EPFL, Switzerland
[4]St.Paul's Hospital, Vancouver BC, Canada;
[5]Rikshospitalet, Oslo, Norway.

Abstract

The pulmonary venous systolic flow wave has been attributed both to left heart phenomena, such as left atrial relaxation and descent of the mitral annulus, and to propagation of the pulmonary artery pressure pulse through the pulmonary bed from the right ventricle. In this study we hypothesized that all waves in the pulmonary veins originate in the left heart, and that the gross wave features observed in measurements can be explained simply by wave propagation and reflection. A mathematical model of the pulmonary vein was developed; the pulmonary vein was modeled as a lossless transmission line and the pulmonary bed by a 3-element lumped parameter model accounting for viscous losses, compliance, and inertia. We assumed that all pulsations originate in the left atrium, the pressure in the pulmonary bed being constant. The model was validated using pulmonary vein pressure and flow recorded 1 cm proximal to the junction of the vein with the left atrium during aortocoronary bypass surgery For a pressure drop of 6 mmHg across the pulmonary bed, we found a transit time from the left atrium to the pulmonary bed of $\tau \approx 150$ ms, a compliance of the pulmonary bed of $C \approx 0.4$ ml/mmHg, and an inertance of the pulmonary bed of 1.1 mmHg s^2/ml. The pulse wave velocity of the pulmonary vein was estimated to be $c \approx 1$ m/s. Waves, however, travel both towards the left atrium and towards the pulmonary bed. Waves traveling towards the left atrium are attributed to the reflections caused by the mismatch of impedance of line (pulmonary vein) and load (pulmonary bed). Wave intensity analysis was used to identify a period in systole of net wave propagation towards the left atrium for both measurements and model. The linear separation technique was used to split the pressure into one component traveling from the left atrium to the pulmonary bed and a reflected component propagating from the pulmonary bed to the left atrium. The peak of the reflected pressure

wave corresponded well with the positive peak in wave intensity in systole. We conclude that the gross features of the pressure and flow waves in the pulmonary vein can be explained in the following manner: the waves originate in the LA and travel towards the pulmonary bed, where reflections give rise to waves traveling back to the LA. Although the gross features of the measured pressure were captured well by the model predicted pressure, there was still some discrepancy between the two. Thus, other factors initiating or influencing waves traveling towards the LA can not be excluded.

To appear in *Heart and Vessels* 1999

ntroduction

he normal flow pattern in extra parenchymal pulmonary veins (PV) is characterized antegrade flow peaks during systole (S waves) and early diastole (D wave), and by rongly reduced or retrograde flow (R wave) into the PV during atrial contraction late diastole (Fig. 1). The pulmonary D wave is caused by LV relaxation and the

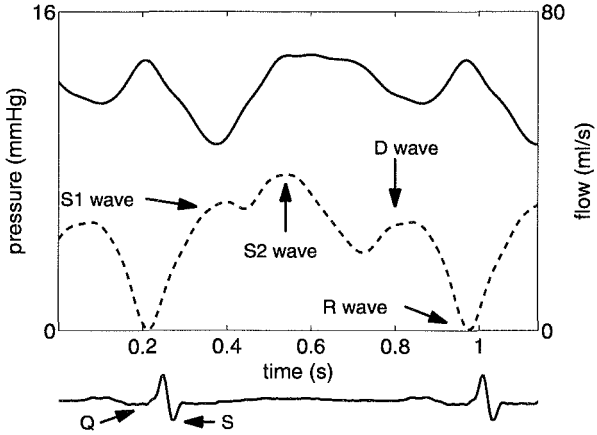

igure 1: Measurements of pressure (solid line; left axis) and flow (dashed line; right axis) the pulmonary vein. Below: corresponding ECG.

bsequent opening of the mitral valve and pressure reduction in the left atrium (LA). he factors that determine the D wave are largely the same as those determining early ansmitral filling (Nishimura et al., 1990).

The pulmonary venous S wave is composed of an early (S1) and a late (S2) systolic ow pulse. The origin of the pulmonary venous S wave, and in particular the S2 wave, not clear. Several experimental studies in dog models conclude that the S wave is enerated predominantly by transmission of the right ventricular flow pulse through ie pulmonary bed (Caro and McDonald, 1961; Pinkerson, 1967; Maloney et al., 1968). owever, other studies, also done in dog models, conclude that the systolic flow pulse the PV is caused by pressure changes in the (LA) (Morgan et al., 1966; Rajagopalan al., 1979). The latter has been attributed to a combined effect of atrial relaxation and stolic descent of the atrioventricular plane, both of which decrease atrial pressure.

To our knowledge, the effects of wave propagation and reflection have not been ldressed to explain the wave features in the PV. In this study we hypothesize that l waves in the pulmonary veins originate in the left heart, and we test this hypothesis means of a mathematical model. Our hypothesis implies that the S2 wave which opagates towards the LA, evident by wave intensity (WI) analysis, can be explained a reflected LA wave.

Methods

The present study was part of a more extensive study on pulmonary venous flow in patients undergoing aortocoronary bypass surgery. The study was approved by the ethics committees at St.Paul's Hospital and the University of British Columbia. All patients gave written informed consent. The measurements were done after the chest had been opened by a median sternotomy and just prior to initiation of extracorporeal circulation. Pulmonary vein flow was recorded by an ultrasonic transit time flow probe (Transonics Systems, Ithaca, NY) placed on the right lower pulmonary vein close to its entrance into the left atrium. The probe was connected to a flowmeter (Transonics Systems, Ithaca, NY). Pulmonary vein pressure was recorded by a micromanometric catheter (model SSD-827, Millar Instruments, Houston, TX, USA) in the pulmonary vein less than 2 cm from its entrance into the left atrium. The analysis in this study was based on measurements on a patient with representative pressure and flow traces.

Further, a mathematical model of the PV and the pulmonary bed was established. The PV was modeled as a lossless transmission line (TL) with a characteristic impedance Z_c, a transit time τ, and a pulse wave velocity c. The pulmonary bed was modeled by a 3-element lumped parameter model that took viscous losses R_p, compliance C, and inertia L into account (Fig. 2).

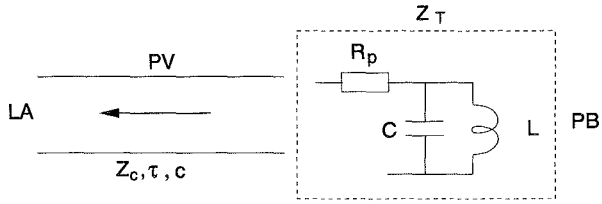

Figure 2: Schematic representation of the model. The pulmonary vein (PV) is modeled as a transmission line (TL) with characteristic impedance Z_c, transit time τ, and pulse wave velocity c. In the pulmonary bed model R_p accounts for peripheral resistance, C for compliance, and L for inertance of the blood.

A constant driving pressure at the lung capillaries was represented by $p_c = \overline{p} + \Delta p$, where $\overline{p}$ is the mean pressure at the LA entrance, and Δp is the pressure drop across the pulmonary bed. The mean flow direction was taken as positive, i.e. flow towards the LA is positive. The input impedance of the model may be presented as (Milnor, 1989):

$$Z_i = Z_c \frac{1 + \Gamma e^{-i2\omega\tau}}{1 - \Gamma e^{-i2\omega\tau}} \tag{1}$$

where the reflection coefficient Γ is:

$$\Gamma = \frac{Z_T - Z_c}{Z_T + Z_c} \tag{2}$$

ith the terminal impedance Z_T representing the impedance of the pulmonary bed:

$$Z_T = R_p + \frac{i\omega L}{1 - \omega^2 LC} \tag{3}$$

he model had five parameters that had to be estimated: Z_c, R_p, τ, L, and C. The haracteristic impedance Z_c was estimated from the measurements by averaging the nput impedance modulus for medium to high frequencies (3-10 harmonics) (Murgo al., 1980). In order to further reduce the number of parameters, R_p was taken as $p/\overline{Q}$. We varied Δp from 2 to 10 mmHg by increments of 2 mmHg, and the mean ressure $\overline{p}$ and flow $\overline{Q}$ were obtained from the measurements.

The remaining three parameters τ, L and C, were estimated for each Δp-value, by inimizing the cost function: $\sum(p_e - p_m)^2$, where p_e and p_m denote estimated and easured pressures, respectively. The estimated pressure was obtained by using the easured flow and the model input impedance. The procedure was implemented in ATLAB, utilizing a Nelder-Mead type simplex search method for non-linear mini- ization. The goodness of fit was evaluated as:

$$RMS = \sqrt{\frac{\sum(p_e - p_m)^2}{N}}$$

here N is the number of samples.

For a given cross-sectional area A and blood density ρ, estimates for pulse wave elocity c and PV length l may be derived from:

$$c = \frac{Z_c A}{\rho}, \quad l = c\,\tau$$

hen estimates for Z_c and τ are available.

The linear separation technique was used to separate the measured and computed ressure waves into one component p_{ap}, propagating from the LA to the pulmonary ed, and a reflected component p_r, propagating towards the LA Westerhof et al. (1972).

$$p_{ap} = \frac{p - Z_c Q}{2}, \quad p_r = \frac{p + Z_c Q}{2} \tag{4}$$

ote that the unconventional signs in the splitting equations are due to the fact that he reflected wave propagates in the positive flow direction. The splitting enabled us o estimate the the transit time from the measurement location to a point of reflection, s the time-lag between the peaks in the p_{ap} and the p_r divided by two.

Finally, WI analysis was used to identify the direction of net rate of energy transport uring the heart cycle. This concept, based on theory for acoustic intensity (Lighthill, 978), was first introduced by Parker et al. in arterial dynamics (Parker et al., 1988; arker and Jones, 1990; Jones et al., 1994). Any finite wave can be analyzed as the um of "wavelets", defined as infinitesimal changes in pressure and flow. Along the haracteristic directions the flow is steady and by following the convention for flow

direction in the present paper, the relationship between wavelets of pressure (dp) and flow (dQ) satisfies:

$$dp_{ap} = -Z_c\, dQ_{ap}, \quad dp_r = Z_c\, dQ_r \tag{5}$$

where the subscripts ap and r, in the same manner as above, denote waves propagating from the LA to the pulmonary bed and reflected waves, respectively. The instantaneous changes in p and Q are the result of intersecting wavelets in the ap-direction and those in the opposite direction at the time and location of measurements:

$$dp = dp_{ap} + dp_r, \quad dQ = dQ_{ap} + dQ_r \tag{6}$$

The wave intensity $WI = dp\, dQ$, is the rate of energy flux associated with the wavelet, and from Eq. (5) and Eq. (6) the following expression for WI may be derived:

$$WI = \frac{-dp_{ap}^2 + dp_r^2}{Z_c} \tag{7}$$

Thus, the WI has the useful property that waves propagating in the ap-direction make a negative contribution to the WI, whereas waves traveling in the opposite direction make a positive contribution. Note that for convenience the WI has been derived with flow and *not* velocity as the primary variable in the present paper. Thus, the WI dimension in the present study is W and not $W\,s^{-2}$ as in (Parker et al., 1988; Parker and Jones, 1990; Jones et al., 1994); i.e. strictly speaking it does not represent wavelet *intensity* but rather wavelet power.

Results

The characteristic impedance of the PV was estimated as: $Z_c = 0.1$ mmHg s/ml. From Z_c, the pulse wave velocity c in the PV can be estimated as: $c \approx 1$ m/s, for a typical cross-sectional area A=0.8 cm^2 and blood density, $\rho = 1.05 \cdot 10^3$ kg/m^3. The estimated model parameters for a range of Δp-values with their corresponding RMS-values, are listed in Table 1. In Fig. 3 the measured and the model predicted pressures are depicted for $\Delta p = 6$ mmHg. From the pulse wave velocity above and a $\tau = 0.15$ s corresponding to a $\Delta p = 6$ mmHg, the PV length was estimated as $l = 15$ cm.

Δp (mmHg)	τ (s)	C (ml/mmHg)	R_p (mmHg s/ml)	L (mmHg s^2/ml)	RMS
2	0.12	0.6	0.08	1.3	1.0
4	0.14	0.4	0.16	1.2	1.0
6	0.15	0.4	0.24	1.1	1.0
8	0.16	0.4	0.32	0.9	1.0
10	0.16	0.4	0.4	0.9	1.0

Table 1: Estimated model parameters for a range of pressure drops across the pulmonary bed (Δp).

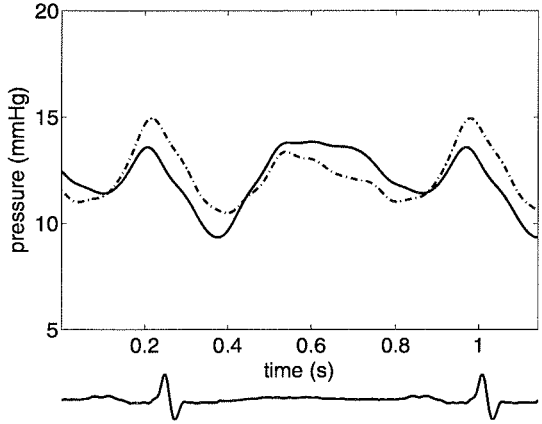

igure 3: Measured (solid line) and model predicted pressure (dash-dotted line) for Δp = mmHg. Below: corresponding ECG.

The presence of a net energy wave transport towards the LA during systole is ident as shown in the upper panel of Fig. 4 by the positive WI peak at t = 0.485 s. The lower panel of Fig. 4 shows the pressure decomposed into one component $_p$ propagating from the LA to the pulmonary bed, and a reflected component p_r opagating towards the LA. The onset of waves propagating towards the pulmonary ed caused by the LA contraction during diastole is observed both in the peak of p_{ap} t=0.21 s, and in the negative WI in the upper panel. A reflected pulse is observed 335 s later, at t=0.545 s. This corresponds to a transit time of $\tau = 0.168$ s.

Discussion

this paper we have shown that the gross features of the pressure and flow waves in e PV may be explained by a simple model, using the principles of wave propagation. particular, the presence of a net rate of energy transport towards the LA during stole, may be explained as a reflection of the wave in the direction of the pulmonary ed initiated in late diastole by the contraction of the LA. This follows from the greement between the positive peak in the WI wave in upper panel of Fig.4 and the flected wave in the lower panel of Fig.4. Therefore, wave transmission through the lmonary bed is not needed to explain the positive WI wave.

We observed a good correspondence between the two independent transit time es- mates, predicted by the model and the wave splitting procedure, respectively. Values r the transit time τ, the compliance C, and the inertance L were found to be within narrow range for variations of the pressure drop across the pulmonary bed (Δp) nging from 4 to 10 mmHg (Table 1). These pressure drops correspond with values und in physiology textbooks (West, 1990). Further, the τ for $\Delta p = 6 - 10$ mmHg rresponds well with the transit time predicted from the wave splitting procedure. hus, we believe that a pressure drop in this range is the best choice.

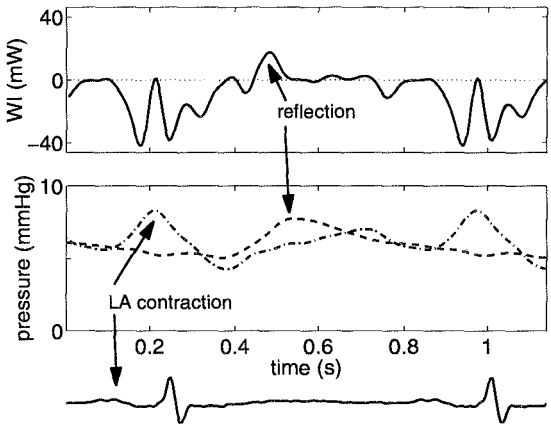

Figure 4: Upper panel: wave intensity (WI) for measurements (solid line). Lower panel: the pressure split into p_{ap}, the component propagating from the LA towards the pulmonary bed (dash-dotted line), and p_r the reflected component propagating towards the LA (dashed line). Below: corresponding ECG.

Information on elastic properties and wave speeds in the venous tree of mammals is scarce. Stress-strain curves have been developed for some veins in the adults Azuma and Masamitsu (1973). By assuming a wall-thickness diameter ratio of $1.5 \cdot 10^{-2}$ (Fung, 1984, pg. 79), we estimated wave speeds in the range 0.5-3 m/s as a function of strain in the jugular, axillary and femoral veins. Estimates from the data on the human saphenous vein Wesley et al. (1975) and the abdominal vena cava of a dog Anliker et al. (1969) yield wave speed ranges of 0.6-6 m/s and 2-6 m/s, respectively. Thus our estimate of a wave speed $c \approx 1$ m/s, is within the range of reported values.

The authors are not aware of available data which can be used to test whether the estimates for the compliance of the pulmonary bed, and the inertia of the blood in the pulmonary bed (Table 1), are within physiological ranges. These issues remain to be investigated.

Although the gross features of the measured pressure were captured well by the model predicted pressure (Fig. 3), quantitative discrepancies between the two were found (RMS = 1 mmHg). An unconventional load has been introduced to terminate the TL in our model. This was motivated by the fact that the impedance pattern of our PV measurements does not look like the impedance pattern of the arterial system. In our measurements, pressure is leading flow indicating an inertia dominated system, characterized by the positive input impedance phase angle, while the opposite is true for the pulmonary and systemic arterial system. Thus, we were led to introduce an inertance term in our model. However, we do acknowledge that a good fit between the measured and predicted pressures does not imply that the elements in the lumped model correspond to real physical quantities. On the contrary, it is known that the three-element Windkessel model provides excellent fit of data, but overestimates the

tal arterial compliance and underestimates the characteristic impedance (Stergiopos et al., 1995). Further, based on the results presented in this paper the modulus the reflection coefficient may be found to be less than unity, i.e. a part of the wave iginating in the LA will propagate through the pulmonary bed. Similarly, if the pulonary bed looks the same to the arterial side as it does to the venous side, this means at waves form the arterial side also will be transmitted through the pulmonary bed. owever, the purpose of the present study was to present an alternative hypothesis ith respect to the origin of the pressure and flow waves, namely that all waves in the ılmonary veins originate in the left heart (in particular the S2-wave). Consequently is hypothesis was tested with a lumped model where possible modifying factors from e right heart were excluded, and we found that the gross wave features observed in e measurements could be represented by this model. Thus, our model suggests that flections of pressure and flow waves at the pulmonary bed should also be taken into ccount. Possible additional contributions from the right heart can then not be exuded. It should be taken into account that the pulmonary venous system operates at w pressures (West, 1990). Pressure and flow waves will therefore be sensitive to perrbations, e.g. breathing and possible transmission of waves through the pulmonary ed.

In conclusion, we have shown that wave transmission and reflection can explain e observed wave features in the PV. A simple transmission line model loaded with inertia dominated lumped parameter model gave fair but not perfect agreement etween measured and predicted pressure waves. Further research is needed to identify her contributing factors and to verify whether the proposed lumped parameter model the proper model for the pulmonary bed.

cknowledgments

ne authors would like to express their sincere gratitude to Professor Kim H. Parker r valuable suggestions and comments. Special thanks also to Stein Inge Rabben MS, dar Sørhus MS, and Professor Bjørn Angelsen for fruitful discussions and suggestions. ne text was revised by Nancy Lea Eik-Nes.

References

Anliker, M., Wells, M., Ogden, E., 1969. The transmission characteristics of large and small pressure waves in the abdominal vena cava. IEEE Trans Biomed Eng 16, 262–273.

Azuma, T., Masamitsu, H., 1973. Distensibility of the vein: from the architectural point of view. Biorheology 10, 469–479.

Caro, C., McDonald, D. A., 1961. The relation of pulsatile pressure and flow in the pulmonary vascular bed. J Physiol 157, 426–453.

Fung, Y., 1984. Biodynamics. Circulation. Springer-Verlag New York Inc, New York.

Jones, C. J., Sugawara, M., Davies, R. H., Kondoh, Y., Uchida, K., Parker, K. H., 1994. Arterial wave intensity: physical meaning and physiological significance, Harwood Publishers, chap. 8. 129–148. Tokyo Symposium on Cardiovascular Mechanics, 1991. Recent progress in cardiovascular mechanics.

Lighthill, J., 1978. Waves in fluids, Cambridge University Press, Cambridge, chap. 2.

Maloney, J. E., Bergel, D. H., Glazier, J. B., Hughes, J. M. B., West, J. B., 1968. Transmission of pulsatile blood pressure and flow through the isolated lung. Circ Res 23, 11–24.

Milnor, W. R., 1989. Hemodynamics. Williams & Wilkins, Maryland, USA, second edn.

Morgan, B., Abel, F., Mullins, G., Guntheroth, W., 1966. Flow patterns in cavae, pulmonary artery, pulmonary vein, and aorta in intact dogs. ajp 210, 903–909.

Murgo, J., Westerhof, N., Giolma, J., Altobelli, S., 1980. Aortic input impedance in normal man: relationship to pressure wave forms. Circulation 62, 105–116.

Nishimura, R. A., Abel, M. D., Hatle, L. K., Tajik, A. J., 1990. Relation of pulmonary vein to mitral flow velocities by transesophageal doppler echocardiography. Effect of different loading conditions. Circulation 81, 1488–1497.

Parker, K., Jones, C., 1990. Forward and backward running waves in the arteries: analysis using the method of characteristics. J Biomech Eng 112, 322–326.

Parker, K., Jones, C., Dawson, J., Gibson, D., 1988. What stops the flow of blood from the heart? Heart Vessels 4, 241–5.

Pinkerson, A. L., 1967. Pulse-wave propagation through the pulmonary vascular bed. ajp 213, 450–454.

Rajagopalan, B., Friend, J., Stallard, T., Lee, G., 1979. Blood flow in pulmonary veins: II. the influence of events transmitted from the right and left sides of the heart. Cardiovasc Res 13, 677–683.

Stergiopulos, N., Meister, J. J., Westerhof, N., 1995. Evaluation of methods for estimation of total arterial compliance. Am J Physiol 4, H1540–8.

Wesley, R., Vaishnav, R., Fuchs, J., Patel, D., Greenfield Jr., J., 1975. Static linear and nonlinear elastic properties of normal and arterialized venous tissue in dog and man. Circ Res 37, 509–520.

West, J. B., 1990. Best and Taylor's Physiological Basis of Medical Practice, Williams & Wilkins, Baltimore, chap. 36. twelfth edn., 529–531.

Westerhof, N., Sipkema, P., Van den Bos, C., Elzinga, G., 1972. Forward and backward waves in the arterial system. Cardiovasc Res 6, 648–656a.